Polyisocyanopeptide Hydrogels as Effective Tissue Engineering Scaffolds

By Annette Kargaard

Thesis presented in partial fulfilment of the requirements for the degree of Master of Science (Polymer Science)

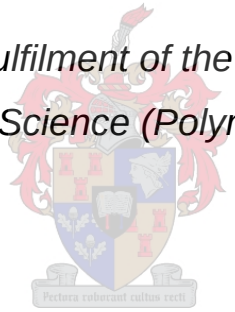

Supervisor: Prof Dr Bert Klumperman

Co-supervisor: Prof Dr Alan Rowan

University of Stellenbosch

Department of Chemistry and Polymer Science

December 2014

Declaration

By submitting this thesis electronically, I declare the entirety of the work contained therein is my own, original work, that I am the owner of the copyright thereof (unless to the extent explicitly otherwise stated) and that I have not previously in its entirety or in part submitted it for obtaining any qualification.

Annette Kargaard September 2014

Abstract

The extracellular matrix (ECM) provides the perfect environment for cells, with regard to mechanical strength, delivery of nutrients, facilitation of cell to cell communication, and more. The most challenging aspects of tissue engineering, the artificial construction of living tissue and organs, is to find a scaffold that is able to create an environment that mimics that of the ECM. In the search of such a scaffold, polyisocyanopeptide hydrogels, functionalised with oligo(ethylene glycol) side chains, have found to be the closest synthetic mimic of the ECM. They mimic, in almost in every way, the microenvironment of the cells. The primary aim of the current study was to decorate these thermo-responsive hydrogels with C**IKVAV** and cyclo(**RGD**fC) epitopes, in order to establish whether they can act as scaffolds in the promotion of neurite outgrowth in neuronal progenitor cells.

The polyisocyanopeptides were prepared by a Ni(II)-catalysed copolymerisation of a spacer monomer and an 'azide monomer' with pendant azide functionality, which was used as a reactive handle to click the C**IKVAV** and cyclo(**RGD**fC) epitopes. Three copolymers were synthesised in two different monomer feed ratios of the 'azide monomer' and 'spacer monomer'. The polymers were then characterised using FT-IR, SEC, AF4, CD and UV-vis analysis. The mechanism of gelation of the polymer was investigated using super-resolution fluorescence microscopy, in an effort to visualise the gelation behaviour in the solution state. It was observed that the polymers accumulate into concentrated clusters of bundles during the transition from solution to gel state.

The polymers were decorated with the epitopes using copper-free click chemistry. This was achieved by clicking alkyne functionalised epitopes to the pendant azide functional groups onto the polymer. The decoration was then verified using the Kaiser test. The functionalised polymers were found to be non-cytotoxic. Thereafter, the decorated polymers were seeded with neuronal GT1-7 progenitor cells, in order to test the process formation of the cells in the gel environment. However, the cell differentiation studies were not very conclusive, the materials do induce cell differentiation, but it is not very extensive. It is necessary to optimise the system, in the future.

Opsomming

Die ekstrasellulêre matriks (ESM) verskaf die perfekte omgewing vir selle met betrekkeing tot hul meganiese krag, aflewering van voedingstowwe, fasiliteite vir sel tot sel kommunikasie en meer. Die mees uitdagende aspek van weefsel manipulasie, die kunsmatige konstruksie van lewende weefsel en organe, is om ‘n steier te vind wat die omgewing van die ESM kan naboots. In die soektog tot so ‘n steier is poliisosiaanpeptied hidrojel gefunksionaliseer met oligo(etileenglikol) sykettings identifiseer as die naaste sintetiese nabootsing van die ESM. Hulle boots na, in byna elke opsig, die mikro-omgewing van die selle. Die primêre doel van die huidige studie was om hierdie termo-responsiewe hidrojel met CIKVAV en siklo(RGDfC) epitope te versier ten einde vas te stel of hulle kan dien as steier in die promosie van die uitbreiding van neurone voorloper selle tot neuriete.

Die poliisosiaanpeptied was voorberei deur ‘n Ni(II) gekataliseerde ko-polimerisasie van ‘n spasiêre monomer en ‘n asied monomeer met hanger asied funktionaliteit wat kon dien as reaktiewe handvatsels om die CIKVAV en siklo(RGDfC) epitope te kliek. Drie ko-polimere is gesintetiseer deur gebruik te maak van twee verskillende invoer verhoudings van die asied monomeer en spasiêre monomeer. Die polimere is gekarakteriseer deur gebruik te maak van FT-IR, SEC, AF4, CD en UV-vis analise. Die meganisme van jelvorming van die polimeer is ondersoek deur gebruik te maak van super-resolusie fluoressensie mikroskopie, in ‘n poging om die jelvorming gedrag in oplossing te visualiseer. Daar is opgelet dat die polimeer akkumileer in gekonsentreerde groepe bondels tydens die transformasie van oplossing to jel toestand.

Die polimeer is versier met die epitoop deur gebruik te maak van koper-vrye kliek chemie. Dit is bereik deur alkyn gefunktionaliseerde epitope te kliek aan die hanger asied gefunktionaliseerde groepe op die polimeer. Die versiering is geverifieer deur die Kaiser toets. Daar is gevind dat die gefunksionaliseerde polimere nie-sitotoksies is nie. Neurone GT1-7 voorloper selle was gekweek in die versierde polimeer ten einde die formasie proses van die selle in die jel omgewing te toets. Die sel differensiasie studies was egter nie baie oortuigend nie. Die material veroorsaak sel differensiasie, maar dit is nie baie ekstensief nie. Dit is nodig om in die toekoms die sisteem te verbeter.

Acknowledgements

I would firstly like to thank my supervisor, Bert Klumperman, for the opportunity to be a part of his research group. I would also like to thank my co-supervisor, Alan Rowan, for allowing me to infiltrate his labs at Radboud University (RU) for three months. On that note, I would like to thank Zaskia Eksteen-Akeroyd for her dedication in teaching me all she knows about polyisocyanides within 3 months, as well as for welcoming me with open arms on my arrival in Holland.

I would like to acknowledge Ben Loos for his help with the physiological aspects of this project as well as help with fluorescent microscopy. A big thanks also to Andre de Toit for his help with cell studies. Furthermore, I would also like to thank Thomas Niesler and Willie Pretorius for their help in simulating the gels.

Thank you to the NRF, Stellenbosch University (SU) and RU for funding. Thank you to the CAF staff as well as all the technical staff at both SU and RU. A special thank you to Calvin Maart, who greets me with a smile every morning at 6.30am, and never fails to surprise me with his helpful and willing nature. Thanks also to Maggie Brand for help with AF4-FFF.

I would like to thank the individual members of the Klumperman group. You have helped me in the lab, with research, and to keep my spirits high. To the Rowan Group, thank you for accepting this nomad into your labs. Thank you for showing me the ropes in research, as well as in the Dutch way of life, including the introduction to Belgian beer and Dutch Bitterballen.

Furthermore, I would like to thank Rueben Pfukwa. You have not only been the best mentor I could have asked for, but also a great friend. For the ridiculous number of times you have motivated me and re-directed me back onto the right research path and for your patience: I thank you.

Thank you to my friends (I won't mention names for fear of missing one out), in Polymer Science, Chemistry and beyond. Thank you for putting up with my complaints of lab stuff not working and my celebrations when it did work. I promise I will stop talking about science, for a few days at least, and drink tea with each and every one of you.

A special and enormous thank you to the most important people in my life: my family. There are too many of you to thank individually, but a few names I cannot leave out. Kiki, thank you for reading through 100 pages of information you don't care about in order to check for a spelling or grammar mistake. To Nina, thank you for always lending an ear, advice and solutions. A massive thank you to Nick and Nina for opening up your home to me. Thank you to Lebo: my rock and my love. And lastly, to my parent: there are no words. Thank you. I love you.

Table of Contents

List of Figures

List of Schemes

List of Tables

List of Acronyms

'Azide monomer'	Isocyanopeptide monomer with tetraethylene glycol side chain containing an azide-functionalised pendant group.
'Click' chemistry	1,3-dipolar cycloaddition of an azide and an alkyne
'Spacer monomer'	Isocyanopeptide monomer with triethylene glycole side chain and a methoxy-functionalised pendent group.
Å	Angstrom
AEMA	2-aminoethyl methacrylate
AF4	Asymmetric flow field flow fractionation
AFM	Atomic force microscopy
Ala	Alanine
ATP	Adenosine triphosphate
BCN	Bicyclo[6.1.0]nonyne
Boc-Ala	*Boc*-alanine
CD	Circular Dichroism
CNS	Central Nervous System
Cryo	cryogenic temperature
Cyclo(RGDfC)	Cyclo(Arg-Gly-Asp-D-Phe-Cys)
Da	Daltons
DAD	Diode Array Detector
DCC	*N,N'*-Dicyclohexylcarbodiimide
DIPEA	*N',N*-Diisopropylethylamine
DMAP	4-Dimethylaminopyramidine
DMAQ	Dimethylasterriquinone

DMEM	Dulbecco's Modified Eagle's medium
ECM	Extracellular Matrix
EDC	1-Ethyl-3-(3-dimethylaminopropyl) carbodiimide
EtOAc	Ethyl acetate
FFF	Field flow fractionation
FT-IR	Fourier Transform Infrared
SEC	Gel permeation chromatography
GT1-7 cells	Hypothalamic Neuronal Mouse Cells
HA	Hyaluronic acid
H-CIKVAV-NH2	H-Cys-Ile-Lys-Val-Ala-Val-amine
HCl	Hydrochloric acid
HEMA	2-hydroxyethyl methacrylate
HOBt	Hydroxybenzotriazole
HPLC	High pressure liquid chromatography
IKVAV	Ile-Lys-Val-Ala-Val
L,*D*,-PIAA	Poly(isocyano-*L*-alanine-*D*-alanine)
L,*L*-PIAA	Poly(isocyano-*L*-alanine-*L*-alanine)
LC	Liquid chromatography
LCST	Lower Critical Solution Temperature
M^{+1}	Molecular ion
MeOH	Methanol
M_n	Number average molar mass
mol%	mole percentage

MS	Mass spectrometry
MTG	MitoTracker Green Stain
M_w	Weight average molecular weight
n	Monomer side chain
Ni(II)	Nickel (II)
NMR	Nuclear magnetic resonance
P(HEMA)	Poly(2-hydroxyethyl methacrylate)
P(HEMA-AEMA)	Co-polymer of 2-hydroxyethyl methacrylate and 2-aminoethyl methacrylate
PA	Peptide Amphiphile
PEG	Poly(ethylene glycol)
PI	Propidium Iodide Stain
Poly(Dex-MA-*co*-AEMA)	Co-polymers of methacrylated dextran and 2-aminoethyl methacrylate
Pov-ray	Persistence of Vision(tm) Ray
RADA16	Arg - Ala - Asp - Ala - Arg - Ala - Asp - Ala - Arg - Ala - Asp - Ala - Arg - Ala - Asp - Ala -NH_2
R_f	Retention factor
RGD	Arg-Gly-Asp-Ser
SEC	Size exclusion chromatography
SEM	Scanning electron microscopy
Sulfo-SMCC	sulfo-succinimidyl-4-(*N*-maleimidomethyl)cyclohexane-1-carboxylate
T	Temperature

t	Time
TLC	Thin-layer chromatography
Trans	Transmission channel
UV-vis	Ultraviolet-visible
YIGSR	Tyr-Ile-Gly-Ser-Arg

Chapter 1: Prologue

1.1 Introduction

Within the field of Tissue Engineering, there is a considerable need for the development of polymer scaffolds that are able to mimic the microenvironment of cells. This scaffold must fulfil certain criteria, which must take into consideration the chemical, physical and topological factors that regulate the development and function of cells.[1-3] These criteria include mechanical strength within a three dimensional, biocompatible network, bio-decomposition of the scaffold after its function has been completed, non-toxicity to cells even of its decomposed parts, ability to direct cell adhesion, differentiation, migration, and proliferation of cells as well as morphology and gene expression. Furthermore, the scaffold must allow for the diffusion of nutrients through the polymer network.[4-6] The scaffold should be easily modified, and therefore, it has been proposed that synthetic polymers are more advantageous as scaffold than naturally-derived polymers.[3,7]

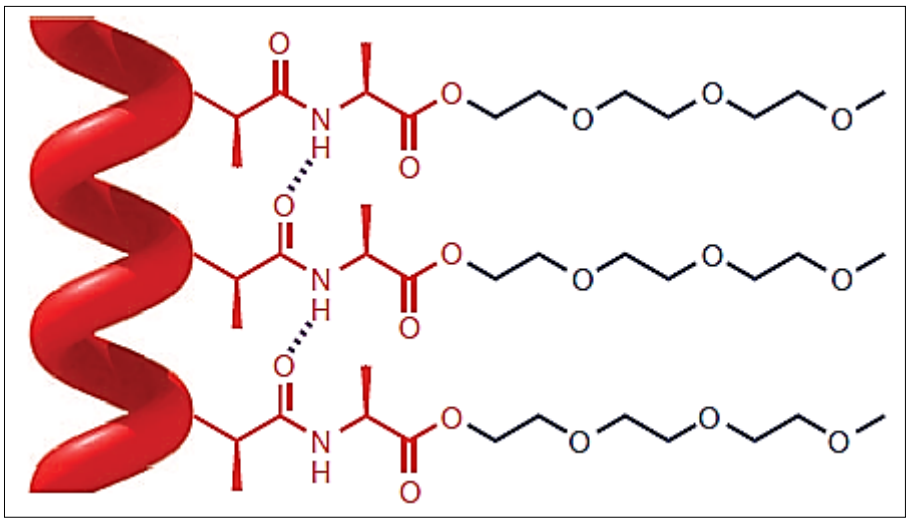

Figure 1.1 A schematic representation of polyisocyanopeptide hydrogels grafted with oligo(ethylene glycol) side chains.[8]

Polyisocyanopeptide hydrogels with oligo(ethylene glycol) side chains, shown in Figure 1.1, have been identified as possible scaffolds in tissue engineering.[8] They have been seen to almost exactly mimic the extracellular matrix (ECM). They

possess a rigid carbon backbone in a helical architecture. As seen in Figure 1.1 and Figure 1.2, each carbon in the backbone has a side chain consisting of two alanine moieties and an oligo(ethylene glycol) chain, with modifiable lengths. The helix is stabilised by intramolecular hydrogen bonds between the alanine moieties on the side chains. These hydrogen bonds are seen in Figure 1.1 by means of dashed lines. The polymer has been seen to have a tuneable and fully reversible, thermal gelation temperature, whereby it is believed that the side chains bundle together to form transparent gels. This occurs even at very low concentrations. The hydrogels are readily modified, due to the possibility of altering each side chain. Therefore, these polymers have been identified as having many possible applications, especially within the biomedical field.

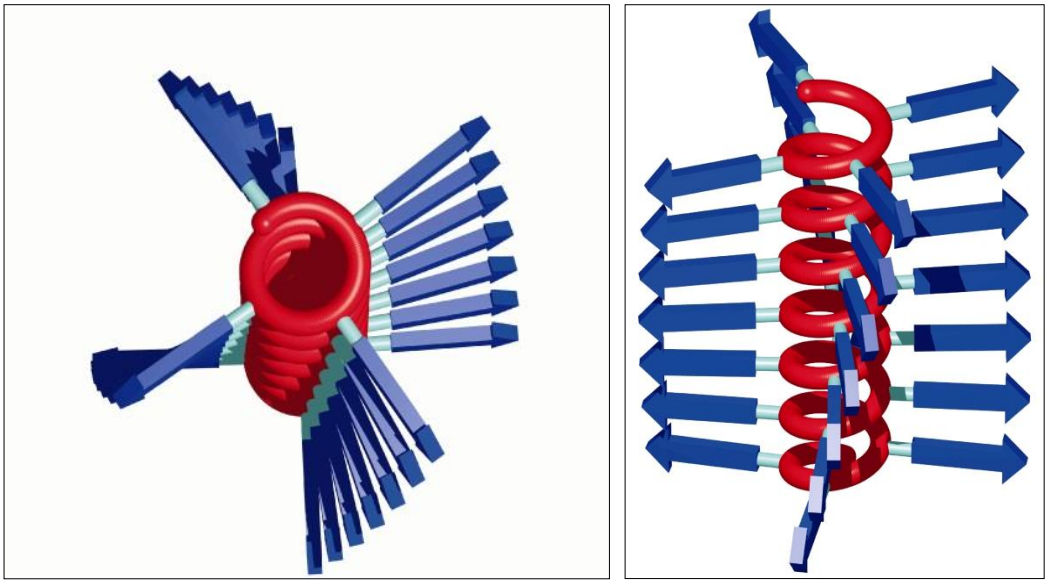

Figure 1.2 A schematic representation from above (left) and from the side (right) of the polyisocyanopeptide hydrogels depicting the manner in which the side chains arrange themselves on the helical, carbon backbone.[8]

1.2 Objectives

The motivation for this work is based on the claim that polyisocyanopeptide hydrogels grafted with oligo(ethylene glycol) side chains are able to almost exactly mimic the ECM.[8] This study proposes the use of polyisocyanopeptide hydrogels functionalised with oligo(ethylene glycol) side chains as a possible scaffold for tissue

engineering. The investigation will incorporate the conjugation of the polymer with **IKVAV** and cyclo(**RGD**fC) epitopes to establish the ability of the scaffold to assist in the cellular activity of these peptides. This was done by seeding GT1-7 cells into a liquid solution of polymer functionalised with the epitopes. After incubating the cell-polymer solution at 37 °C, the cells were monitored to see whether neurite outgrowth was successfully promoted.

The current study also investigates the mechanism of gelation of these polyisocyanopeptide hydrogels in aqueous medium. This research used fluorescent microscopy to visualise the polymers in the gel state. A concentration gradient study was undertaken whereby the gels were analysed under the fluorescent microscope at super resolution. These z-stack images were then compiled into a 3D simulation of the gel. Furthermore, a thermal, time lapse fluorescent microscopy study was done, whereby the polymers in aqueous medium were visualised during the transition from solution state to gel state. The following goals were set for the research described in this thesis.

1. To synthesise isocyanopeptide monomer with an azide functionalised end group, or the 'azide monomer'.
2. To copolymerise and fully characterise the bought, non-functional monomer, or spacer monomer, with the synthesised azide monomer, in different monomer ratios.
3. To visualise the polymer in gel and solution phase using fluorescent microscopy and then recreate the gel with 3D simulations based on the z-stack images.
4. To conjugate the polymers with C**IKVAV** and cyclo(**RGD**fC) epitopes and establish the scaffolding ability of the polymer *in vitro*, by visualising the cell - polymer interaction under the fluorescent microscope.
5. To establish the cytotoxicity of the polymers *in vitro,* as well as the extent of promotion of progenitor cells into neuronal cells.

1.3 Layout of Dissertation

The dissertation comprises 6 chapters.

Chapter 1: Prologue

Chapter 1 gives a brief introduction to previous research conducted within the area of this dissertation as well as an overview of the objectives and aims of the study.

Chapter 2: Literature Review

Chapter 2 gives a comprehensive literature review that gives an overview of tissue engineering and scaffolds for tissue engineering with a focus on scaffolds used in the promotion of neurite outgrowth. The overview also gives a summary of the work that has previously been carried out on polyisocyanopeptide hydrogels.

Chapter 3: Monomer Synthesis and Characterisation

Chapter 3 addresses the synthetic protocol and characterisation of the synthesis of the azide-functionalised monomer, isocyano-*D*-Ala-*L*-Ala-$(EG)_4$-N_3.

Chapter 4: Polymer Synthesis and Characterisation

Chapter 4 describes the copolymerisation and characterisation of polyisocyano-peptide hydrogels with different monomer ratios and molecular weights. It further addresses the gelation properties of the polymers.

Chapter 5: Polymer Conjugation and Physiological Testing

Chapter 5 addresses the conjugation of the polymers synthesised in Chapter 4 with C**IKVAV** and cyclo(**RGD**fC) epitopes. It also describes the results of the physiological testing of these conjugated polymers in the presence of cells.

Chapter 6: Conclusion

Chapter 6 gives a brief overview of the results obtained in this dissertation as well as recommendations for future research to develop the knowledge and understanding of polyisocyanopeptide hydrogels with oligo(ethylene glycol) side chains as possible scaffolds for tissue engineering.

1.4 References

(1) Putnam, A. J.; Mooney, D. J. *Nat Med* **1996**, *7*, 824.
(2) Vacanti, J. P.; Langer, R.; Upton, J.; Marler, J. J. *Adv Drug Deliv Rev* **1998**, *33*, 165.
(3) Brandl, F.; Sommer, F.; Goepferich, A. *Biomaterials* **2007**, *28*, 134.
(4) O'Brien, F. J. *Materials Today* **2011**, *14*, 88.
(5) Carletti, E.; Motta, A.; Migliaresi, C. *Methods Mol Biol.* **2011**, *695*, 17.
(6) Chan, B. P.; Leong, K. W. *Eur Spine J* **2008**, *4*, 467.
(7) Lee, K. Y.; Mooney, D. J. *Chem Rev* **2001**, *101*, 1869.
(8) Kouwer, P. H. J.; Koepf, M.; Le Sage, V. A. A.; Jaspers, M.; van Buul, A. M.; Eksteen-Akeroyd, Z. H.; Woltinge, T.; Schwartz, E.; Kitto, H. J.; Hoogenboom, R.; Picken, S. J.; Nolte, R. J. M.; Mendes, E.; Rowan, A. E. *Nature* **2013**, *493*, 651.

Chapter 2: Literature Review

2.1 Tissue Engineering: A General Overview

Tissue engineering is the artificial manufacturing of living tissue and systems, such as organs, which can be done using various methods.[1] These methods include the manipulation of stem cells to differentiate into specific phenotypes, as well as the combination of polymer scaffolds with cells in such a way that the natural microenvironment of the cells is mimicked, as depicted in Figure 2.1.[2,3] This current study will focus on the latter approach.

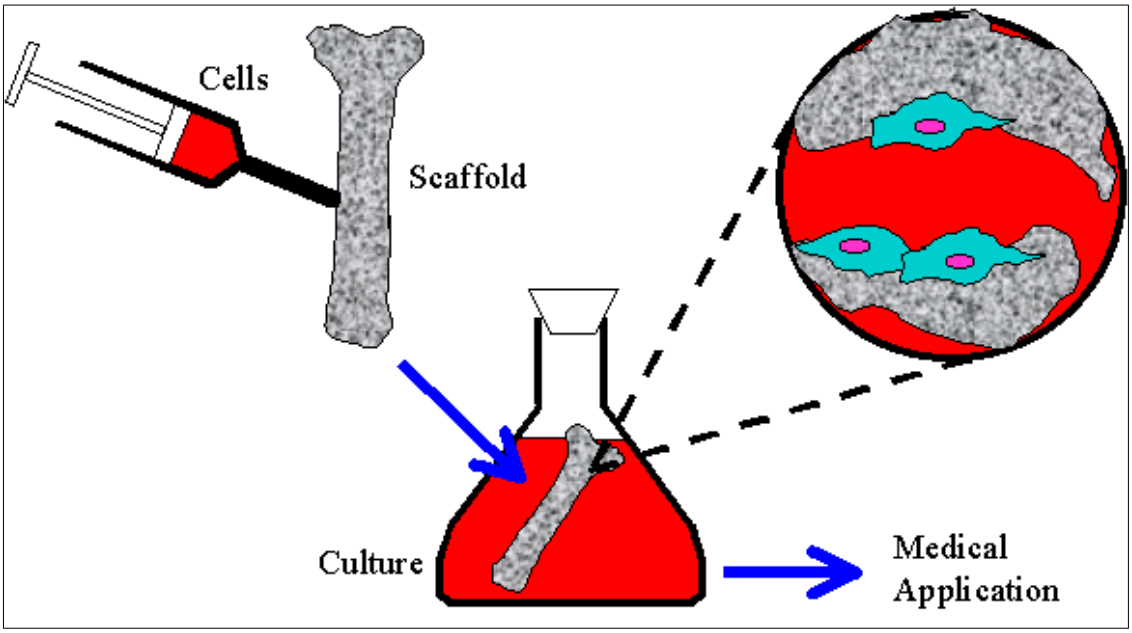

Figure 2.1 Tissue engineering using a polymer scaffold as a mimic of the extracellular matrix (ECM) of the cells. Illustration by Goldstein, A. S. (http://www.tissue.che.vt.edu/home_frame.htm)

2.2 Scaffolds

Due to cell function and the development of tissue and organs being regulated by chemical, physical and topographical factors, efficacious tissue engineering of biomaterials must consider all of these factors.[2-4] Thus, to properly understand the requirements needed to effectively design a three-dimensional scaffold, the

extracellular microenvironment of cells must be understood. This complex microenvironment is able to guide the development and maintenance of cell function by providing bound, multifunctional adhesion proteins, including fibronectin, vitronectin and laminin.[5,6] These proteins are responsible for the mechanical properties of the hydrogel network.[7] Furthermore, the matrix is able to direct cell adhesion, differentiation, proliferation, morphology, as well as gene expression.[8-10] Each of these variables have specific signalling pathways and, through the adjustment of any of these factors, it is possible to tailor the biomaterials for a large range of applications.[4] West *et al*.[11] proposed that effective tissue engineering requires a three-dimensional scaffold that can mimic the extracellular microenvironment of the cells, thus allowing it to promote cell growth at the same time as controlling cell function and tissue organisation. It is then possible for the scaffold to direct the cells to their desired location, act as a site for the tissue to grow, as well as control the function and structure of the engineered tissue.[2,3,12] They were able to demonstrate examples of such scaffolds via the synthesis of hydrogels that were decorated with Arg-Gly-Asp-Ser (**RGD**S) cell adhesive, peptide sequences in a three-dimensional conformation. When cells were placed in the environment of this scaffold, they were seen to exclusively invade and migrate into regions containing **RGD**S.[11]

2.3 Scaffolds that Mimic the Extracellular Matrix

The importance of the extracellular matrix (ECM) is vast and inconceivable. It is largely comprised of various peptides and proteins that mediate intracellular contact, control cell function and tissue structure, as well as facilitate diffusion of nutrients, metabolites and growth factors. This underscores the critical importance of the polymer scaffold that is utilised in tissue engineering, as the scaffold must act as a substitute for the ECM.[5,13,14] Bissell *et al*.[15] previously showed that, due to interactions with the cellular microenvironment, the phenotype is able to supersede the genotype and hence concluded that the function and gene expression, and ultimately protein expression, of cells is influenced by their microenvironment. Thus, the function of a scaffold is more than just a three-dimensional vehicle, as it must also be synthesised with the view that it is part of the pathways that direct the specific cellular phenotype.[7] Moreover, it is now believed that cells should be cultured in a microenvironment that mimics the ECM of the cell, including the

mechanical and biochemical signals that are present in this microenvironment.[16] Furthermore, these three-dimensional scaffolds should facilitate hierarchical processes of the cells, including migration and tissue organisation.[7]

Cells are cultured in a single layer when a two-dimensional scaffold is utilised.[7] The tissue engineering investigations undertaken using two-dimensional scaffolds have paved the way for what is now known about complex biological systems within molecular biology, stem cell differentiation, and tissue development.[17] However, Bissell *et al*. discovered that cell cultures grafted on two-dimensional scaffolds had a tendency towards developing into tumours. This tumour formation was not detected when using a three-dimensional scaffold.[18] Three-dimensional scaffolds are more effective than two-dimensional scaffolds, since monolayer matrices restrict the cultures to a planar environment, which creates an environment that does not allow for the complex morphologies that are seen in nature.[5,7] Zhang *et al*.[19] explain this phenomenon by describing how the two-dimensional scaffold actually polarises the cells in a manner that subsequently only allows a segment of the cell to be available to interact with its microenvironment, and with other cells. Hendzel *et al*.[20] concluded that the phenotypic fate is then affected, the intracellular signalling is disrupted, and unnatural interactions occur between soluble factors. This influences cell migration, intercellular communications and cell differentiation.[7] In essence, the two-dimensional structures are unable to provide a platform with the environmental signals that are seen in the natural microenvironments of the cells.[21] Thus, two-dimensional scaffolds are unsuccessful in mimicking the natural environment of the cell,[22] and a scaffold with a three-dimensional, hierarchical architecture is necessary for effective cell culture growth.[18,22]

Evidence has shown that it is possible, to sufficiently create a model system of the ECM using three-dimensional scaffolds. The cell cultures are provided with the mechanical cues[23] and regulatory signals that are necessary for natural growth, and a platform for cell-cell interactions. Furthermore, such a scaffold has been shown to be able to develop natural cellular behaviour patterns by providing the necessary composition, stiffness and topography necessary for the behaviour and morphology of the cells, as well as tissue development.[21,22,24]

ECMs have inspired the use of polymers that are similar in architecture, *i.e*. a three-dimensional, porous network on which the cells are able to adhere and proliferate. Scaffolds for tissue engineering applications must fulfil certain criteria. These criteria include physical parameters, such as degradation and mechanics, as well as performance constraints within the biological sector, such as cell adhesion and biocompatibility with the host.[12,25] The components produced during the gradual degradation should also be non-toxic and should be easily eliminated from the human body.[24] Only when these criteria are reached, can polymers be seen as successful scaffolds. There are several factors that must be considered when regarding polymers as viable scaffolds, including biocompatibility, biodegradability, mechanical properties, scaffold architecture, as well as the manufacturing technology.[10] Furthermore, a minimally intrusive procedure is preferable when the cell culture, incorporated into the polymer scaffold, is transplanted into the human body. Injection is often a favoured method, and is possible with polymer systems such as hydrogels and amphiphiles.[26,27]

The activity of proteins is directly related to their structure due to the 'lock-and-key' model. Therefore, the secondary structure, based on hydrogen bonding, is essential for the function of the protein. In the same manner, scientists have tried to create scaffolds that are activated through secondary structures, via self-assembly of the scaffold. Self-assembly is a process driven by free energy, whereby the molecules are organised into ordered structures. It is possible to regulate self-assembly using environmental conditions, *e.g*. pH, solvents and temperature. One of the main factors that drive self-assembly in physiological conditions is hydrophobicity. This self-assembly is then stabilised by secondary forces, such as electrostatic interactions, intramolecular interactions, etc.[28,29] It is important to note that the intended goal of self-assembly is not to solely yield stable nanostructures, but rather for the nanostructure to carry out a specific function. Indeed, *in vivo*, it is desirable for the scaffold to degrade once it has performed its function.[10,30] The degradation process of peptide-based scaffolds sees them dissipate into natural, non-toxic amino acids, which is perfect for applications within living systems. Furthermore, the function of the final nanostructure is controlled by the information contained within each individual building block. This allows for the tuning of nanostructures for use in different applications. This is especially important within medical applications.

There has been a large amount of research surrounding the use of polymers as scaffolds for amino acid sequences such as **RGD**, Ile-Lys-Val-Ala-Val (**IKVAV**) and Tyr-Ile-Gly-Ser-Arg (**YIGSR**). Cells that are exposed to a scaffold containing the laminin-derived epitope, **IKVAV**, have been observed to differentiate into neurons far more effectively, especially in comparison to those that have been exposed to laminin itself.[31] This research field has especially been pioneered by Samuel Stupp and his co-workers.

2.4 Amphiphiles as Scaffolds

Prior to Stupp's research, the majority of the work in this field encompassed the use of scaffolds made from biodegradable, non-bioactive polymers, such as poly(*L*-lactic acid), poly(glycolic acid) and combinations thereof,[32] as well as from biomaterials, for example collagen, alginate and fibrin.[33] Cells from the tissue were seeded into these pre-assembled scaffolds, and thereafter these structures were either implanted into the living system, or they were allowed to develop in a bioreactor, and subsequently transferred to their final destination.[34] Amphiphiles are one class of polymers that have been investigated in this regard. They are compounds that contain both a hydrophobic (water-hating) and a hydrophilic (water-loving) moiety, as illustrated in Figure 2.2. The original proposal of a peptide amphiphile (PA) as a scaffold was designed by Kunitake.[35]

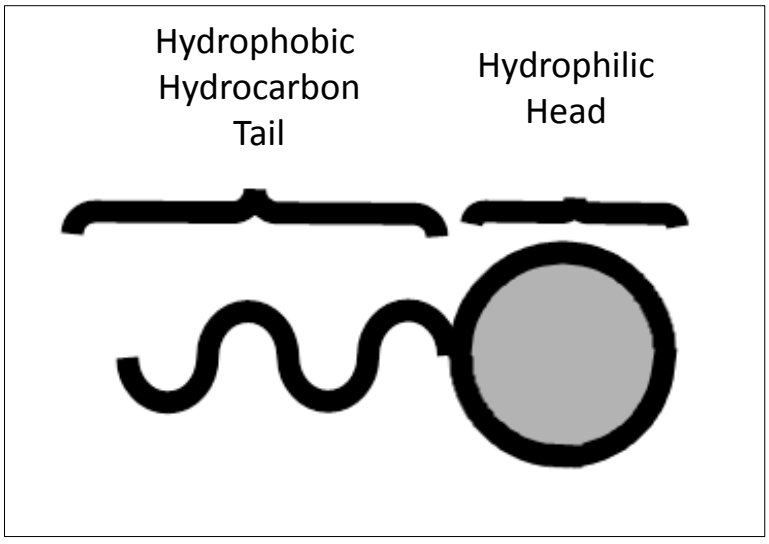

Figure 2.2 Amphiphiles contain a hydrophilic (water-loving) head and a hydrophobic (water-hating) hydrocarbon tail.

Lin *et al*. studied the effect of cell adhesion and differentiation when cells were exposed to polystyrene surfaces, and a number of other support systems, coated with LA-2, which is a multi-domain, synthetic polymer containing **IKVAV** and a heparin-binding domain.[36] They observed that using this multi-domain peptide showed more cell adhesion than just exposing the cells to **IKVAV**. They further concluded that the peptide coating could be used to enhance cell adhesion and differentiation in implants for tissue engineering.

Zhang *et al*.[37] developed a self-assembling peptide amphiphile (PA), RADA,[16] which was tested as a scaffold for neural tissue engineering in mice with injured brains.[38] RADA[16] is a peptide-based hydrogel, which is able to self-assemble at very low concentrations into a three-dimensional, ECM-mimicking structure. When triggered, the PA was able to organise itself into a β-sheet structure under physiological conditions. It was observed that the scaffold not only promoted neurite extension and differentiation of neuronal stem cells, but also acted as a support structure for tissue development.

Silva *et al*.[33] prepared a two-part scaffold containing two peptide amphiphiles, one positively charged and the other negatively charged at neutral pH. These amphiphiles consist of four parts (see Figure 2.3), where the hydrophobicity increases systematically from very hydrophilic, to very hydrophobic from one side of the molecule to the other ('**d**' to '**a**'). In Figure 2.1, '**a**' represents the hydrophobic region, which is usually an alkyl chain. Attached to this hydrophobic region is a section of hydrophobic peptide sequences ('**b**' in Figure 2.1) that allow for hydrogen bonding between amphiphile units. These intermolecular hydrogen bonds usually form β-sheets giving rise to the one-dimensional nature of the self-assembled nanostructures.[39] The interactions in this region are responsible for the high packing density of the molecules. The mechanical properties and shape of the nanostructures can be tuned by controlling this peptide region. Thereafter, is region '**c**', which is typically composed of charged amino acids. These amino acids promote electrostatic repulsion between the amphiphiles and this region is accredited for the self-assembly of the peptide amphiphiles. The number of charges must be controlled. There must be enough charge to ensure solubility and allow for the purification of the peptide amphiphiles, but not too high a charge as this would interfere with the intermolecular interactions that ensure the 1D self-assembly of the

amphiphiles. The final, hydrophilic region ('**d**') contains bioactive signals, usually epitopes, which are able to interact with cells and proteins.

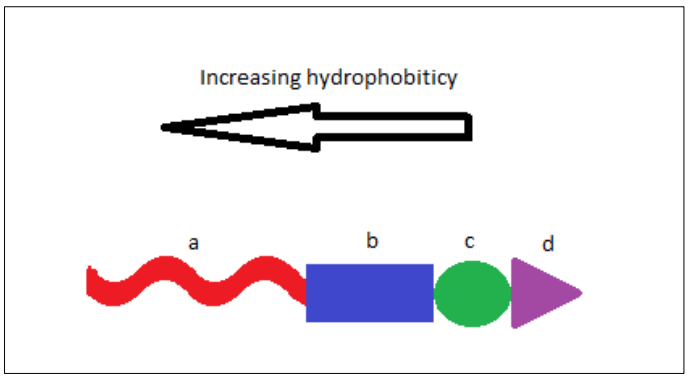

Figure 2.3 A schematic representation of the amphiphiles used in the self-assembly of gel scaffolds by Stupp *et al*., where a represents the hydrophobic region, usually an alkyl chain, b represents a short peptide sequence that is able to form hydrogen interactions, c contains charged amino acids which promotes the electrostatic repulsion, involved in self-assembly and d is the region containing bioactive signals, usually an epitope.

These PAs self-assemble into cylindrical 'micelle'-like aggregates, and gel at concentrations above 5 mg/mL in aqueous medium. The self-assembly can be tuned due to the weak base and acid nature of the charged amino acid region by changing the pH of the system, or by changing the concentration of electrolytes. Thus, the amphiphiles can be injected into a living system as a liquid and, upon exposure to a change of pH, the molecules self-assemble into nanofibers, which subsequently bundle to form gelled networks. Due to the hydrophobic region, the peptide amphiphiles are able to assemble in such a way that the bioactive signals are on the periphery of the nanofiber surface.[40] The high density of these molecules, due to region '**b**' (Figure 2.1), allows for a high concentration of epitopes to appear on the fibre surface. This can be controlled by the length of the alkyl chains in the hydrophilic region. The possibility of the self-assembly being due to the hydrophobic collapse of the alkyl chains of either of the two amphiphiles was dismissed due to the solubility of both amphiphiles at a neutral pH. In addition to the electrostatic forces, hydrogen bonding occurs between the amino acid moieties on the amphiphiles, and

hydrophilic and hydrophobic interactions in aqueous medium cause the PAs to take their assembled shape. The final shape, size and interfacial curvature of the self-assembled systems results from a balance between each of the contributing factors. The double amphiphile molecule allows for dual functionalisation of these gels, whereby they have been labelled with **RGD**, **IKVAV** and **YIGSR** amino acid sequences.[41]

More recently, Stupp and his coworkers have looked at other self-assembling charged nanostructures, where they combine an aqueous solution of positively charged PAs and an aqueous solution of negatively charged, high molecular weight hyaluronic acid (HA).[42] The PAs self-assemble in the same manner as the other PA systems explored by Stupp *et al.*[39,43-47] When these two solutions come into contact with each other they form a dense fibrous layer within milliseconds at the interface of the two liquids.[42,48] This layer prevents the two solutions from mixing. Reptation of the HA solution occurs through the diffusion barrier into the PA solution due to the unbalanced osmotic pressure between the two solutions, thus there are three zones, shown in Figure 2.4, of the hierarchical HA/PA membrane.[42,48,49] These three layers are firstly an amorphous gel (**1**), then there is the diffusion barrier which is made up of nanofibers aligned parallel to the interface (**2**), and lastly there is a layer of HAs and PAs that have complexed due to electrostatics (**3**). This layer lies perpendicular to the interface. The ordered microstructure seen in this membrane is due to the molecular interactions between the PA nanostructures and the polyelectrolytes. No further processing is necessary. As in the other PAs described by Stupp, bioactive peptides can be incorporated into these membranes.[49]

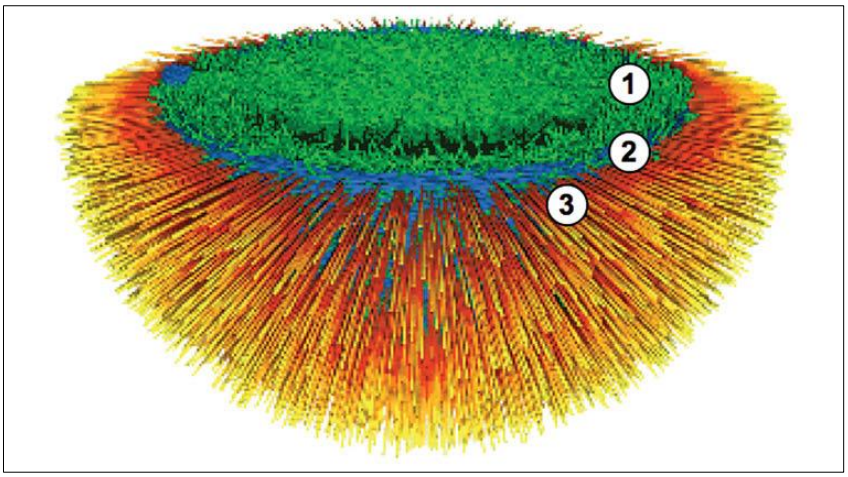

Figure 2.4 A schematic representation of the three hierarchical zones of the PA/HA membrane, where 1) is the amorphous gel layer, 2) is the nanofibers that align parallel to the plane of the membrane, and 3) represents the electrostatically complexed HA-PA nanofibers that align perpendicular to the membrane.[49]

A number of other gelling PA polymers have been studied as possible polymer scaffolds, including work done by Zhang,[50] Xu[51] and others.

Another such study involved the use of the PA, $C_{16}H_{31}O\text{-}A_3G_4D_2$ **IKVAV**, whereby the 3D nanofiber matrix, consisting of 99.5 wt% water, provided mechanical support, as well as a porous medium, through which the diffusion of nutrients, biofactors and oxygen, as well as cell migration was possible. The hydrogel allowed for the proliferation of cells due to the **IKVAV** epitope.[52] Copolymers of methacrylated dextran and aminoethyl methacrylate (Poly(Dex-MA-*co*-AEMA)) with sulfhydryl-terminated peptides, crosslinked using sulfo-succinimidyl-4-(*N*-maleimidomethyl)cyclohexane-1-carboxylate (sulfo-SMCC), have also been investigated as possible scaffolds in tissue engineering. The primary amine groups allowed for the covalent functionalisation of the macroporous scaffold with epitopes. These amphiphiles showed positive results with regards to neurite outgrowth. There was a higher cellular response when an extended laminin derivative was used, such as CQAAS**IKVAV**, rather than a single standing epitope, *e.g*. S**IKVAV**.[53]

2.5 Polymer Hydrogels as Scaffolds

Polymer hydrogels are another class of polymer systems that have been investigated for their potential use as scaffolds. Hydrogels are typically hydrophilic polymers that are composed of cross-linked networks of polymer chains that contain

high concentrations of water, up to thousands of times their own (dry) mass.[54,55] Hydrogels can be made up of polymers, proteins or peptides. The use of peptides as hydrogels is advantageous, as they do not need any additional factors to promote cell attachment or neurite outgrowth. However, the problem is that these peptides are expensive and complex to synthesise.[56] Polymer-derived hydrogels are usually created from natural polymers, such as proteins, e.g. collagen, or from synthetic polymers, such as poly(vinyl alcohol) or poly(acrylic acid). These gels have been shown to act as effective scaffolds due to their high porosity and three-dimensional nature.[7] Thus, hydrogels form an integral part of tissue engineering.[5] The limitations of two-dimensional scaffolds, as well as three-dimensional scaffolds that mimic fibrillar extracellular proteins, can be overcome by using hydrogels as scaffolds. The main reason for this is the ability of hydrogels to imitate the physiochemical characteristics of natural extracellular matrixes.[5,7]

A major advantage of hydrogels is their biocompatibility (especially when derived from natural polymers[12]), physiochemical properties, as well as their ability to be easily synthesised.[5] Limitations associated with naturally derived polymers, such as difficulty in functionalising/modification, have caused scientists to alter these natural polymers or use synthetic polymers instead. These synthetic polymers are chosen based on their chemical and physical properties. Another major advantage of synthetically derived hydrogels is their ability to incorporate growth factors and mechanical signals, which improve their scaffolding abilities.[12] The characteristics that are incorporated into the hydrogel assist in providing the cell cultures with the appropriate environment needed for cell adhesion, migration, growth and differentiation.[4] The cells are unable to adhere to hydrogels, due to the lack of proteins that bind to the cellular receptors. However, this can be adjusted by covalently coupling peptides or proteins to the hydrogels, which would then allow the cells to adhere to the polymers. In a similar way, specific peptide sequences can be added to the polymer chains, in order to adjust the influence of the scaffold on the growth and phenotype of the cell cultures.[4] A limitation to the addition of these growth factors, as well as the adhesion peptide sequences, is the lack of control over the even distribution of these bonded receptors on the hydrogel.[56]

Hydrogel formation typically takes place under mild chemical conditions that do not affect the viability of cell cultures. As a consequence, the formation of hydrogels can

be carried out *in vivo*. This underscores the ability of the hydrogel scaffolds to mimic extracellular microenvironments.[5] Although the porosity and highly hydrated, random chain network of the hydrogels allow for diffusion characteristics that mimics that in the natural ECM, these characteristics also cause the platform to have poor mechanical strength.[57] It is evident that when these gels are combined with cells, the mechanical properties improve.[58,59] In tissue engineering, it is crucial that the hydrogel scaffold is able to provide the necessary support for the cells, until such a time when the cells have produced their own extracellular microenvironment.[4] After this time, the mechanical properties of the hydrogel are no longer needed, and thus they do not need to be retained.[12] However, the scaffold must also be able to biodegrade in a non-toxic fashion.[57]

The building blocks of the hydrogels are manipulated to ensure that the hydrogel provides the correct mechanical support necessary for the desired outcome of the cell cultures. Thus, the hydrogels are specifically designed for a particular function, and it is crucial to take this function into consideration when designing and synthesising the hydrogel. Every specific monomer unit of the hydrogel has a role to play in the overall outcome of the hydrogel, and this includes the molecular weight and the chemical make-up, be it hydrophobicity, ability to form intra/intermolecular interactions, etc. The hydrophilic nature of hydrogels, as well as the amount of water in the hydrogel, assists them in ensuring that the proteins of the ECM are not absorbed.[55] Other factors also influence the properties of the hydrogels, such as the manner in which the polymer chains were cross-linked, be it physically (reversible) or chemically (permanent or reversible).

A study on a two-dimensional cell culture was conducted using a PEG hydrogel as a scaffold, where proteolytic degradation sites, as well as growth factors and cell adhesion ligands, were incorporated into the hydrogels. The scaffolds were seen to promote neurite outgrowth of PC12 cells. This system showed less neurite outgrowth than that of scaffolds that display a 3D matrix,[60] such as agarose gels.[61]

Another hydrogel that has been investigated is poly(2-hydroxyethyl methacrylate) (PHEMA). It is considered to be a good polymer scaffold due to its high mechanical strength, versatility in structure, and elasticity. It is possible to copolymerise 2-hydroxyethyl methacrylate (HEMA) with reactive comonomers containing pendant groups, such as carboxylic acids and amino acids, to obtain super porous hydrogels

that are readily modified. The radical copolymerisation of HEMA with 2-aminoethyl methacrylate (AEMA) yielding P(HEMA-AEMA) was subsequently modified with the **IKVAV** epitope. This modified scaffold was seen to promote neurite outgrowth and cell adhesion.[62] The non-degradability of the P(HEMA) remains an issue.

Further investigation for a viable scaffold has yielded a thiolated, water-soluble methacrylamide chitosan which was coupled to GQASS**IKVAV** through a maleimide-thiol bond, as seen in Scheme 2.1. A study investigating the cell penetration into the scaffold matrix, and the cell adhesion to the three dimensional, porous scaffolds were done. Positive results were obtained regarding both of these aspects, as well as the biodegradability of the chitosan upon the addition of lysozyme.[63] Another chitosan scaffold has been developed, using a tendon chitosan tube with triangular section.[64] Tendon chitin is obtained from crabs and then deacetylated into tendon chitosan. A triangular steel bar was inserted into circular chitosan, upon heating, and the chitosan took on the shape of the bar, as seen in Figure 2.5 When the bar was removed, the chitosan shrunk. Due to the presence of hydrogen bonds among the chitosan molecules, the triangular shape of the tube remained. When placed in solution, this triangular shape of the chitosan remained stable. This tube showed increased mechanical strength compared to previous chitosan materials, and was therefore plausible for scaffold functionality. The study included the addition of **IKVAV** sequences to the tubes. Results showed that these tubes assisted nerve tissue extension.

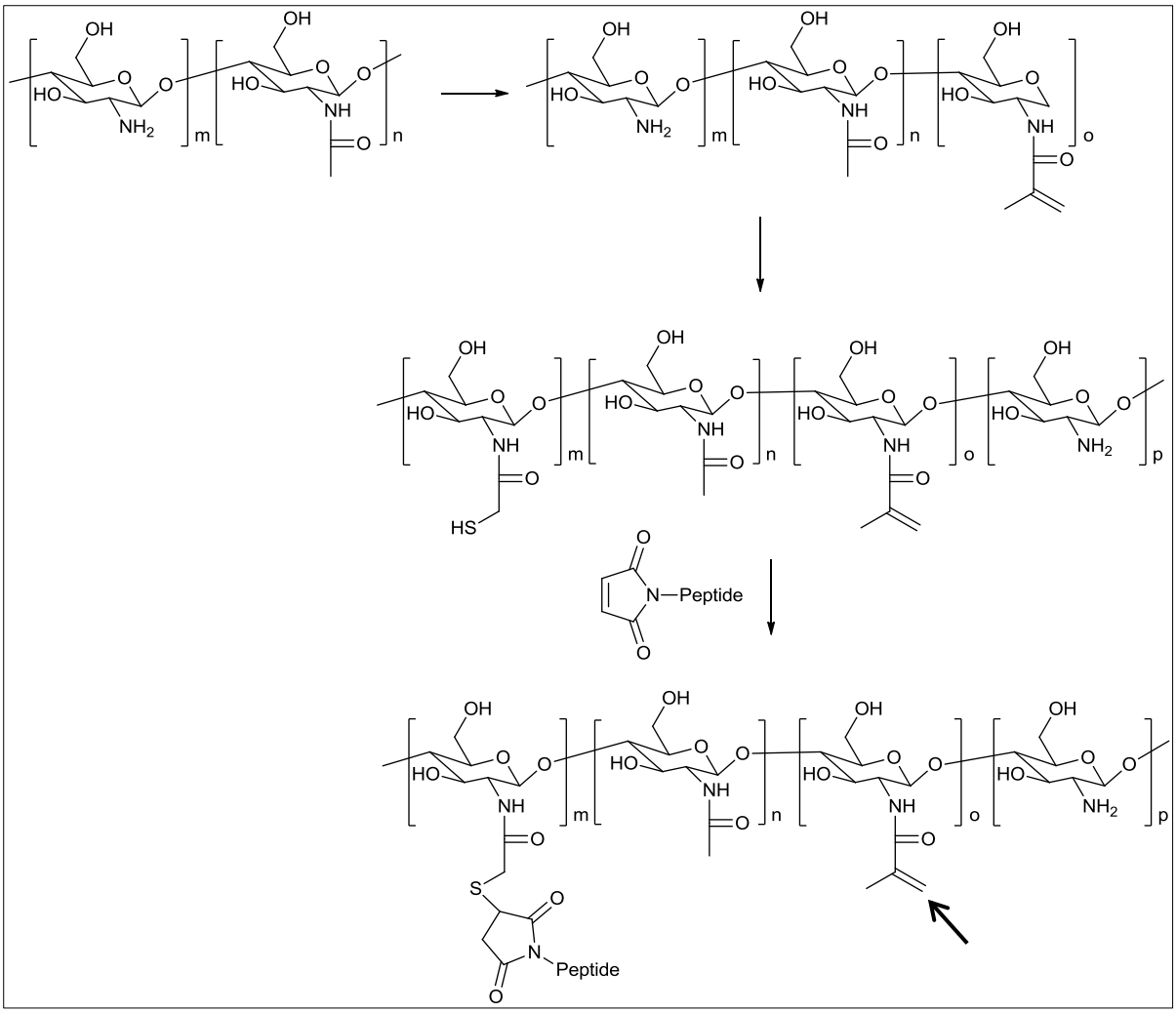

Scheme 2.1. Methacrylamide chitosan is synthesised by reacting chitosan and methacrylic anhydride. This product undergoes free radical polymerisation, producing in a methacrylamide chitosan hydrogel. The primary amine functional groups are reacted with thioglycolic acid via an EDC-mediated cross-linking to finally produce the thiolated methacrylamide chitosan. A Michael addition reacts the thiol with a maleimide-containing peptide to produce the peptide-functionalised, thiolated methacrylamide chitosan. The arrow shows the site where cross-linking occurs. [63]

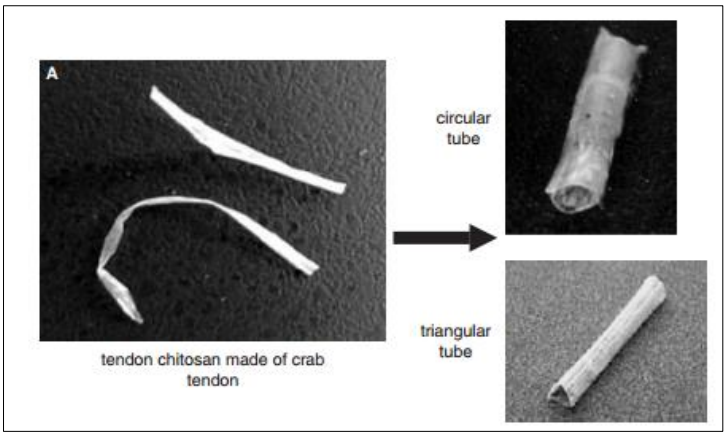

Figure 2.5 Chitin from crab tendons are transformed into triangular chitosan tubes by moulding circular chitosan tubes with a triangular steel rod.[64]

HA hydrogels have also been investigated as possible scaffolds, decorated with an **IKVAV** epitope. HA, a long negatively charged glycosaminoglycan, is a large component of the ECM of brain tissue. This highly hydrated acid is known for its assistance in healing wounds, and has been shown to play a crucial role in the development of the central nervous system (CNS). When conducting this study, they implanted the scaffold into the injured brains of rats. Although they observed temporary inflammation in the implanted area, this effect was fixed by the presence of the hydrogel. Thus, they concluded that their scaffold showed biocompatibility *in vivo.* It also showed favourable results with regard to cell ingrowth and angiogenesis.[65]

A limitation for all of the above mentioned polymer systems is that they have not proven to be perfect ECM-mimics. In the hope of finding such a scaffold, the intention of this current study is to explore the use of polyisocyanopeptide hydrogels as scaffolds for neurite outgrowth. These polymers have shown promise as ECM mimics. Through a Ni(II)-catalysed polymerisation of isocyanopeptides, analogues of β-helices, with β-helix motifs that are similar to naturally occurring β- sheet helices, as seen in Scheme 2.2, have been obtained.[66] These polyisocyanopeptides are defined as rigid polymers. They contain a carbon backbone whereby each carbon is attached to a side chain substituent containing a dipeptide. [66]

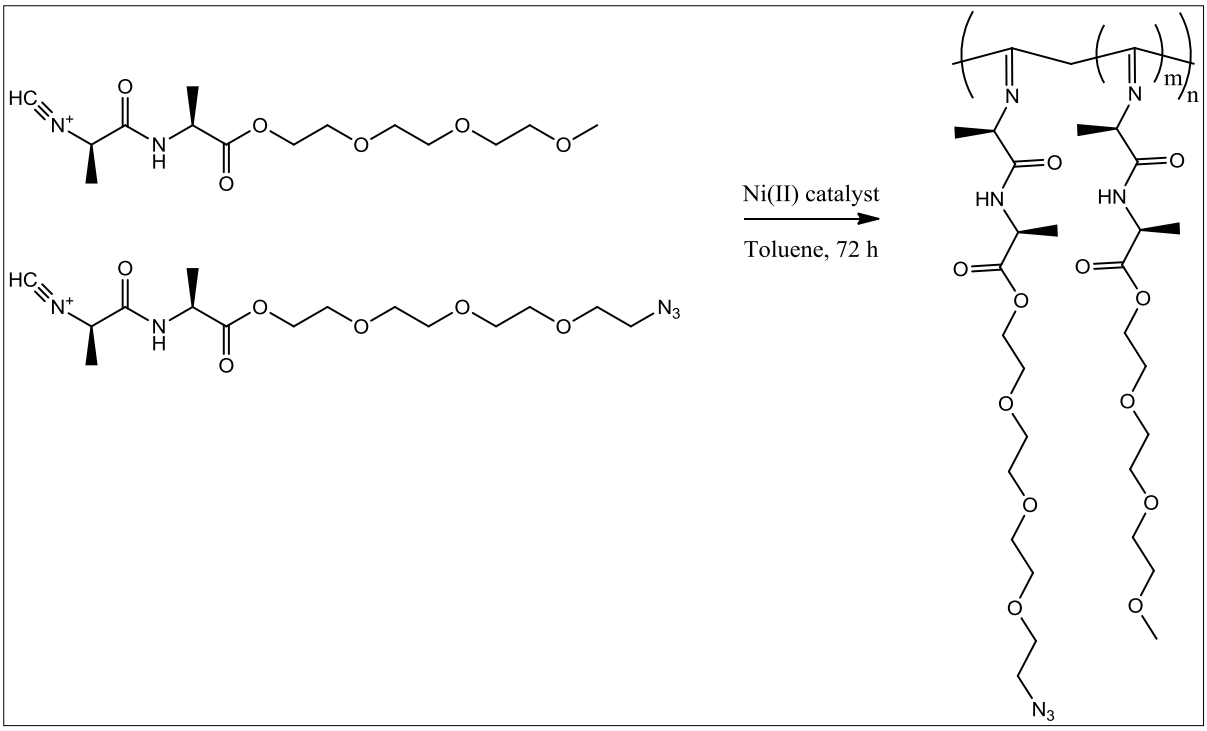

Scheme 2.2 The Ni(II) catalysed random copolymerisation of the isocyanopeptide monomers investigated in the current study.

2.6 Polyisocyanopeptide Hydrogels

The substituents on the polymer backbone are considered to resemble individual β-strands, and the overall arrangement of the polymer is then regarded as having a β-sheet-like organisation.[66] Due to each carbon in the backbone having a substituent, a restricted rotation around the backbone is seen, which then leads to a stiff polymer chain.[67] This stiffness and the chirality of the side chain lead to stereoisomerism (atropisomerism) in the backbone of the polymer. Therefore, it was proposed by Millich, on the basis of molecular models, that these dipeptide polymers adopt a $\sim 4_1$ (approximately four repeat units per turn) helical conformation.[68] This proposed conformation was supported by chromatographic evidence carried out by Nolte and co-workers, whereby an achiral *tert*-butyl isocyanide polymer was resolved into two antipodes. This optical activity could only exist due to the helical conformation of the backbone of the polymer.[68] It was further found that this conformation, in aqueous medium and in gel phase, was stable at elevated temperatures, of 70 °C.[69] The $\sim 4_1$ helical conformation of the polymer can be viewed as a 'polymeric spring'. The stretching of this spring causes the carbon backbone to elongate and the rods to

shorten in diameter. In NMR studies of the polymers, a helical pitch of 4.5 Å has been reported. Furthermore, an average spacing of 4.7 Å between one monomer side chain, *n*, and the next, parallel monomer side chain, (*n* + *4*) was measured.[66] Moreover, studies using atomic force microscopy (AFM) were done in order to visualise the stiffness of the dipeptide polymer chains. In these studies, it was possible to visualise the individual molecules with lengths of up to 200 nm. It has recently been revealed that the adopted 'spring conformation' is the lowest energy conformation. This is especially true when the substituents on the side groups of the backbone are bulky.[68] Conversely, when smaller side chain substituents are present, the helix slowly uncoils when the polymer is allowed to stand in solution.[66] Thus, the stability of the helical secondary structure is dependent on the bulkiness of the side groups,[67] as well as the substituent's ability to form intramolecular hydrogen bonds between the side chains.[68]

Due to the occurrence of hydrogen bonding, polyisocyanopeptides are very rigid polymers.[68] It has been noted that it is possible to 'denature' these helical structures in a manner similar to the denaturation of proteins, whereby the hydrogen interactions are disturbed by exposing the polymers to a strong acid, by increasing the temperature, or by stretching the bonds to such an extent that they break.[7,66,70] Thus, it is possible to fine-tune the polymers' architecture and properties by manipulating the network of hydrogen bonding interactions.[66] The helical structure of the polyisocyanides has been studied using circular dichroism (CD) spectroscopy by monitoring the n-π^* transition, at 250-350 nm, of the imine functionality attached to the backbone of the polymers.[69] The Cotton effect of the n- π^* transition is influenced by contributions from the side-chains on the backbone. Thus, the determination of the helical sense of the polymer is slightly prejudiced. It is interesting to note that the hydrogen bonding can be reflected in the Cotton effect of the CD spectrum of the polymers, and the denaturation of these interactions can be visualised by changes in the spectrum. Hence, these spectra can be used as a tool for studying the hydrogen bonding and the denaturation of the polymers.[7]

The twist sense of the helical backbone, *i.e*. left-handed (M) or right-handed (P), can be manipulated by controlling the stereochemistry of chiral monomer side chains used, or by using an optically active Ni(II) catalyst.[66,67] For example, the kinetically controlled, Ni(II)-catalysed polymerisation of the *L*-Alanine monomer causes all *L*-

alanine-based polymers to have the same stereochemistry.[7] It has been seen that polyisocyanides derived from *L*-*D*-di-alanine (*L,D,*-PIAA) are more stable than those from *L*-*L*-di-alanine (*L,L*-PIAA). This is due to the unfavourable steric interactions in the latter polymer, caused by the second alanine methyl group being in van der Waal contact with the methyl group of the first alanine moiety. In the former polymer, this interaction is absent due to the positions of the proton and the methyl group swapping in the *L*,*D*-di-alanine monomer, causing the greater stability of the polymer. This differs from the *L*,*L*-di-alanine monomer. Due to this stability, it was seen that it is possible to polymerise *L*,*D*-di-alanine monomers in the absence of the Ni(II) catalyst to produce chiroptical polymers similar to the ones formed through the catalysed polymerisation.[7,66] Clearly, subtle changes in the configuration of the side-chains of the backbones, due to steric interactions and hydrogen bonding, are able to influence the formation of these polymers.[7]

There is a large variety of possible polyisocyanides that can be synthesised, all with different characteristics. This is due to the different combinations of natural and unnatural amino acids that can be polymerised.[71] Additionally, these polymers can be varied further with a diverse range of side chains and pendent functional groups, including nonlinear optical chromophores, which can be attached to these stable and robust backbone peptides.[71] One example of these polyisocyanopeptides is a charged block polymer, which consists of styrene and an optically active isocyanodipeptide, isocyano-*L*-*L*-di-alanine or isocyano-*L*-alanine-*L*-histidine. These superamphiphilic diblock copolymers were the pioneers in forming chiral superstructures with chiral nano-architecture in aqueous solution, in similar manner to low-molecular weight surfactants. The helical structures of these polymers are based on the chirality of the side chains of the monomers. As in the above mentioned isocyanopeptide polymers, the helical structure of these diblock-copolymers is due to interactions caused by the sterically bulky side-chains attached to the backbone of the polymer, which are then stabilised by the hydrogen interactions between the parallel side-chains initiated by the amide functionality of the amino acids, as shown through infrared spectroscopy.[72] These helical polymers have applications within material science and catalysis.[72]

It has recently been claimed that polyisocyanopeptides functionalised with oligo(ethylene glycol) side chains are able to, in almost every way, mimic the ECM

of cells.[69] With this in mind, the current study will focus on the particular polyisocyanopeptides.

2.6.1 Polyisocyanides with oligo(ethylene glycol) side chains

The incorporation of the PEG side chains onto polymers has been noted in various studies, *e.g*. in polystyrene[73] and poly(methacrylates).[73-75] The interest in PEG-functionalised polymers is due to their water solubility, as well as their inert nature and biocompatibility.[76] The balance between hydrophilic and hydrophobic units allows for a control over the solubility of the polymer. It has been shown that the hydrophilicity of PEG is dependent on temperature, through a sharp order-disorder phase transition at the LSCT.[69] Thus, when incorporated, it allows for a thermo-responsive polymeric system.[77,78] These styrene- and methacrylate-derived PEG polymers are highly flexible, and when heated above their thermal transition temperature, in aqueous solution, they are seen to coil or globulate.[79] Methacrylate derived PEG analogues can be classed as reference point for these PEG-derived macromolecules, due to the fact that they are so well studied.[76] Its phase transition has been seen to be fast and independent of external factors or the degree of polymerisation and their LCST are highly tunable. These properties have been accredited to the inability of the oligo(ethylene glycol) side chains to form inter- or intramolecular interactions, neither by hydrogen bonding nor covalent bonding. Due to the flexible backbones of these polymers, as well as the inert nature of the PEG-side chains, the polymers are unable to gel, even at high concentrations. Interestingly, when PEG side-chains were incorporated into poly(methacrylates) with linear or star-like conformations using initiators such as the example is seen in Figure 2.6 (top), it was possible to observe gelation with tunable transition temperatures for high concentrations of the polymers.[74,75] The gelation of these polymers is seen in Figure 2.6 (bottom).

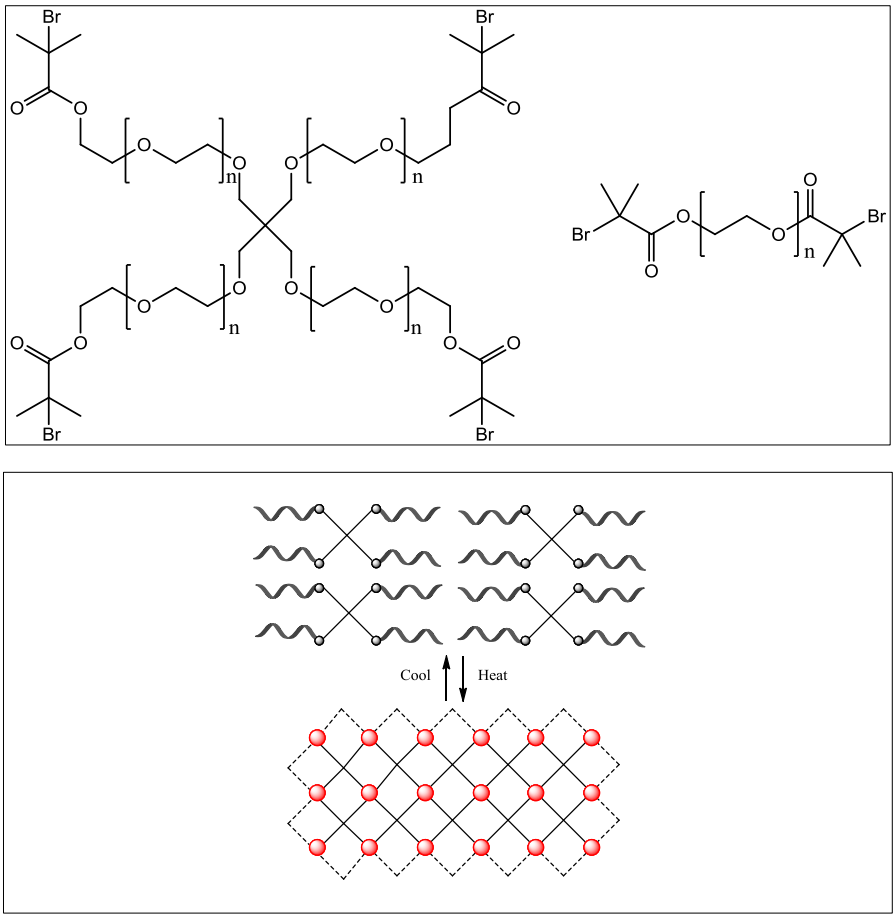

Figure 2.6 Top: An example of a four armed 'star-shaped' (left) and a linear (right) oligo(ethylene glycol) methyl ether methacrylate initiators. Bottom: A schematic representation of the thermal gelation of the 'star-shaped' poly(methacrylate) derived PEG analogues.[75]

Furthermore, Rowan *et al*. showed that the incorporation of these PEG side chains onto polyisocyanides, containing a rigid polymer backbone and a well-defined helical secondary structure, allows for a thermo-responsive polymer in aqueous solutions at very low concentrations (0.1 wt.%).[80] The ethylene glycol allows for the polymers to be soluble in aqueous medium. These polymers are able to mimic gels that are prepared from intermediate filaments in almost every aspect.[69] Until now, there have been no other synthetic polymers or low-molecular weight gels possessing the ability to display control over the mechanical responses, such as strain stiffening, as seen in gels of cytoskeletal proteins, such as actin, fibrin, intermediate filaments, collagen and microtubules. These proteins are able to self-assemble into helical structures and superstructures.[69] All parts of living systems require mechanical responsiveness,

from organs and tissues, and even individual cells. These polyisocyanopeptide hydrogels have been prepared through a Ni(II)-catalysed polymerisation, with different ratios of oligo(ethylene) glycol dipeptide monomers (see Scheme 2). The gelation of these poly(isocyanidopeptides) is due to the polymers self-assembling into supramolecular structures, *i.e*. superhelices, controlled by non-covalent interactions such as hydrogen bonding, van der Waal forces and hydrophobic effects.[66] Due to the linear relationship between transition temperature and the length of the ethylene glycol chain, the transition temperature of these polyisocyanides, from solution state to gel, can be adjusted according to the length of the oligoethylene group. The gelation transition temperature is 18 °C and 40 °C for triethylene and tetraethylene moieties, respectively.[69] By controlling the ratio of monomers containing tri- and tetraethylene groups in the polymer, it is possible to tune the transition temperature between these values.

It is possible to functionalise these polymers by copolymerisation with monomers containing pendant functional groups, such as azides, as seen in Scheme 2.2.[81] Once polymerisation has occurred, it is then possible to use ‘click’ chemistry to functionalise the polymer with peptide sequences.[82] The employment of copper-free ‘click’ chemistry will be discussed in Chapter 4.

The ease with which these polyisocyanopeptide hydrogels can be modified makes them highly versatile and useful in many different applications, especially in the biomedical field.[69] One noteworthy example of this is their use as effector molecules, which possess the ability to dock onto T cells, thereby causing the activation of these cells, as depicted in Figure 2.7.[83]

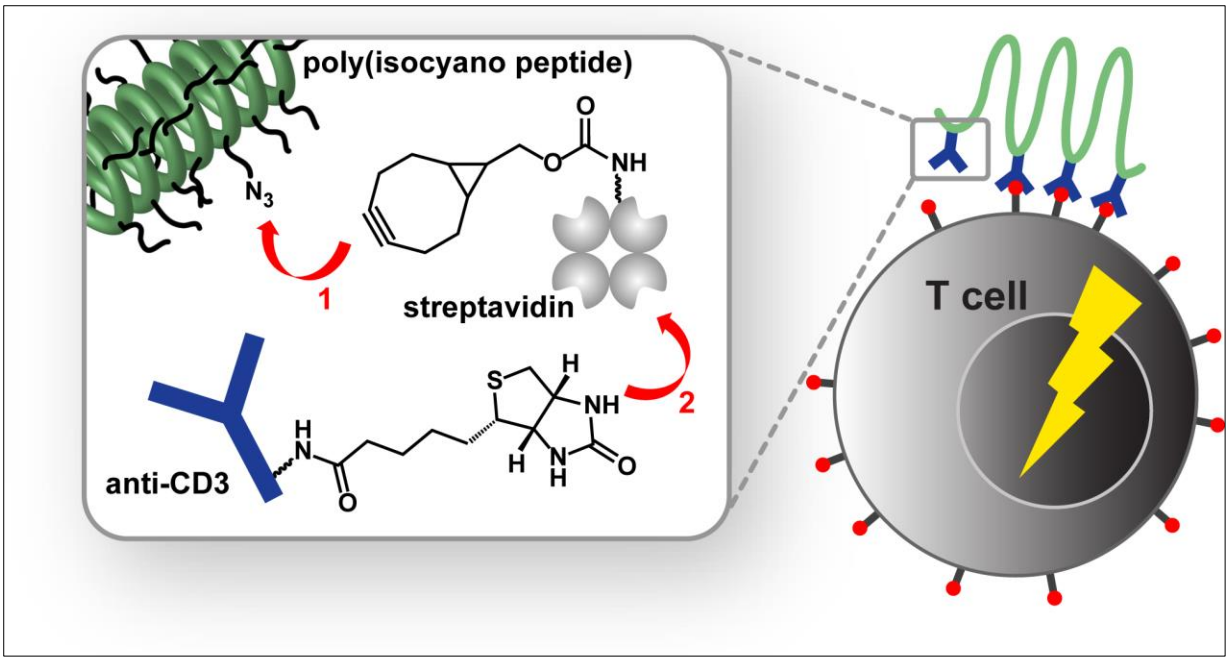

Figure 2.7 Polyisocyanides grafted with oligo(ethylene glycol) side chains and functionalised with antibodies act as synthetic dendritic cells, causing activation of the T cell. [83]

As with other polyisocyanopeptides, hydrogen bonding occurs between the alanine moieties on parallel side chains. The interaction forms between the amide on the alanine (**Ala 1**) closest to the oligoethylene group, and the oxygen on the alanine (**Ala 2**) closest to the carbon backbone, as seen in Figure 2.8.[67] This causes the polymers to have a stiff, helical structure, as shown in other isocyanopeptides.[69] CD and IR experiments confirmed the helical structure of these polymers, as well as the gel's conformational stability, up to 70 °C.[69]

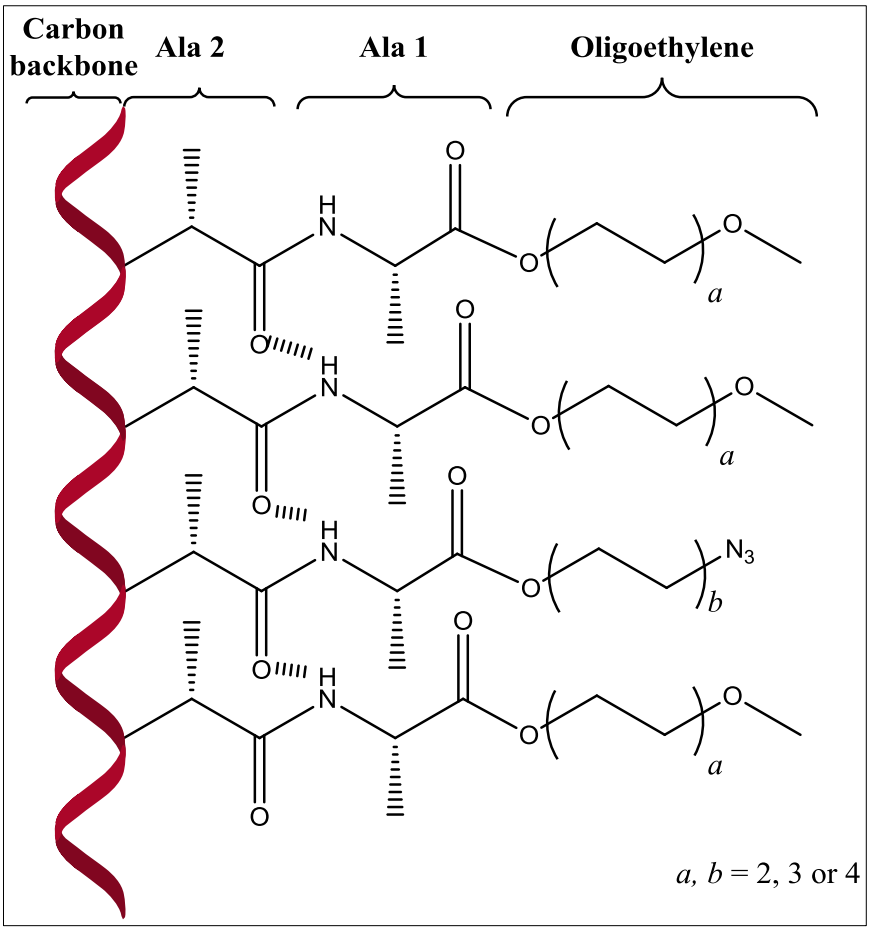

Figure 2.8 The helical polyisocyanopeptide hydrogel with hydrogen bonding occurring between the alanine moieties of the side chains.

Due to the ease with which these intermediate filament-mimicking hydrogels can be manipulated, the potential applications for these polymers are virtually limitless.[69] Therefore, the objective of this study is to synthesise the isocyanide monomers needed for the polymerisation of polyisocyanides grafted with oligoethylene glycol chains. Thereafter, the polymers will be functionalised with the **IKVAV**-laminin-derived epitope. Based on previous scaffolds used for the epitope, this polymer may possess the potential to direct the differentiation of stem cells into neurons. If successful, these results would pioneer a new class of tissue-engineering scaffolds for the treatment of neurological disorders.

2.7 References

(1) Griffith, L. G. *Ann NY Acad Sci* **2002**, *961*, 83.
(2) Putnam, A. J.; Mooney, D. J. *Nat Med* **1996**, *7*, 824.
(3) Vacanti, J. P.; Langer, R.; Upton, J.; Marler, J. J. *Adv Drug Deliv Rev* **1998**, *33*, 165.
(4) Brandl, F.; Sommer, F.; Goepferich, A. *Biomaterials* **2007**, *28*, 134.
(5) Lutolf, M. P.; Hubbel, J. A. *Nat Biotechnol* **2005**, *23*, 47.
(6) Discher, D. E.; Janmey, P.; Wang, Y.-l. *Science* **2005**, *310*, 1139.
(7) Tibbitt, M. W.; K.S., A. *Biotechnol Bioeng* **2009**, *103*, 655.
(8) Carletti, E.; Motta, A.; Migliaresi, C. *Methods Mol Biol.* **2011**, *695*, 17.
(9) Chan, B. P.; Leong, K. W. *Eur Spine J* **2008**, *4*, 467.
(10) O'Brien, F. J. *Materials Today* **2011**, *14*, 88.
(11) Hahn, M. S.; Miller, J. S.; West, J. L. *Adv Mat* **2006**, *18*, 2679.
(12) Lee, K. Y.; Mooney, D. J. *Chem Rev* **2001**, *101*, 1869.
(13) Shin, H.; Jo, S.; Mikos, A. G. *Biomaterials* **2003**, *24*, 4353.
(14) Silva, E. A.; Mooney, D. J. In *Curr Top Dev Biol*; Academic Press: 2004; Vol. 64, p 181.
(15) Le Beyec, J.; Xu, R.; Lee, S.; Nelson, C. M.; Rizki, A.; Alcaraz, J.; Bissell, M. J. *Exp Cell Res* **2007**, *313*, 3066.
(16) Hubbell, J. A. *Curr Opin Biotech* **2003**, *14*, 551.
(17) Jaiswal, N.; Haynesworth, S. E.; Caplan, A. I.; Bruder, S. P. *J Cell Biochem* **1997**, *64*, 295.
(18) Petersen, O. W.; Ronnov-Jessen, L.; Howlett, A. R.; Bissell, M. J. *Proc Nati Acad Sci* **1992**, *89*, 9064.
(19) Zhanga, S.; Gelainb, F.; Zhaoc, X. *Semin Cancer Biol* **2005**, *15*, 413.
(20) Gieni, R. S.; Hendzel, M. J. *J Cell Biochem* **2008**, *104*, 1964.
(21) Serban, M. A.; Liu, Y.; Prestwich, G. D. *Acta Biomat* **2008**, *4*, 67.
(22) Hosseinkhani, H.; Hiraoka, Y.; Li, C.; Chen, Y.; Yu, D.; Hong, P.; Ou, K. *ACS Chem Neurosci* **2013**, *4*, 1229.
(23) Wong, J. Y.; Leach, J. B.; Brown, X. Q. *Surf Sci* **2004**, *570*, 119.
(24) Panda, J. J.; Dua, R.; Mishra, A.; Mittra, B.; Chauhan, V. S. *Appl Mater Interfaces* **2010**, *2*, 2839.
(25) Liu, W. F.; Chen, C. S. *Mater Today* **2005**, *8*, 28.
(26) Christman, K. L.; Vardanian, A. J.; Fang, Q.; Sievers, R. E.; Fok, H. H.; Lee, R. J. *J Am Coll Cardiol* **2004**, *44*, 654.
(27) Hou, Q.; De Bank, P. A.; Shakesheff, K. M. *J Mat Chem* **2004**, *14*, 1915.
(28) Nune, M.; Kumaraswamy, P.; Krishnan, U. M.; Sethuraman, S. *Curr Protein Pept Sc* **2013**, 70.
(29) Zhang, S. *Mater Today* **2003**, 20.
(30) Mikos, A. G.; McIntire, L. V.; Anderson, J. M.; Babensee, J. E. *Adv Drug Deliv Rev* **1998**, *3*, 111.
(31) Matson, J. B.; Stupp, S. I. *Chem Commun* **2012**, *48*, 26.

(32) Mikos, A. G.; Lyman, M. D.; Freed, L. E.; Langer, R. *Biomaterials* **1994**, *15*, 55.
(33) Silva, G. A.; Czeisler, C.; Niece, K. L.; Beniash, E.; Harrington, D. A.; Kessler, J. A.; Stupp, S. I. *Science* **2004**, *303*, 1352.
(34) Langer, R.; Vacanti, J. P. *Science* **1993**, *260*, 920.
(35) Kunitake, T. *Angew Chem Int Edit* **1992**, *31*, 709.
(36) Lin, X.; Takahashi, K.; Liu, Y.; Zamora, P. O. *Biochim Biophys Acta* **2006**, *1760*, 1403.
(37) Zhang, Z. X.; Zheng, Q. X.; Wu, Y. C.; Hao, D. J. *Biotechnol Bioproc E* **2010**, *15*, 545.
(38) Cheng, T.; Chen, M.; Chang, W.; Huang, M.; Wang, T. *Biomaterials* **2012**, *34*, 2005.
(39) Velichko, Y. S.; Stupp, S. I.; de la Cruz, M. O. *J Phys Chem B* **2008**, *112*, 2326.
(40) Cui, H.; Webber, M. J.; Stupp, S. I. *Peptide Sci* **2009**, *94*, 1.
(41) Niece, K. L.; Hartgerink, J. D.; Donners, J. J. J. M.; Stupp, S. I. *J Am Chem Soc* **2003**, *125*, 7146.
(42) Capito, R. M.; Azevedo, H. S.; Velichko, Y. S.; Mata, A.; Stupp, S. I. *Science* **2008**, *319*, 1812.
(43) Behanna, H. A.; Donners, J. J. J. M.; Gordon, A. C.; Stupp, S. I. *J Am Chem Soc* **2005**, *127*, 1193.
(44) Niece, K. L.; Hartgerink, J. D.; Donners, J. J. J. M.; Stupp, S. I. *J Am Chem Soc* **2003**, *125*, 7146.
(45) Hartgerink, J. D.; Beniash, E.; Stupp, S. I. *Science* **2001**, *294*, 1684.
(46) Hartgerink, J. D.; Beniash, E.; Stupp, S. I. *P Nat A Sci* **2002**, *99*, 5133.
(47) Rajangam, K.; Behanna, H. A.; Hui, M. J.; Han, X.; Hulvat, J. F.; Lomasney, J. W.; Stupp, S. I. *Nano Letters* **2006**, *6*, 2086.
(48) Carvajal, D.; Bitton, R.; Mantei, J. R.; Velichko, Y. S.; Stupp, S. I.; Shull, K. R. *Soft Matter* **2010**, *6*, 1816.
(49) Bitton, R.; Chow, L. W.; Zha, R. H.; Velichko, Y. S.; Pashuck, E. T.; Stupp, S. I. *Small* **2014**, *10*, 500.
(50) Zhang, S.; Holmes, T.; Lockshin, C.; Rich, A. *P Natl Acad Sci* **1993**, *90*, 3334.
(51) Yang, Z.; Liang, G.; Wang, L.; Xu, B. *J Am Chem Soc* **2006**, *128*, 3038.
(52) Song, Y.; Zheng, Q.; Guo, X.; Zheng, J. *J Wuhan Univ Technol* **2009**, *24*, 753.
(53) Lévesque, S. G.; Shoichet, M. S. *Biomaterials* **2006**, *27*, 5277.
(54) Anseth, K. S.; Bowman, C. N.; Brannon-Peppas, L. *Biomaterials* **1996**, *17*, 1647.
(55) Hoffman, A. S. *Adv Drug Delivery Rev* **2002**, *54* 3.
(56) Yan, H.; Saiani, A.; Gough, J. E.; Miller, A. F. *Biomacromolecules* **2006**, *7*, 2776.
(57) Hutmacher, D. W. *J Biomat Sci - Polym E* **2001**, *12*, 107.
(58) Hu, J. C.; Athanasiou, K. A. *Biomaterials* **2005**, *26*, 2001.

(59) Kazakia, G. J.; Nauman, E. A.; Ebenstein, D. M.; Halloran, B. P.; Keaveny, T. M. *J Biomed Mater Res A* **2006**, 688.
(60) Mann, B. K. In *The second Joint EMBS/BMES conference* Houston, Texas, 2002, p 695.
(61) Bellamkonda, R.; Ranieri, J. P.; Aebischer, P. *J Neurosci Res* **1995**, *41*, 501.
(62) Kubinová, S.; Horák, D.; Kozubenko, N.; Vanecek, V.; Proks, V.; Price, J.; Cocks, G.; Syková, E. *Biomaterials* **2010**, *31*, 5966.
(63) Yu, L. M.; Kazazian, K.; S., S. M. *J Biomed Mater Res A.* **2007**, *82*, 243.
(64) Itoh, S.; Suzuki, M.; Yamaguchi, I.; Takakuda, K.; Kobayashi, H.; Shinomiya, K.; Tanaka, J. *Artif Organs* **2003**, *27*, 1079.
(65) Wei, Y. T.; Tian, W. M.; Yu, X.; Cui, F. Z.; Hou, S. P.; Xu, Q. Y.; Lee, I. *Biomed mater* **2007**, *2*, 142.
(66) Cornelissen, J. J. L. M.; Donners, J. J. J. M.; de Gelder, R.; Graswinckel, W. S.; Metselaar, G. A.; A.E., R.; Sommerdijk, N. A. J. M.; Nolte, R. J. M. *Science* **2001**, *293*, 676.
(67) Cornelissen, J. J. L. M.; Sommerdijk, N. A. J. M.; Nolte, R. J. M. *Macromol Chem Physic* **2002**, *202*, 1625.
(68) Cornelissen, J. J. L. M.; Graswinckel, W. S.; Rowan, A. E.; Sommerdijk, N. A. J. M.; Nolte, R. J. M. *J Poly Sci* **2003**, *41*, 1725.
(69) Kouwer, P. H. J.; Koepf, M.; Le Sage, V. A. A.; Jaspers, M.; van Buul, A. M.; Eksteen-Akeroyd, Z. H.; Woltinge, T.; Schwartz, E.; Kitto, H. J.; Hoogenboom, R.; Picken, S. J.; Nolte, R. J. M.; Mendes, E.; Rowan, A. E. *Nature* **2013**, *493*, 651.
(70) van Buul, A. M.; Schwartz, E.; Brocorens, P.; Koepf, M.; Beljonne, D.; Maan, J. C.; Christianen, P. C. M.; Kouwer, P. H. J.; Nolte, R. J. M.; Engelkamp, H.; Blank, K.; Rowan, A. E. *Chem Sci* **2013**, *4*, 2357.
(71) Schwartz, E.; Koepf, M.; Kitto, H. J.; Nolte, R. J. M.; Rowan, A. E. *Polym Chem* **2011**, *2*, 33.
(72) Cornelissen, J. J. L. M.; Fischer, M.; Sommerdijk, N. A. J. M.; Nolte, R. J. M. *Science* **1998**, *280*, 1427.
(73) Wang, X. S.; Armes, S. P. *Macromolecules* **2000**, *33*, 6640.
(74) Badi, N.; Lutz, J.-F. *J Controlled Release* **2009**, *140*, 224.
(75) Fechler, N.; Badi, N.; Schade, K.; Pfeifer, S.; Lutz, J.-F. *Macromolecules* **2008**, *42*, 33.
(76) Koepf, M.; Kitto, H. J.; Schwartz, E.; Kouwer, P. H. J.; Nolte, R. J. M.; Rowan, A. E. *Eur Polym J* **2013**, *49*, 1510.
(77) Neugebauer, D. *Polym Int* **2007**, *56*, 1469.
(78) Lutz, J. *Adv Mater* **2011**, *23*, 2237.
(79) Lutz, J.-F.; Weichenhan, K.; Akdemir, Ö.; Hoth, A. *Macromolecules* **2007**, *40*, 2503.
(80) Rowan, E. A.; Nolte, R. J. M.; Conrelissen, J. J. L. M.; Kitto, H. J.; Schwartz, E.; Koepf, M. The Netherlands, 2011.

(81) Kitto, H. J.; Schwartz, E.; Nijemeisland, M.; Koepf, M.; Cornelissen, J. J. L. M.; Rowan, A. E.; Nolte, R. J. M. *J Mater Chem* **2008**, *18*, 5615.
(82) Rostovtsev, V. V.; Green, L. G.; Fokin, V. V.; Sharpless, K. B. *Angew Chem Int Ed* **2002**, *41*, 2596.
(83) Mandal, S.; Eksteen-Akeroyd, Z. H.; Jacobs, M. J.; Hammink, R.; Koepf, M.; Lambeck, A. J. A.; van Hest, J. C. M.; Wilson, C. J.; Blank, K.; Figdo, C. G.; Rowan, A. E. *Chem Sci* **2013**, *4*, 4168.

Chapter 3: Monomer Synthesis and Characterisation

Abstract

In this study, the functional 'azide monomer' for copolymerisation of polyisocyano-peptides with oligo(ethylene glycol) side chains was synthesised using an altered version of the protocol previously reported.[1] The monomers were characterised by ^{1}H NMR and ^{13}C NMR spectroscopy, IR spectroscopy and mass spectrometry.

3.1 Introduction

Polyisocyanopeptide hydrogels decorated with oligo(ethylene glycol) side chains have previously been synthesised by the Rowan group.[2] The bulk of the polymer is made up of the spacer monomer, seen in '**a**' of Figure 3.1. This monomer can either have a tri- or tetraethylene glycol side chain, and the length of this side chain controls the gelation temperature of the polymer. It is also possible to copolymerise the spacer monomer with azide-functional monomers ('azide monomer'), as seen in '**b**' of Figure 3.1. The pendant azide functionality on the polymer can later be modified through (copper-free) click chemistry, as will be elaborated on in Chapter 4.

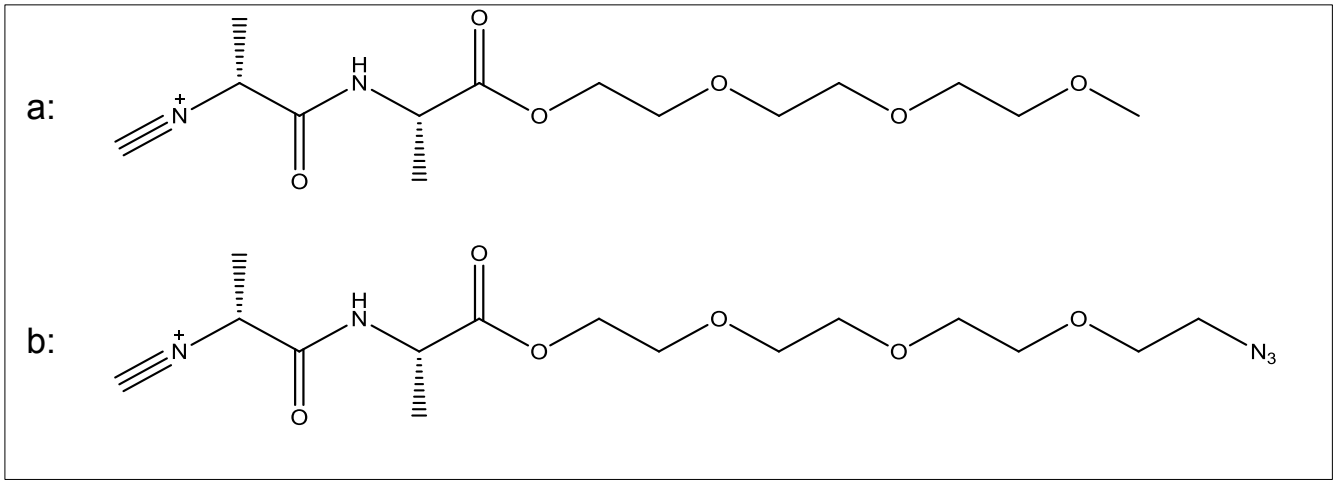

Figure 3.1 The structures of the monomers used to make the polyisocyanopeptides in this study where, a) is the 'spacer monomer' and b) is the azide monomer

In the general protocol for the synthesis of the monomers, seen in Scheme 3.1, the alanine moieties are coupled to the glycol through two consecutive *N,N*'-dicyclohexylcarbodiimide (DCC) or 1-ethyl-3-(3-dimethylaminopropyl)carbodiimide (EDC) mediated coupling reactions. For this reaction, the amine functionality of the alanine is protected by a *tert*-butyloxycarbonyl (*Boc*) protecting group, which can be readily removed after each coupling, using hydrochloric acid in dioxane. The second *Boc*-Alanine is then coupled and de-protected in a manner similar to the first coupling. Thereafter the amine is converted to a formyl group, which is then dehydrated to a cyano functional group using methyl *N*-carbamate (Burgess reagent).

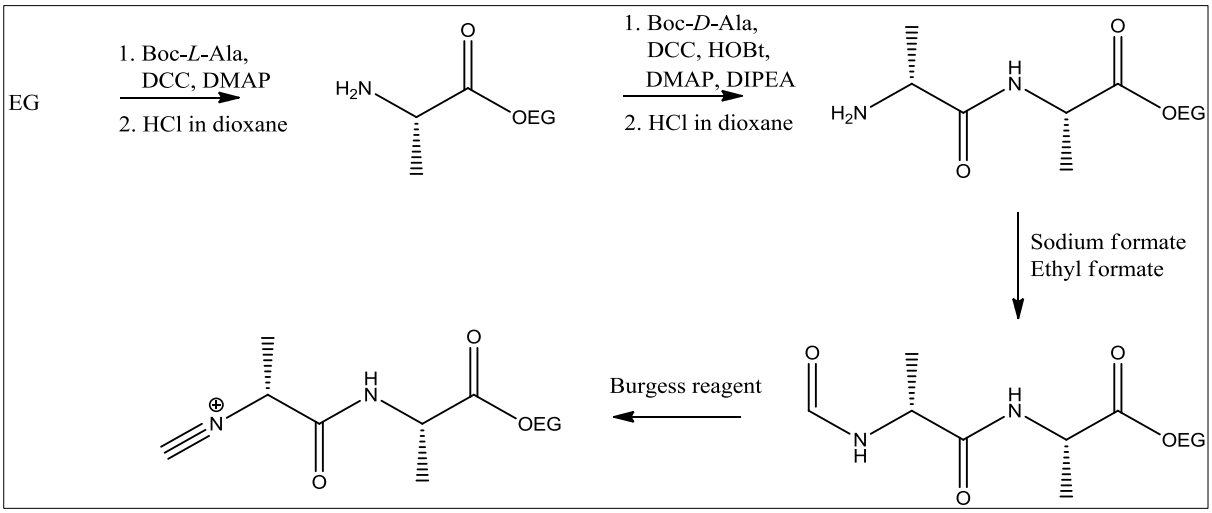

Scheme 3.1 General protocol used in the synthesis of isocyanide monomers

It is very important to ensure that no racemisation of the stereochemistry of the alanine moieties occurs during either of the two coupling reactions, more so during the second coupling step. It is ensured by using HOBt in the reaction mixture, which also serves to improve the efficiency of the peptide synthesis.

In this chapter, the aim was to synthesise an azide monomer with a tetraethylene glycol side chain. This azide monomer can then be copolymerised with the spacer monomer, which was purchased from Chiralix. It has been seen that the gelation temperature is controlled by the length of the ethylene glycol side chain, where triethylene glycol side chains result in a gelation temperature of 18 °C and

tetraethylene glycol side chains produce hydrogels with a gelation temperature of 40 °C. During polymerisation of the two monomers, the spacer monomer will ensure that the gelation temperature of the polymer is approximately 18 °C, which means that the polymer will be a gel at physiological conditions. By manipulating the fraction of the azide monomer in the copolymerization mixture, we could control the gelation temperature of the eventual polymer hydrogel.

3.2 Results and Discussion

A number of routes were undertaken in attempts to synthesise the azide monomer. Scheme 3.2, depicts a previously reported synthetic route towards the azide monomer.[1] It follows a similar protocol to that described under the general method (see Section 3.1), in which a tosylated tetraethylene glycol is first coupled to the two alanine moieties, yielding **4** (see Scheme 3.2). Thereafter, the protocol follows a different path from the spacer monomer to that described in literature,[2] as the tosyl-group undergoes nucleophilic attack by sodium azide to yield the azide functionality. Subsequently, the amine is then converted to a formyl and then dehydrated into the isocyanide group.

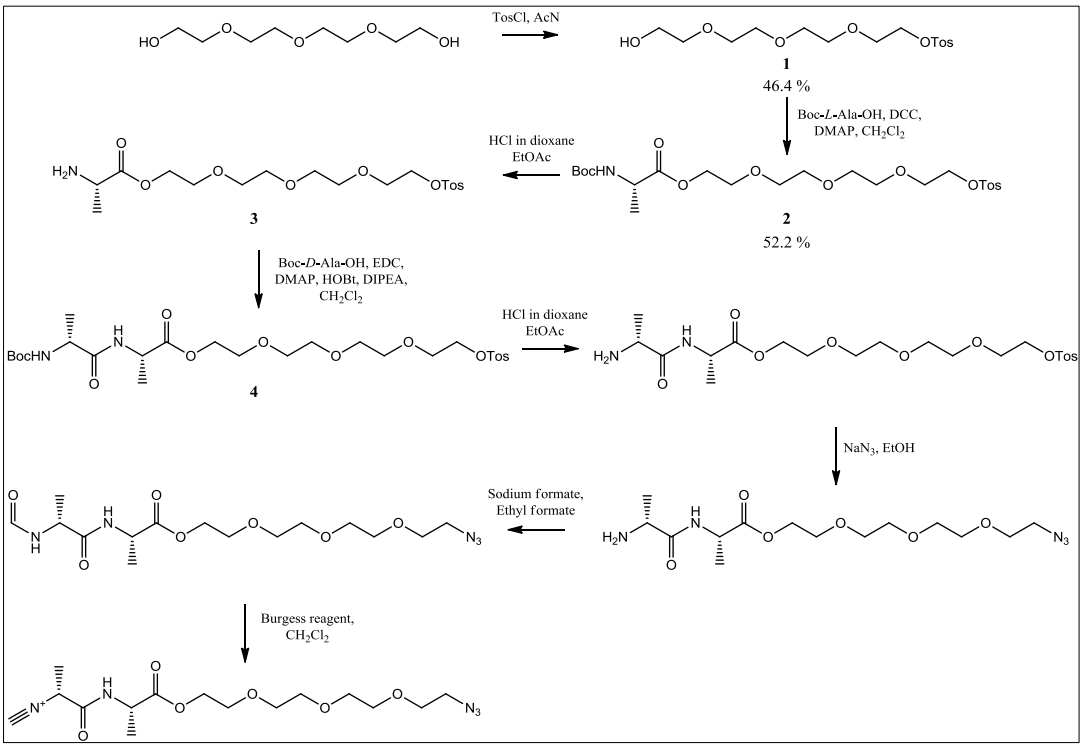

Scheme 3.2 The complete synthesis of HCN^{+}-D-Ala-L-Ala-$(PEG)_4$-N_3 using the method described by Rowan et al.[1]

The product from the second coupling step, compound **4** (Scheme 3.2), proved difficult to purify using column chromatography, as described in literature. Although, thin-layer chromatography (TLC) analysis, using 10 % methanol in dichloromethane as an eluent, showed a compound at the R_f reported in literature, that particular compound could not be isolated after running the crude product through the silica column. It is possible that the compound degraded on the column. Therefore, prep-HPLC was used in an attempt to purify the crude product.

First, the crude product was analysed using analytical HPLC to determine which peak correlates to the desired product, **4** (Scheme 3.2). The chromatogram (shown in Figure 3.2) showed that there were many impurities in the sample, which was expected for a crude product. As shown in Figure 3.2, a peak with a parent m/z of 591.23 eluted at 4.8 minutes (taking the 0.1 min delay between diode array detector (DAD) and MS into account). This m/z, seen in the insert of Figure 3.2, corresponds to the M^{+1} of **4**, and therefore this peak was targeted.

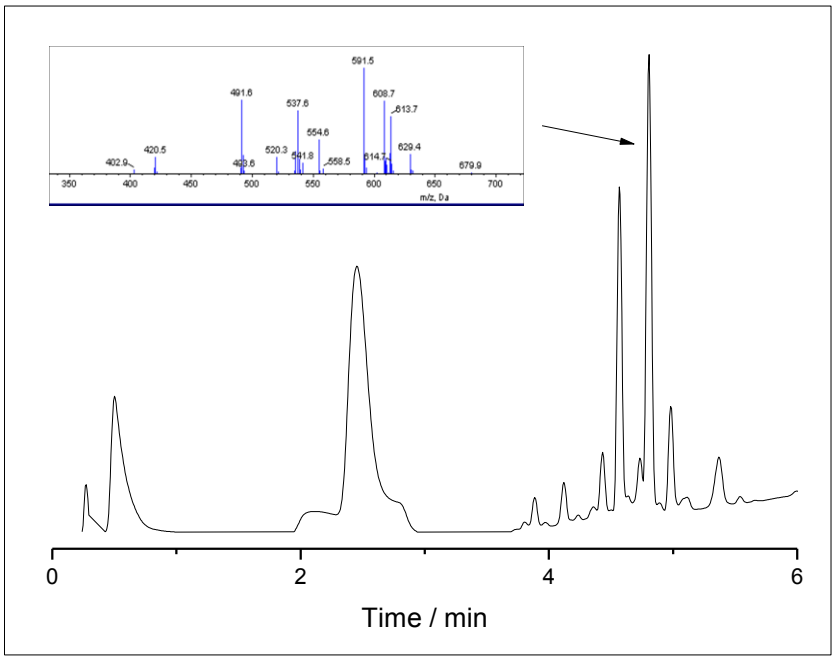

Figure 3.2 The analytical HPLC chromatograph of the crude product, whereby the arrow points to a product in which the MS results show a parent m/z peak correlating to the M^{+1} (591.5 Da) of 4. The mass spectrum for this peak is seen in the insert.

The isolation of the compound that eluted at 4.8 minutes, Figure 3.3, allowed for NMR analysis of the compound, shown in Figure 3.4. From the ^{1}H NMR spectrum, it is possible to see that the isolated compound is not the desired product. This is clear from the peaks in the aromatic region (7 – 8.2 ppm), which should show only two doublets, each with integrations of 2H. Instead, the NMR spectrum is a conglomeration of many peaks that cannot be assigned to what should be a completely pure compound. It is possible that **4** rearranged itself through intramolecular hydrogen bonds between the PEG end chain and the alanine moieties. This will be discussed later in this chapter.

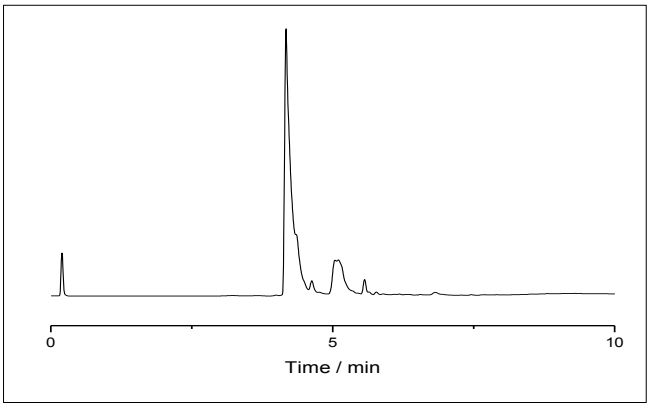

Figure 3.3 HPLC-DAD analysis of the purified peak

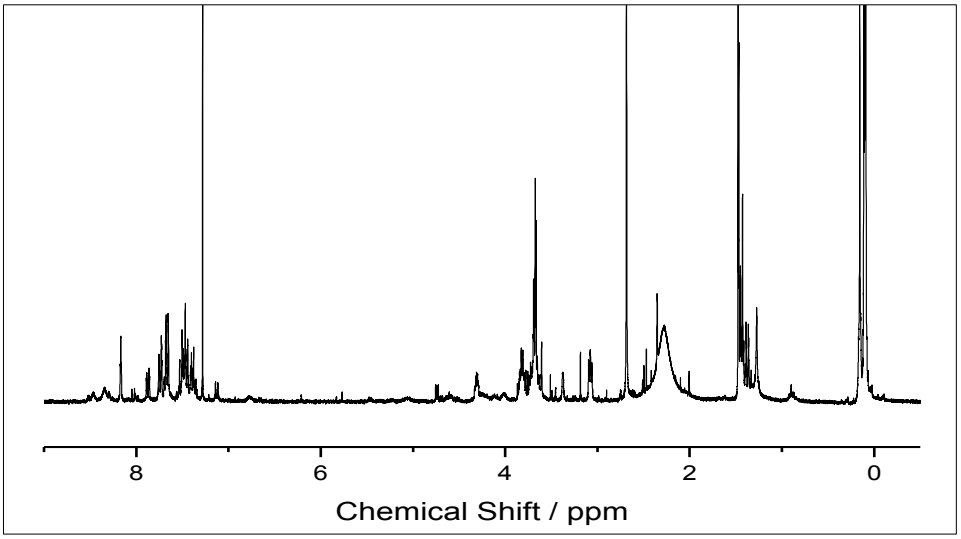

Figure 3.4 ^{1}H NMR spectrum of the product, isolated from prep-HPLC, that eluted at 4.8 min

It seemed curious that the synthesis of the spacer monomer, where the product from the second coupling step is chemically similar to **4**, was performed without problems. The only structural difference between the two was the end-groups of the PEG chains. Therefore, it was hypothesised that the tosyl group could be the issue. A new method, as seen in Scheme 3.1, was attempted, whereby the two alanine moieties were first coupled and then added to the PEG moiety. This was done rather than sequentially coupling the alanine moieties to the PEG chain, one after the other. This methodology of coupling the alanine moieties together has been used in synthesising polyisocyanopeptides in the past by Nolte *et al*.[3] One problem identified with this method is that protected amino acids can undergo racemisation.[4,5] Thus, it would be essential to test the final unprotected dipeptide's optical rotation, and compare the results to the values obtained by Nolte *et al*.[3] According to Reetz,[4] racemisation is minimized if only cold solvents are used and the α-amino acids are freshly prepared.

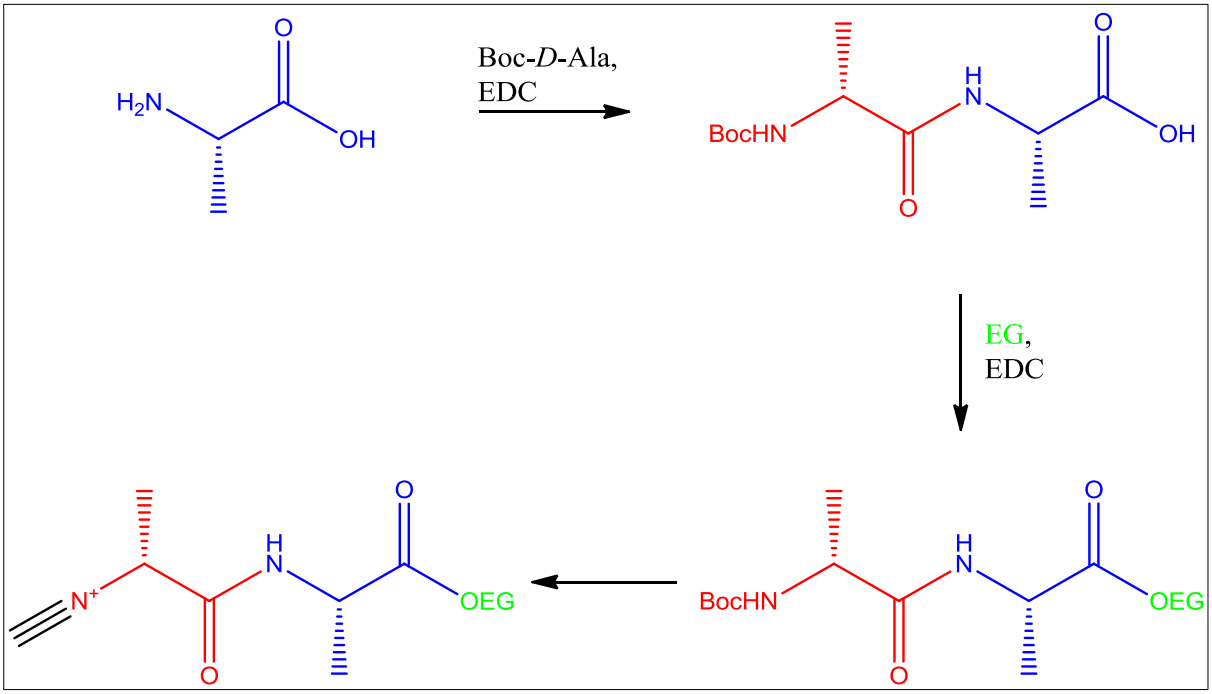

Scheme 3.3 A general outline of the second method that was attempted in the synthesis of the azide monomer.

To obtain a stereochemically pure dipeptide and avoid self-condensation, it was necessary to protect the carboxylic acid of the *L*-alanine with a protecting group that can be removed selectively without removing the *Boc*-protection group, before coupling the dipeptide to the PEG. The best protecting groups are readily installed and removed quantitatively, under mild conditions, without forming byproducts that are difficult to separate from the product. Another important requirement of the protecting group is that it must not influence the reactivity of the adjacent functional groups of the amino acid. The most common form of carboxy-protection for amino acids is esterification. Therefore, the synthetic protocol in Scheme 3.4 was attempted. In this protocol, the *L*-Alanine-OH was protected as a methyl ester. This protection was attempted using the method described by Avinash and Govindaraju,[6] which entailed purifying the product by recrystallization, however, this was unsuccessful. Therefore, commercial *L*-Ala-OMe·HCl was used instead. Thereafter, an EDC-mediated coupling reaction was used to obtain **7a**.

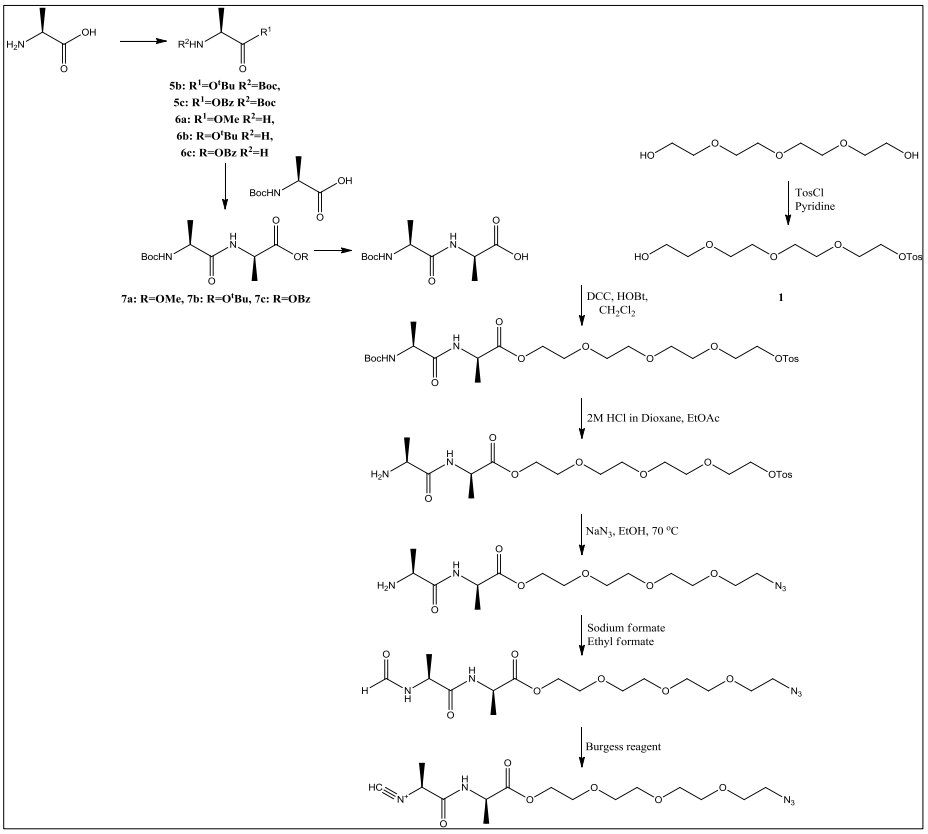

Scheme 3.4 Synthesis of the azide monomer using method 2 whereby the dipeptide was first synthesised and thereafter coupled to the tetraethylene glycol moiety

The deprotection of **7a** was attempted in a number of ways, following methods described by Casida *et al*.,[7] Joullié *et al*.,[8] and Prabhakaran.[9] However, all were deemed unsuccessful as proven through NMR and MS analyses. Shortcomings in using methyl ester protection groups have been reported previously.[5] The use of other protecting groups was studied due to the difficulty in de-protecting the methoxy ester protecting group without de-protecting the *Boc*-group. These included benzyl and *t*-butyl esters. If obtained, these compounds would have then followed the same protocol, in order to convert them into the azide-functionalised monomer, as seen in Scheme 3.4. *t*-Butyl esters have been widely used as carboxy-amino protecting groups due to their stability when exposed to bases, nucleophiles and catalytic hydrogenation. Benzyl ester protecting groups are the most widely used in solution chemistry.[10]

The method used to synthesise **5b** was described by Olsen *et al*.[11] This protocol, shown in Scheme 3.4, entailed reacting a *Boc*-protected amino acid with *t*-butyl alcohol in an EDC-mediated coupling reaction. The *Boc*-protection was then removed using the same method as in **3**, using hydrochloric acid to yield **6b** with a yield of 77 %. Thereafter, the coupling of the two alanine moieties followed the same method as described above for the methoxy ester protected alanine, with a yield of 48 % being obtained for **7b**. The de-protection of **7b**, following the method described by Yadav *et al*.[12] was unsuccessful. Literature reveals that the cleavage mechanism of *t*-butyl protecting groups is very similar to *Boc*-protecting groups. Thus, it is possible that the *Boc*-protecting group was affected during the cleavage step.[5] It was hoped that using a benzyl ester protecting group would allow for deprotection of the dipeptide without affecting the *Boc*-protection. Benzyl groups are widely used as protecting agents in organic chemistry due to their stability.[13] In previous work, it has been shown to be difficult to remove the benzyl protecting group, while not removing other protecting groups.[14] However, Hirota *et al*.[14] developed a method in which the benzyl group is removed under mild conditions. This method uses hydrogenation in the presence of a nitrogen-containing base. Thus, the same synthetic strategy as with the *t*-butyl ester protecting group, **6b**, was attempted in order to synthesise the benzyl-protected alanine, **6c**, seen in Scheme 3.4. Compound **6c** was obtained in good yield (96 %), and the dipeptide, **7c**, was then synthesised in the same manner as with **7a.**

The deprotection via hydrogenation, in the presence of a nitrogen-containing base, was then done in order to remove the benzyl protecting group. According to ^{1}H NMR spectroscopy, the reaction was unsuccessful. The spectrum revealed that the *Boc*-protection group was not only removed, but the product did not contain the two alanine moieties. Therefore, a different approach, described by Perosa *et al*.[15] was attempted. This reaction used potassium hydroxide instead of a nitrogen-containing base, and heated the solution to 50 °C, rather than allowing the mixture to stir at room temperature. However, this strategy was also proved to be unsuccessful by ^{1}H NMR spectroscopy. Similar conclusions were drawn from the NMR spectrum regarding the resulting product as for the previous reaction.

Although, the strategy of creating a dipeptide first and then connecting it to the PEG seemed plausible, the difficulties encountered at the de-protection step made this option less viable. Therefore, a new strategy was required. With this in mind, the azide-functionalised monomer and the spacer monomer were compared. The general procedure for these isocyanopeptide monomers, described by Rowan and his coworkers in Scheme 3.1, was re-examined and the different pendent functionalities of the two monomers were studied. It was rationalised that the tosyl group must be the reason **4** could not be purified. Thus, it was hypothesised that by swapping the order in which the monomer is functionalised, it could be possible to complete the synthesis and obtain the azide monomer. Thus, the azide functionality of the monomer was put in place before the two peptide coupling steps, as seen in Scheme 3.5. This approach, towards the azide monomer, was successful.

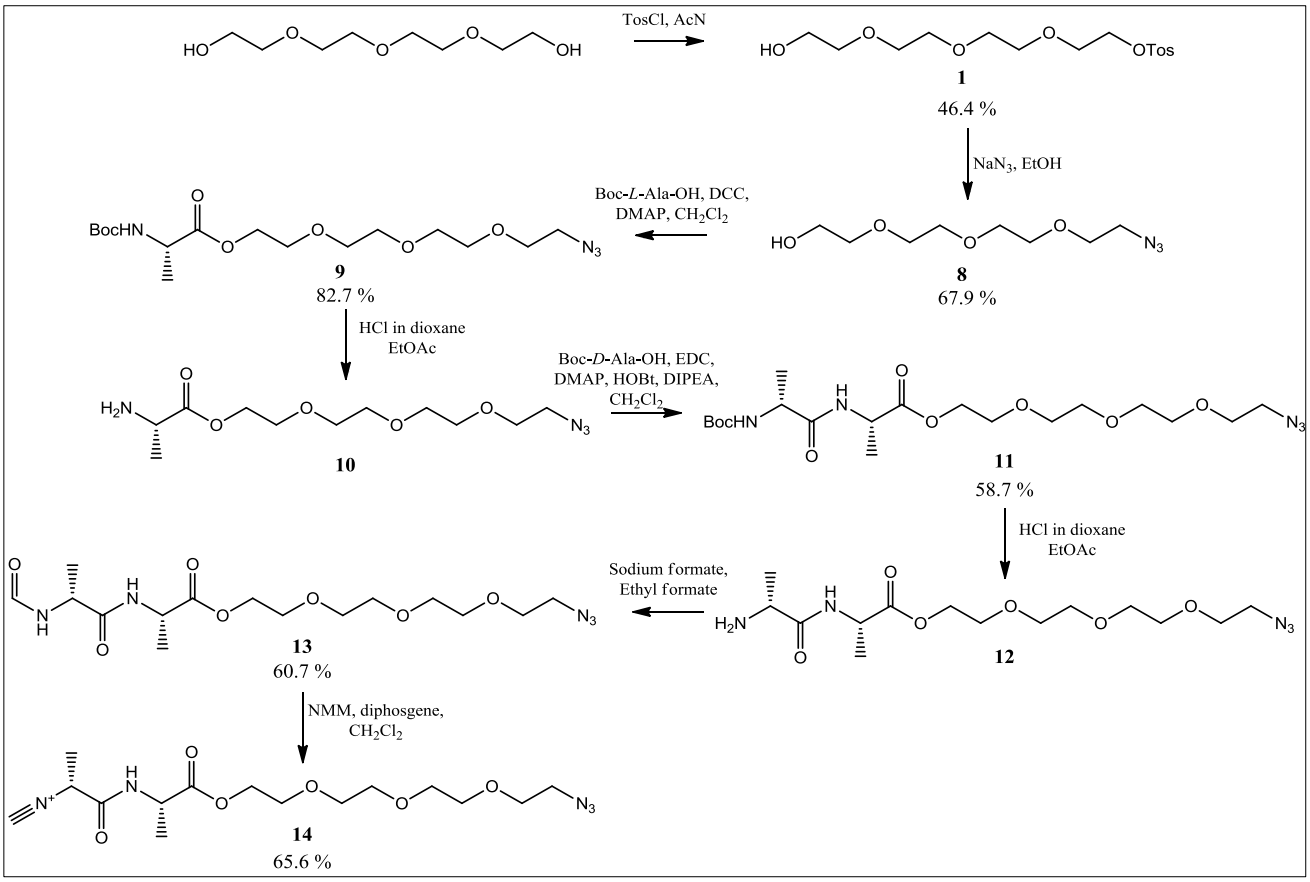

Scheme 3.5 Alternative approach for the azide monomer synthesis.

Compound **11** was purified, via silica gel chromatography, albeit with some difficulty, because it co-eluted with *Boc-D*-alanine. It is hypothesised that this co-elution was due to the formation of a synthon,[16,17] whereby two intermolecular hydrogen bonds form between the *Boc*-alanine and **11** in a spatially arranged manner. It would be necessary to expand this theory using computational models, whereby the energy associated with the formation of such a synthon and the 'gain' in stability energy would be calculated. These calculations are beyond the scope of this study. However, this co-elution impurity was removed easily, two steps later, after the formylation step.

3.3 Conclusion

It was seen that the strategy sited in literature was unsuccessful for the synthesis of the azide-functionalised monomer. Another approach was attempted, whereby the two alanine moieties were initially coupled, with the intention of thereafter coupling

the dipeptide to the ethylene glycol chain. However, the necessity of protecting the carboxylic acid functionality during the dipeptide coupling introduced another complication, as the carboxylic acid and amine functionalities could not be deprotected orthogonally. A new synthetic strategy of first changing the tosyl end-group to the azide-functional end group, and thereafter coupling the two alanine moieties to the tetraethylene chain proved successful. The azide-functionalised monomer was obtained by following this slightly modified protocol.

3.4 Experimental

3.4.1 General

Chemicals

All chemicals were purchased from Merck or Sigma Aldrich and used without further purification, unless stated otherwise.

NMR analysis

^{1}H NMR and ^{13}C NMR spectra were measured using a Varian VXR-Unity (400 MHz) spectrometer, a Varian Gemini 300 spectrometer or a Varian 600 MHz Inova spectrometer. Chemical shifts were reported in parts per million (ppm) and the samples were dissolved in *deuterated* $CHCl_3$. The spectra were referenced to the residual solvent proton peaks. MestReNova (version 6.0.2) was used for data analysis.

FT-IR analysis

All FT-IR measurements were performed using Thermo Nicolet iS10 FT-IR spectrometer. Omnic software (version 6.0a) was used for instrument control and data analysis. 32 scans were performed for each sample, and they were scanned between 650 and 4100 cm^{-1}.

MS analysis

MS was performed on a Waters Synapt G2 with an ESI probe injected into a stream of acetonitrile (and 0.1 % formic acid). ESI positive, Cone Voltage 15 V, was used for detection. MassLynx software (version 4.1) was used for instrument control and data acquisition.

TLC analysis

All reactions were monitored using Machery-Nagel Silica gel 60 plates.

Preparative HPLC Instrumentation

Preparative HPLC separations were performed on a modular Waters HPLC system (Waters, Tygervalley, South Africa) consisting of a 2767 sample manager, 2545 quaternary gradient pump, 1500 series column heater, and a 2998 photodiode array detector (PDA) with a Prep 2998 flowcell. MassLynx software (version 4.1) was used for instrument control and data acquisition, while FractionLynx software (version 4.1) was used to control the collection of HPLC fractions. A Waters Xbridge C_{18}, OBD 19 x 250 mm preparative HPLC column was used for the fractionations and purifications. Xbridge C_{18}, 5 µm, 4.6 x 20 mm and Xbridge C_{18}, 5 µm, 19 x 10 mm guard column was connected to the inlet of the preparative HPLC column.

For the analytical run, an Agilent 1200 Rapid Resolution (600 bar) HPLC system consisting of a binary pump, degasser, auto sampler and diode array detector (DAD) was used. Chemstation software (V) was utilised for instrument control and data acquisition.

HPLC gradient grade acetonitrile and formic acid (98 – 100%) was purchased from Sigma-Aldrich (Kempton Park, South Africa). Water was purified by a Millipore Synergy water purification system (Merck South Africa).

Analytical HPLC method

Injection volume was 10 µL, the mobile phase flow rate was 0.6 mL/min and the column temperature was maintained at 35 °C. The mobile phase A was 0.1% formic acid, and mobile phase B was 0.1% formic acid in acetonitrile. A gradient elution was used initially 0% B for 1.2 minutes, and then it went from 0-100% B over 7.5 minutes, maintained at 100% B for 7.5 minutes, and then returned to starting conditions. The total run was 20 minutes.

Preparative HPLC method

Sample solutions for purification / fractionation were prepared at *ca.* 0.5 g/mL in 50% methanol. Injection volumes ranged between 50 µL and 1 mL. The mobile phase flow rate was 20 mL/min and the column heater was set at 35 °C. A mobile phase gradient was used, using the same mobile phase employed for the analytical HPLC analysis.

3.4.2 Synthetic Procedures

The syntheses of **1, 2, 3** and **4** were carried out as in literature.[1]

HO-$(EtO)_4$-OTos (**1**)

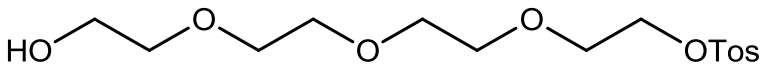

1 was yielded as a pale yellow oil (18.60 g, 53.39 mmol, 46.3 %).

^{1}H NMR (400 MHz, $CDCl_3$) δ 7.79 (aromatic, d, *J* = 8.3 Hz, 2H), 7.33 (aromatic, d, *J* = 8.1 Hz, 2H), 3.80 – 3.48 (CH_2, m, 16H), 2.44 (CH_3, s, 3H)

m/z 349.1313 **(calculated 348.41 for $[M+H]^+$),** 371.1139 **(calculated 371.40 for [M+Na])**

R_f (100 % EtOAc) = 0.6; R_f(10 % MeOH/DCM) = 0.6

Boc-L-Ala-$(EtO)_4$-OTos (**2**)

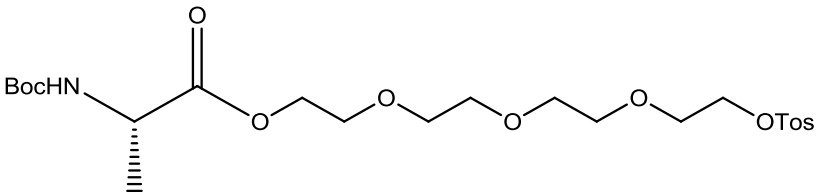

2 was obtained as a yellow oil (13.02 g, 25.06 mmol, 52.2 %).

^{1}H NMR (300 MHz, $CDCl_3$) δ 7.86 – 7.78 (aromatic, m, 2H), 7.39 – 7.33 (aromatic, m, 2H), 5.08 (NH, s, 1H), 4.33 – 4.28 (CH, m, 1H), 4.21 – 4.11 (CH_2, m, 3H), 3.80 – 3.56 (CH_2, m, 13H), 2.46 (CH_3, s, 3H), 1.46 (CH_3, s, 9H), 1.40 (CH_3, dd, J = 7.2, 2.8 Hz, 3H).

L-Ala-$(PEG)_4$-OTos (**3**)

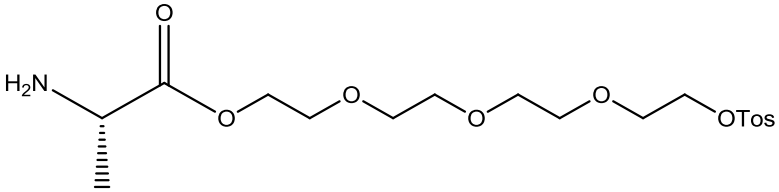

3 was obtained and used without further purification.

^{1}H NMR (300 MHz, $CDCl_3$): δ 7.85 – 7.78 (aromatic, m, 2H), 7.39 – 7.33 (aromatic, m, 2H), 4.20 – 4.15 (CH, m, 1H), 3.80 – 3.60 (CH_2, m, 16H), 2.46 (CH_3, s, 3H), 1.73 (CH_3, d, J = 7.2 Hz, 3H).

Boc-*D*-Ala-*L*-Ala-$(EtO)_4$-OTos (**4**)

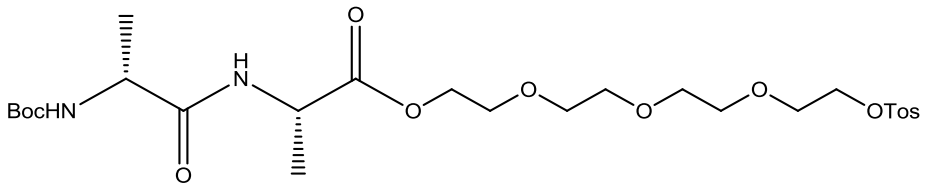

The purification as described in literature did not yield product, as explained in the Results and Discussion section. Therefore, prep-HPLC purification was used.

Boc-D-Alanine-*L*-Alanine methyl ester (**7a**)

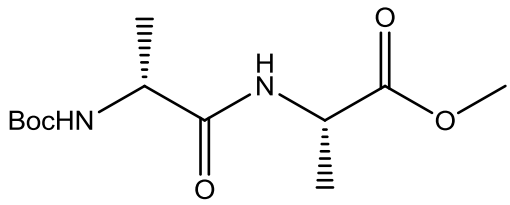

Acetonitrile (57.5 mL) was added to *L*-alanine methyl ester hydrochloride (2.15 g, 0.015 mmol) and cooled to 0 °C. Triethylamine (2.1 mL, 15.06 mmol) was added to the solution and stirred for 30 min. HOBt (2.43 g, 18 mmol) and Boc-D-Ala-OH (1.8 g, 15 mmol) were added to the solution at 0 °C. The reaction mixture was removed from the ice bath and it was heated slightly to ensure that all the contents were fully dissolved. The ice bath was then replaced. EDC (3.25 g, 17 mmol) was added portion-wise, and the solution was stirred for 3 h at 0 °C. Thereafter, the solution was filtered and the solvent was removed under reduced pressure. The product was re-dissolved in ethyl acetate (80 mL), and triethyl ammonium chloride was filtered off. The organic layer was washed with water (4 mL), dried over $MgSO_4$, filtered, and the solvent was removed under reduced pressure. The crude product was purified by column chromatography (eluent gradient: 1:1 to 1:3, Pentane:ethyl acetate) to yield product, **7b**, as a white solid (1.58 g, 5.76 mmol, 38.4 %).

^{1}H NMR (400 MHz, $CDCl_3$) δ 6.69 (NH, s, 1H), 4.94 (NH, s, 1H), 4.56 (CH, p, *J* = 7.3 Hz, 1H), 4.11 (CH, q, *J* = 7.1 Hz, 1H), 3.74 (OCH_3, s, 3H), 1.45 ($3CH_3$, s, 14H), 1.40 (CH_3, d, *J* = 7.2 Hz, 5H), 1.35 (CH_3, d, *J* = 7.1 Hz, 5H)

Boc-L-Alanine *t*-butyl ester (**5b**)

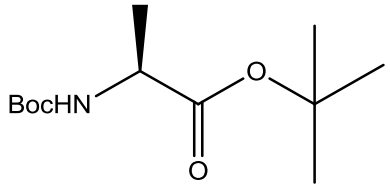

A solution of Boc-*L*-Ala-OH (1.0 g, 5.29 mmol), DMAP (0.32 g, 2.645 mmol) and t-butyl alcohol (0.45 g, 6.01 mmol) was dissolved in CH_2Cl_2 (19 mL). The solution was cooled to 0 °C in an ice bath and EDC (1.12 g, 5.82 mmol) was added portion-wise, with stirring. The reaction mixture was stirred at 0 °C for 2 h and thereafter stirred at r.t. overnight. The solution was concentrated under reduced pressure (making sure that the pressure did not go below 300 mbar, so that the product did not sublime). The remaining product was re-dissolved in ethyl acetate (60 mL) and water (12 mL). The organic layer was collected and washed with saturated sodium bicarbonate (2 x 36 mL), dried over MgSO4, filtered, and the solvent was removed under reduced pressure (again ensuring that the pressure did not go below 300 mbar so that the product did not sublime). The crude product was purified by column chromatography (eluent: 100 % ethyl acetate) to obtain product, **5b**, in the form of a white powder (0.5 g, 4.08 mmol, 77%).

^{1}H NMR (400 MHz, $CDCl_3$) 4.99 (NH, s, 1H), 4.22 (CH, q, J = 7.1, 1H), 1.46 ($3CH_3$ (Boc), s, 9H), 1.44 ($3CH_3$ (*t*-butyl), s, 9H), 1.33 (CH_3, d, J = 7.1 Hz, 3H).

L-Alanine *t*-butyl ester (**6b**)

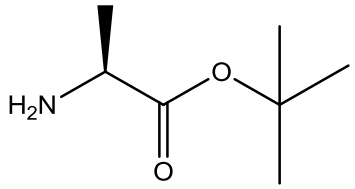

5b (0.55 g, 2.24 mmol) was dissolved in dry ethyl acetate (5 mL), and thereafter 4 M HCl (8 mL) in dioxane was added in a drop-wise manner. The mixture was stirred for 2h. The solvent was carefully removed under reduced pressure, so as to not remove the product. Any remaining HCl was removed by adding 1 mL *t*-BuOH to the solution. The excess *t*-BuOH was removed azeotropically by adding 10 mL DCM and then removing the solvents under reduced pressure. 10 mL DCM was again added and removed under reduced presseure, this was repeated twice. Product, **6b**, was used without any further purification. It contained a slight dioxane impurity, as seen on ^{1}H NMR.

Boc-D-Alanine-*L*-Alanine *t*-butyl ester (**7b**)

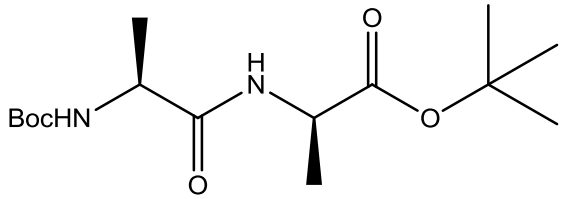

The same method was used as with **7a** to yield **7b** (2.93 g, 10.68 mmol, 71.2 %).

^{1}H NMR (400 MHz, $CDCl_3$) δ 6.70 (NH, s, 1H), 6.60 (NH, s, 1H), 4.45 (CH, m, 1H), 4.14 (CH, m, 1H), 1.48 ($3CH_3$, s, 9H), 1.47 ($3CH_3$, d, *J* = 0.9 Hz, 9H), 1.39 (CH_3, d, *J* = 7.1 Hz, 3H), 1.37 (CH_3, d, *J* = 7.1 Hz, 3H).

Boc-L-Alanine benzyl ester **5c**

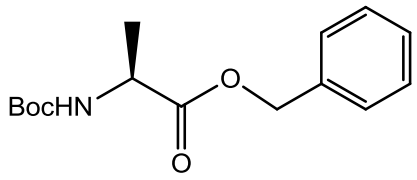

The same method was used as with **5b** to yield **5c** in the form of a white powder (1.42 g, 5.08 mmol, 96.0 %).

^{1}H NMR (400 MHz, $CDCl_3$) δ 7.40 – 7.29 (CH,m, 5H), 5.17 (CH_2, ABq, *J* = 12.3 Hz, 2H), 5.03 (NH, s, 1H), 4.36 (CH, m, 1H), 1.43 ($3CH_3$ (Boc), s, 9H), 1.39 (CH_3, d, *J* = 7.2 Hz, 3H).

L-Alanine benzyl ester **6c**

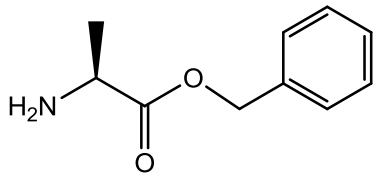

6c (0.57 g, 2.04 mmol) deprotected in the same manner as **6b**.

Boc-D-Ala-*L*-Ala-O*t*Bu **(7c)**

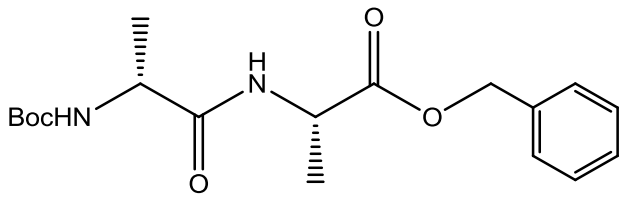

For **6c** (0.50 g, 2.54mmol), the same procedure was used as in **7b**, however, the eluent for the column chromatography was 1:1 to 1:3 hexane:ethyl acetate. This yielded product **7c** (0.56 g, 1.6 mmol, 63 %).

^{1}H NMR (300 MHz, $CDCl_3$) δ 7.45 – 7.32 (CH, m, 5H), 6.72 (NH, s, 1H), 5.26 – 5.12 (CH_2, ABq, 2H), 4.90 (NH, s, 1H), 4.69 – 4.57 (CH, p, 1H), 4.25-4.16 (CH, m, 1H), 1.47 (3 CH_3, s, 9H), 1.44 (CH_3, d, *J* = 7.2 Hz, 3H), 1.37 (CH_3, d, *J* = 7.1 Hz, 3H).

HO-$(EtO)_4$-N_3 (**8**)

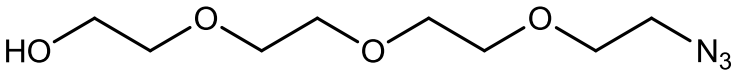

1 (14.72 g, 48.41 mmol) was dissolved in absolute ethanol (150 mL). Sodium azide (31.47 g, 484.1 mmol) was added to the solution, and the reaction mixture was refluxed for 12 h. Once cooled to r.t. the precipitate was filtered off, and the solvent was removed under reduced pressure. The crude product was purified using column chromatography (eluent: EtOAc), to yield the product, **8**, as a pale yellow liquid (7.40 g, 33.75 mmol, 69.7%)

^{1}H NMR (300 MHz, $CDCl_3$) δ 3.78 – 3.31 (m)

^{13}C NMR (150 MHz, $CDCl_3$) δ 72.63 (CH_2, s), 71.53 (CH_2, s), 70.69 (CH_2, s), 70.51 (CH_2, s), 70.20 (CH_2, s), 61.92 (CH_2, s), 50.83 (CH_2, s), 42.77 (CH_2, s)

R_f (EtOAc) = 0.4

Boc-L-Ala-$(EtO)_4$-N_3 (**9**)

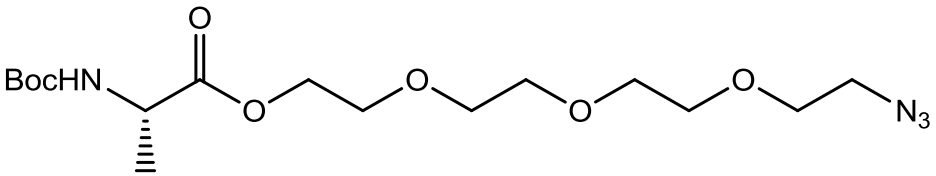

8 (6.7 g, 30.56 mmol), Boc-*L*-Ala-OH (5.78 g, 30.56 mmol) and DMAP (0.37 g, 3.06 mmol) were dissolved in freshly distilled CH_2Cl_2 (100 mL) and cooled to 0 °C. DCC (6.31 g, 30.56 mmol) was added portion-wise at 0 °C. The reaction mixture was stirred at 0 °C for 1 h and then at r.t. for a further 3 h. The precipitate was filtered off and washed with EtOAc. The solvent was removed under reduced pressure. The crude product was re-dissolved in a minimum amount of EtOAc and placed in the fridge for 12 h. The precipitate was then filtered off using a funnel with a cotton wool plug and gravity. The solvent was removed under reduced pressure, and the crude product was purified using column chromatography (eluent: EtOAc) to yield product, **9**, as a yellow/orange liquid (9.87 g, 25.28 mmol, 82.7 %).

^{1}H NMR (300 MHz, $CDCl_3$) δ 5.13 – 5.00 (NH, bs, 1H), 4.32 – 4.25 (CH, m, 1H), 3.79 – 3.35 ($8CH_2$, m, 16H), 1.44 ($3CH_3$, s, 9H), 1.38 (CH_3, d, J = 7.2 Hz, 3H)

^{13}C NMR (75 MHz, $CDCl_3$) δ 173.45 (C, s), 171.26 (C, s), 71.50 (C, s), 70.17 (CH_2, s), 69.05 (CH_2, s), 64.43 (CH_2, s), 60.52 (CH_2, s), 50.82 (CH_2, s), 49.27 (C, s), 42.84 (CH_2, s), 28.40 ($3CH_3$, s), 18.90 (CH_3, s), 14.39 (s)

m/z 391.2195 (Calculated 391.44 for **$[M+H]^+$**)

R_f (EtOAc) = 0.7

L-Ala-$(EtO)_4$-N_3 (**10**)

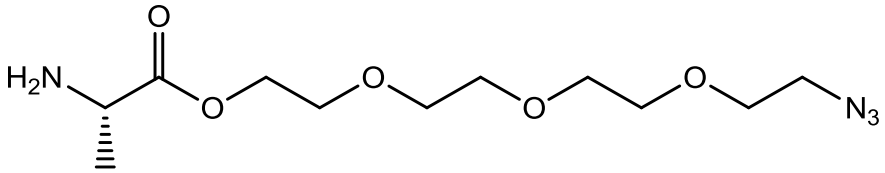

9 (9.87 g, 25.28 mmol) was deprotected in the same manner as described in literature.[1] The product, **10**, was used without further purification.

Boc-D-Ala-*L*-Ala-$(EtO)_4$-N_3 (**11**)

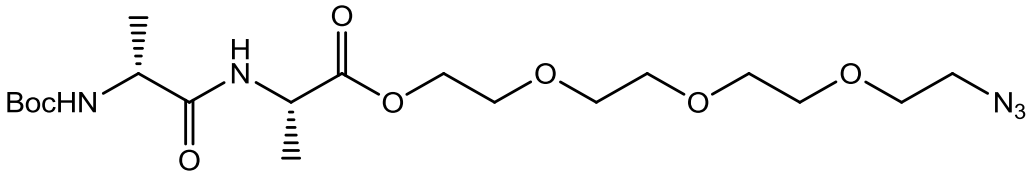

10 (7.33 g, 25.28 mmol), Boc-*D*-Ala-OH (4.78 g, 25.28 mmol) and HOBt (3.42 g, 25.28 mmol) were dissolved in freshly distilled CH_2Cl_2 (150 mL). The pH was adjusted to pH 8 by the addition of DMAP. DIPEA (4.41 mL, 25.28 mmol) was added in a drop-wise manner at r.t. as the reaction mixture stirred. The mixture was stirred at r.t. until all the contents had completely dissolved. Thereafter, the reaction mixture was cooled to 0 °C and EDC (3.92 g, 28.28 mmol) was added in a portion-wise manner. The reaction was stirred at 0 °C for 1 h and then for a further 5 h at r.t. The solvent was then removed under reduced pressure. The crude product was re-dissolved in chloroform and washed with water (3 x 15 mL) and then conc. $NaHCO_3$ (aq). The aqueous layers were extracted with mL chloroform (2 x 100). The combined organic layers were dried over $MgSO_4$, filtered, and the solvent was removed under reduced pressure. The crude product was purified, with difficulty, using column chromatography (gradient eluent: pentane: EtOAc, 1:1, to EtOAc,

flushed with 2 % MeOH/EtOAc) to yield product, **11**, as a yellow oil (11.44 g, 24.78 mmol, 81.1 %). The product coeluted with Boc-*D*-Ala.

R_f (EtOAc) = 0.5

D-Ala-*L*-Ala-$(EtO)_4$-N_3 (**12**)

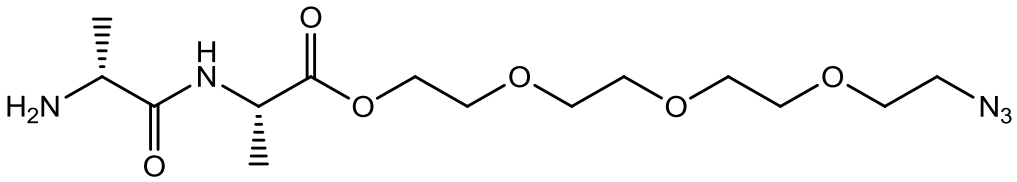

The same procedure as described for **9** (10.00 g, 21.67 mmol) was followed. The product, **12**, was used with no further purification.

Formyl-*D*-Ala-*L*-Ala-$(EtO)_4$-N_3 (**13**)

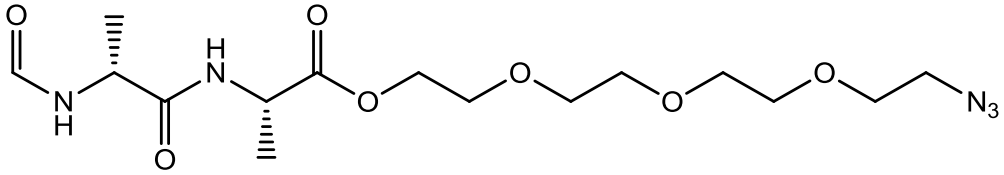

13 (5.12 g, 13.15 mmol, 60.7 %) was synthesised as in literature[1].

^{1}H NMR (400 MHz, $CDCl_3$) δ 8.17 (CH, s, 1H), 6.95 (NH, t, *J* = 6.4 Hz, 1H), 6.71 (NH, d, *J* = 7.0 Hz, 1H), 4.58 (CH, m, 1H), 4.26 (CH_2, m, 2H), 4.09 (CH, q, J=7.1, 1H), 3.79 – 3.56 (CH_2, m, 12H), 3.40-3.35 (CH_2, m, 2H) 1.41 (CH_3, d, *J* = 7.2 Hz, 3H), 1.38 (CH_3, d, *J* = 7.0 Hz, 3H)

^{13}C NMR (75 MHz, $CDCl_3$) δ 172.53 (C, s), 171.48 (C, s), 161.30 (C, s), 72.46 (CH_2, s), 71.32 (CH_2,), 70.32 (CH_2, s), 70.00 (CH_2,), 68.92 (CH_2, s), 64.42 (CH_2, s), 61.70 (CH_2, s), 50.65 (CH_2, s), 48.32 (C, s), 47.19 (C, s), 42.73 (CH_3, s), 17.89 (CH_3, s)

m/z 390.1993 (calculated 390.41 for **$[M+H]^+$**), 412.1812 (calculated 412.39 for **$[M + Na]^+$**)

IR 3282. (N-H), 2871. (C-H), 2105 (N_3), 1738. (C=O), 1655 (N-H), 1522. (N-H), 1454 (C-H), 1135 (C-O)

R_f (10% MeOH/CH_2Cl_2) = 0.1

Cyano-*D*-Ala-*L*-Ala-$(EtO)_4$-N_3 (**14**)

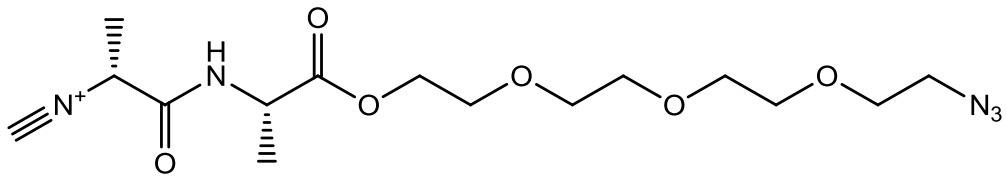

13 (0.5 g, 1.28 mmol) was dissolved in CH_2Cl_2, (150 mL) and Burgess reagent (0.49 g, 1.92 mmol) was added to the solution. The solution was refluxed for 3-4 h. The solvent was then removed under reduced pressure and the crude product was purified using column chromatography (packed with CH_2Cl_2 and eluted with 10% ethyl acetate / CH_2Cl_2), and then purified again with column chromatography eluted with a gradient eluent of 100 % pentane to 100 % ethyl acetate) to obtain pure product, **14**, as a yellow oil (219 mg, 0.59 mmol, 66 %).

R_f (10% MeOH/CH_2Cl_2) = 0.7

^{1}H NMR (300 MHz, $CDCl_3$) δ 7.05 (NH, s, 1H), 4.56 (CH, m, 1H), 4.34 (CH_2, m, 2H), 4.24 (CH, m, 1H), 3.79-3.70 (CH_2, m, 2H), 3.69–3.66 (CH_2, m, 10H), 3.42 – 3.32 (CH_2, m, 2H), 1.62 (CH_3, d, *J* = 7.0 Hz, 3H), 1.45 (CH_3, d, *J* = 7.2 Hz, 3H).**^{13}C NMR** (75 MHz, $CDCl_3$) δ 196.38 (HCN, s), 172.21 (C, s), 159.64 (C, s), 152.85 (CH, s), 71.49 (CH_2, s), 70.18 (CH_2, s), 68.96 (CH_2, s), 68.93 (CH_2, s), 64.80 (CH_2, s), 50.81 (CH_2, s), 48.26 (C, s), 42.85 (CH_2, s), 24.49 (CH_2, s), 23.93 (CH_3, s), 18.24 (CH_3, s)

m/z 372.1889 (calculated 372.40 for **$[M^+]$**), 394.1707 (calculated 394.38 for **$[M + Na]^+$**)

IR 3319 (N-H), 2920 (N-H), 2140 (C≡N), 2098 (N_3), 1744 (C=O), 1678 (N-H), 1530 (N-H), 1454 (C-H), 1094 (C-O)

3.5 References

(1) Mandal, S.; Eksteen-Akeroyd, Z. H.; Jacobs, M. J.; Hammink, R.; Koepf, M.; Lambeck, A. J. A.; van Hest, J. C. M.; Wilson, C. J.; Blank, K.; Figdor, C. G.; Rowan, A. E. *Chemical Science* **2013**, *4*, 4168

(2) Kouwer, P. H. J.; Koepf, M.; Le Sage, V. A. A.; Jaspers, M.; van Buul, A. M.; Eksteen-Akeroyd, Z. H.; Woltinge, T.; Schwartz, E.; Kitto, H. J.; Hoogenboom, R.; Picken, S. J.; Nolte, R. J. M.; Mendes, E.; Rowan, A. E. *Nature* **2013**, *493*, 651.

(3) Cornelissen, J. J. L. M.; Graswinckel, W. S.; Adams, P. J. H. M.; Nachtegaal, G. H.; Kentgens, A. P. M.; Sommerdijk, N. A. J. M.; Nolte, R. J. M. *J Pol Sci* **2001**, *39*, 4255.

(4) Reetz, M. T. *Angew Chem Int Ed* **1991**, *30*, 1531.

(5) Sureshbabu, V. V.; Narendra, N. In *Amino Acids, Peptides and Proteins in Organic Chemistry*; Hughes, A. B., Ed.; Wiley: 2011; Vol. 4, p 1.

(6) Avinash, M. B.; Govindaraju, T. *J Phys Chem Lett* **2013,**, *4*, 583.

(7) Latli, B.; Tomizawa, M.; Casida, J. E. *Bioconj Chem* **1997**, *8*, 7.

(8) Javier Adrio, J.; Cuevas, C.; Manzanares, I.; Joullie, M. M. *J Org Chem* **2007**, *72*, 5129.

(9) Prabhakaran, E. N.; Science, I. I. o., Ed.; Indian Institute of Science: India, 2010; Vol. US 2010/0261871Al, p 1.

(10) Isidro-Llobet, A.; A´lvarez, M.; Albericio, F. *Chem Rev* **2009**, *109*, 2455.

(11) Dhaon, M. K.; Olsen, R. K.; Ramasamy, K. *J Org Chem* **1982**, *47*, 1963.

(12) Yadav, J. S., Balanarsaiah, E., Raghavendra, S. & Satyanarayana, M. *Tetrahedron Lett* **2006**, *47*, 4921.

(13) Sajiki H., K., H. & Hirota, K. *Tetrahedron Lett* **1998**, *39*, 7127.

(14) Sajiki H., K., H. & Hirota, K. *Tetrahedron Lett* **1997**, *38*, 399.

(15) Perosa, A., Tundo, P. & Zinovyevb, S. *Green Chem* **2002**, *4*, 492.

(16) Corey, E. J. *Pure Appl Chem* **1967**, *14*, 19.

(17) Desiraju, G. R. *Angew Chem Int Edit* **1995**, *34*, 2311.

Chapter 4: Polymer Synthesis and Characterisation

Abstract

Polyisocyanides were obtained in a Ni(II) catalysed polymerisation of the monomers that were synthesised in Chapter 3. Five polymers were synthesised with spacer to azide-functionalised monomer feed ratios of 1:100 and 1:200. These polymers were characterised by FT-IR SEC, AF4, CD and 'dye test' experiments.

The gelation behaviour of the hydrogels was investigated using fluorescence microscopy. Using a thermal, time-lapse study, it was possible to visualise the hydrogels in aqueous medium, while they undergo the transition from solution state into gel state. It was seen that the polymers congregate and form organised clusters of bundles. Due to the limited resolution of the confocal lens, it was not possible to visualise the discrete bundles. Furthermore, a concentration study was undertaken, whereby the hydrogels were analysed under super-resolution at different polymer concentrations in aqueous medium. The z-stacks were then reconstructed into a three dimensional simulation of the gel. These simulations were able to give a better impression of the manner in which the polymers gelled since the images are a true three dimensional representation of the gels in their solvated state.

4.1 Introduction

The current study focused on the preparation and characterisation of polyisocyanopeptides with oligo(ethylene glycol) side chains. The azide-functionalised ('azide monomer') and an unfunctionalisable spacer monomer were co-polymerised by the method depicted in Scheme 4.1.

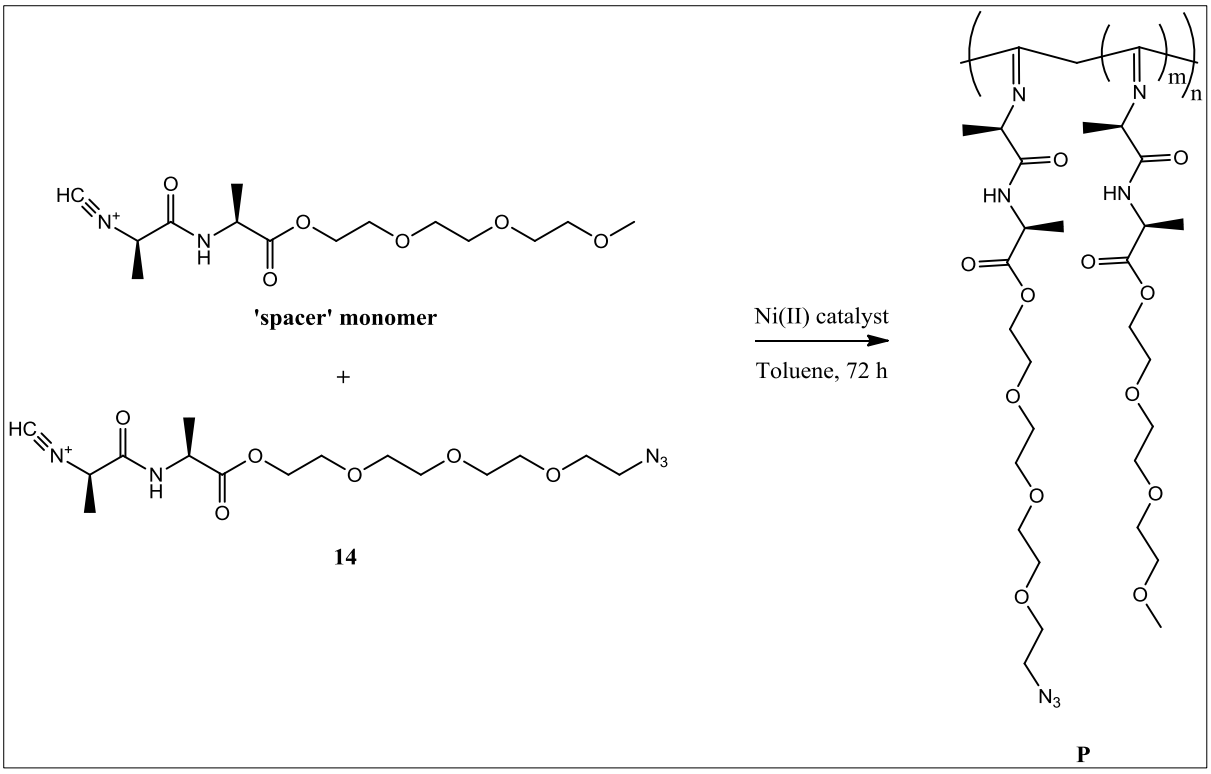

Scheme 4.1 Polyisocyanide hydrogels with oligo(ethylene glycol) side chains were prepared via the Ni(II)-catalyzed co-polymerisation of 'spacer monomer' and azide monomer.

4.1.1 Ni(II)-catalysed polymerisation of polyisocyanides

The first polyisocyanides were prepared by Millich[1] via an acid-coated glass system with a radical initiator or air. As mentioned in Chapter 2, the regular method for the polymerisation of isocyanopeptides is now a Ni(II)-catalysed reaction, discovered by Drenth *et al*.[2] These catalysts are usual Ni(II) salts, such as $NiCl_2.6H_2O$ or $Ni(Acac)_2$.[3] A superficial overview of this mechanism would show that the lone pair on the carbon of the isocyanide moiety of the monomer coordinates to the Ni(II) centre. Four isocyanides are able to coordinate to the catalyst, causing the Ni(II) centre to obtain a square-planar configuration.[3] Nucleophilic attack occurs on the monomer ligand by an alcohol or amine, which subsequently initiates the polymerisation.[4] This nucleophilic attack renders the Carbon-Ni bond nucleophilic. Thereafter, this new nucleophile is able to attack another monomer that is coordinated to the catalyst, incorporating it into the growing polymer chain through an α-insertion. In the presence of a chiral centre on the monomer, one of the two neighbouring monomers will be favoured above the other. This will create a chiral bias.[4] This cycle continues as the polymer grows through a number of consecutive α-

insertions, as seen in Scheme 4.2. This allows for a sort of “merry-go-round” polymerisation.[2] In this manner, the fifth side-group of the monomer is inserted in a manner in which it is positioned above the side group of the first monomer, and the ninth is above the fifth, etc. In this way a 4_1 helical configuration of the polymer chain is obtained.[5] The energy released from the conversion of the monomer’s divalent carbon into a tetravalent carbon is the driving force behind this polymerisation reaction.[3]

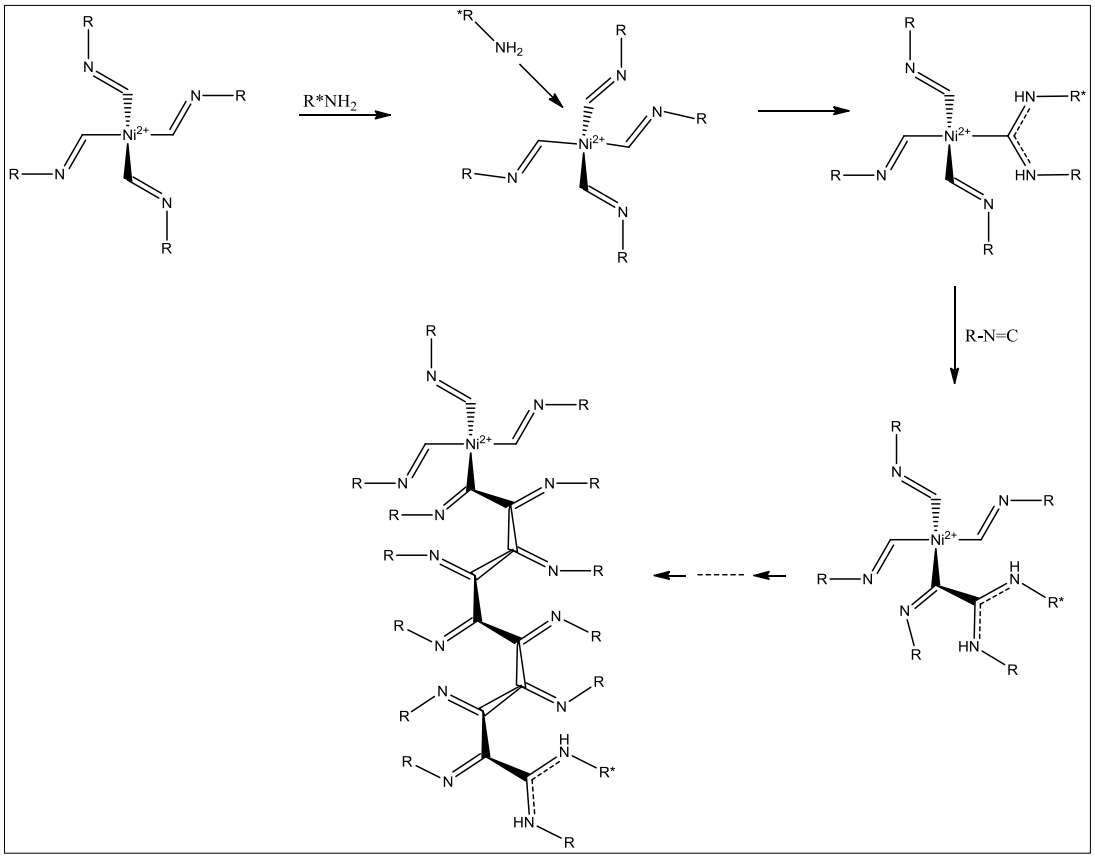

Scheme 4.2 A scheme representing the polymerisation mechanism, catalysed by a Ni(II) species.

A more in depth investigation of this mechanism would include studies in which the reaction was followed using electron spin resonance, cyclic voltammetry and magnetic susceptibility measurements.[4] The mechanism is believed to be more complex due to the presence of Ni(I) species, as well as due to the observed impact that the presence of oxygen has on the polymerisation process. This need for aerobic conditions was shown by Novak *et al*.[6] It has been witnessed that in the

absence of oxygen, the polymerisation rate decreases. The inverse can be seen in the presence of oxygen. However, it has also been seen that the presence of oxygen can cause the isocyanide monomers to be converted into isocyanates.[6] It is important to note that, in the presence of an excess of 10 equivalents of the isocyanide compared to the catalyst, the catalyst is reduced to Ni(I). However, in the presence of oxygen, an oxidation reaction reactivates the Ni-centre.[6]

The Ni(II)-catalysed polymerisation of isocyanides is greatly influenced by the concentration of the Ni(II) catalyst, as well as the solvent in which the polymerisation takes place. The influence of the solvent was studied by Rowan and co-workers[7], where their investigations incorporated polymerisation studies using toluene, dichloromethane, tetrahydrofuran and methanol. It was discovered that the most effective solvent for the polymerisations is toluene, as it produced the highest yields. Furthermore, the degree of polymerisation for polymers that were polymerised in toluene or tetrahydrofuran was higher than that of polymers synthesised in dichloromethane or methanol. The rate of polymerisation, studied using the isocyanide infrared (IR) stretching band, was also seen to be influenced by the solvent used. Toluene was observed to induce the fastest polymerisation, followed by dichloromethane. The lowest rate seen was for a polymerisation conducted in tetrahydrofuran, where the kinetic rate could not be studied for methanol. The conclusion drawn from this was that a decrease in solvent polarity increases the rate of polymerisation.[7]

4.1.2 Gelation properties of poly(isocyanidopeptide) hydrogels

It is believed that the thermal transition from solution to gel state occurs due to the ability of the side chains to bundle together.[8] The thermal transition has been shown to be fully reversible, and the transformation from solution state to gel state has been shown to occur within seconds. The gel state polymer was visualised using atomic force spectroscopy (AFM) and cryo scanning electron microscopy (cryo-SEM), as seen in Figure 4.1. It was observed that the polymers formed bundles of polymer chains. The extent of bundling was analysed, using AFM, as well as the approximate bundle number, *i.e*. the average number of polymer chains per bundle, and was estimated to be 6.9.[8] It was noted that the bundle dimensions were independent of the concentration of the polymer in solution. Solutions with larger concentrations showed a larger number of bundles, rather than thicker bundles.[8] Rowan *et al*. have

also done single-particle tracking studies on the gel state of polymers grafted with triethylene glycol side chains. The preliminary results from this study showed that the nanoparticle diffusion coefficients are dependent on the concentrations.[8] This indicates that, with a higher concentration of polymers, there are more bundles that lead to smaller pore sizes. Hence, the diffusion is more restricted through higher concentrations of polymer. The belief is that these results are related to the helical structure of the polymer, as well as to the intrinsic stiffness of the polymers, which is vital for the polymer's ability to effectively mimic intermediate filaments. Moreover, the intrinsic stiffness of the polymer chains is also vital for the mechanical properties of the polyisocyanides.[8]

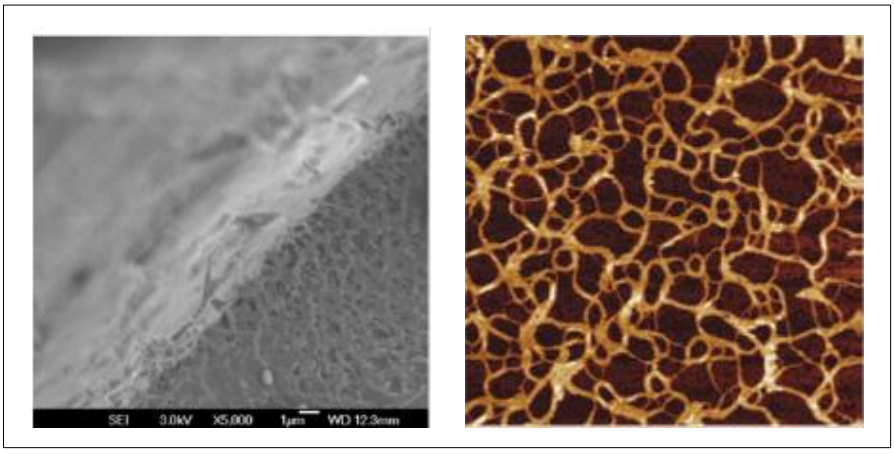

Figure 4.1 Left: AFM image showing the polymer in the gel state. The pore sizes are seen to be around 100 nm and the bundles are approximately 1.4 nm, and made up of 6.9 polymer chains. Right: Cryo-SEM image of the polymer in gel state. The nanopore network is similar to that seen in the AFM image.[8]

4.1.3 Functionalising polyisocyanopeptide hydrogels

The incorporation of the azide monomer allows for further functionalisation of the polymer. As mentioned in Chapter 3, this functionalization can be carried out using so-called 'click' chemistry, which in this case is a 1,3-dipolar cycloaddition of an azide and an alkyne, producing a linking 1,2,3-triazole ring.[9,10] This post-polymerisation functionalisation has proven to be a better strategy than pre-modifying the monomer with the desired functional group, as the process of pre-modifying the monomer is costly and tedious.[10] A normal 'click' reaction requires the

presence of a copper (I) catalyst in approximately 5-10 mol% concentrations (relative to the azide/alkyne), which would compromise the potential use of the resulting hydrogels in contact with living cells or tissue. Thus, the copper-catalysed version of the click reaction is unsuitable for the functionalisation of such systems.[11] To ensure that there are no toxic side effects for the cells, due to the presence of the copper catalyst, copper-free click chemistry can be utilised instead.[12] This reaction has been shown to occur under ambient conditions without the need for a catalyst. The reaction between the azide and a cyclooctyne occurs spontaneously due to the ring-strain of the cyclooctyne system. The ring-strain found in this eight-membered ring has been calculated to be 18 kcal.mol^{-1}, and it has been seen to release this strain when the triazole is produced.[13] Due to the absence of any auxiliary agents, this 'click' reaction causes no negative-effects for the viability of living cells.[12] These reactions have become a useful tool for labelling, or functionalising, polymers and proteins with probes.[12]

4.2 Results and Discussion

4.2.1 Synthesis and characterisation of polyisocyanopeptide hydrogels

Three polymers, with different spacer monomer to "azide monomer" ratios and with different catalyst to monomer ratios, were synthesised, as shown in Table 4.1. The Ni(II) catalyst was dissolved in ethanol, which acts as the necessary nucleophile to activate the polymerisation. The molecular weight of the polymer chains can be controlled due to the relationship between the molecular weight and the monomer to catalyst ratio ([M]/[cat]).

Table 4.1 A summary of the results obtained from polymerisations P1, P2 and P3.

Sample	Theoretical ratio (N_3:spacer)	Catalyst: monomer ratio	Yield (%)	M_w (SEC) (kg/mol)	M_n (SEC) (kg/mol)	$Đ_{SEC}$	M_w (AF4) (kg/mol)	M_n (AF4) (kg/mol)	Actual ratio (N_3:spacer)
P1	1:200	1:10000	84.7	15644	5668	2.7	5876	3780	1:130
P2	1:100	1:2000	85.6	669	321	2.1	18.20	16.42	1: 25
P3	1:200	1:2000	58.7	668	321	2.1	19.09	18.03	1:135

The Ni(II) catalyst, which could be cytotoxic, was removed by precipitating the polymer in diisopropyl ether. The polymer was also purified using dialysis after conjugation. Thus, it is expected that all Ni(II) would be removed before the polymer has contact with cells. This was checked by doing a cytotoxicity study, in Chapter 5, where it was found that cells were viable in the presence of the polymer. Thus, it was concluded that the Ni(II) catalyst was sufficiently removed from the polymer system.

The yield of the polymerisation ranged from 58.6 – 85.6 %. The infrared (IR) spectrum, see Figure 4.2 **c**, of **P1** shows that the isocyanide band (2140 cm^{-1}), seen in the IR spectra of the monomers, Figure 4.2 **a** and **b**, disappeared and was replaced with an imine absorption band at approximately 1596 cm^{-1}. This indicated the formation of the polyisocyanide. Previous studies have shown that the amide vibration band shifts to a lower wavenumber after polymerisation.[14] This shift is due to the formation of hydrogen bonds between the amide on side chain n and (n+4). These results can be seen in Figure 4.2, where the IR spectra for both of the monomers and **P1** are shown, where the shifts from 3301 cm^{-1} to 3270 cm^{-1} can be seen when comparing the spectra of the spacer monomer to that of **P1**, the vertical line can be used as a visual aid.

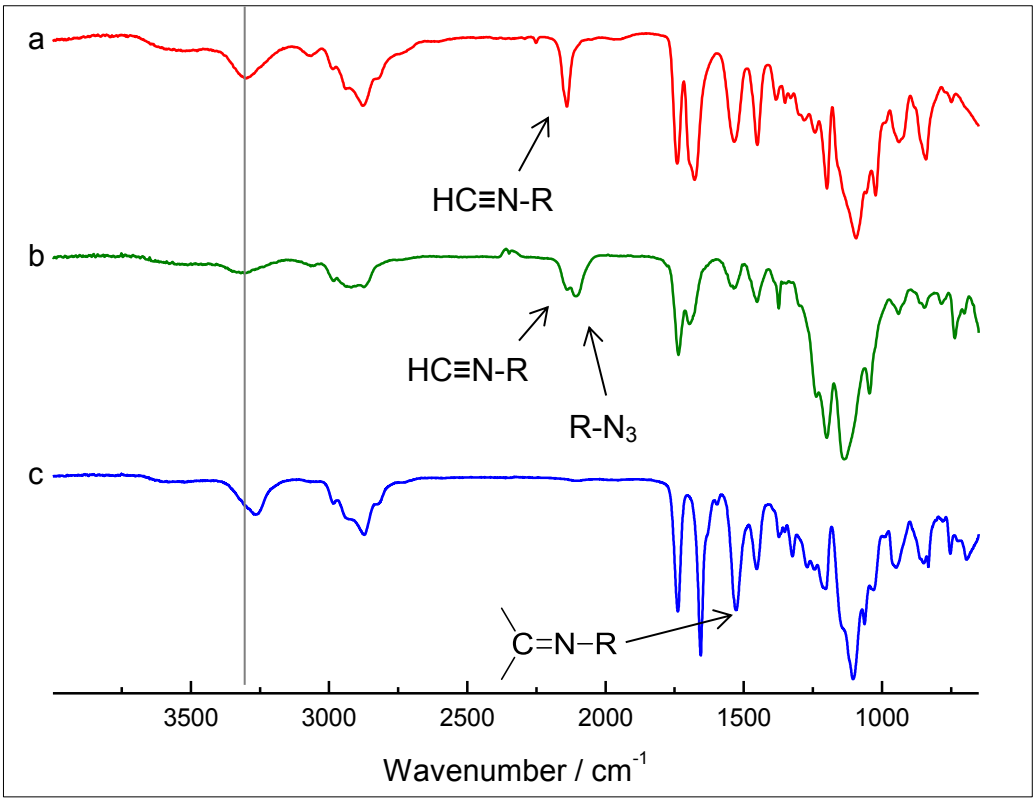

Figure 4.2 A comparison of the IR spectra of a) the 'spacer monomer', b) the azide monomer and c) the polymer (P1)

Due to the rigidity of the helical carbon backbone of polyisocyanides, it is well known that SEC is an inefficient method of measuring the absolute molecular weight of the polymers.[15] Instead it is possible to use viscometry, AFM and field flow fractionation (FFF). FFF was first described by Giddings,[16,17] and it allows for the separation of compounds based on their physicochemical properties, especially size, causing the compound's retention times to differ within a narrow channel in which there is a field or a gradient. The retention is driven by a cross-flow field in flow FFF, as well as by a temperature gradient in thermal FFF. The compounds are then observed by the detector. The asymmetric flow field flow fractionation (AF4) results for **P1-P3** are seen in Table 4.1. The results show a very high molecular weight for **P1**. It was thought that perhaps the high molecular weight was due to the [M]/[cat] ratio. **P2** and **P3** were synthesised with a lower [M]/[cat]) ratio (1:2000 rather than 1:10 000), with the aim to obtain polymers with a molecular weight of approximately 350-400 kg.mol^{-1}.[18] According to SEC, the number average molecular weight (M_n) obtained for **P2** and **P3** was 321 kg.mol^{-1}, which is almost the targeted molecular weight. The degree

of polymerisation (DP) for both polymers was 1014. The high polydispersity was most probably due to the inefficiency of analysing polyisocyanides using SEC. However, the molecular weights obtained for **P2** and **P3** using AF4 are not within the targeted molecular weight. The eluent system used for these two polymers (an aqueous system) was different to that of **P1** (acetonitrile and methanol). During analysis, the AF4 chamber is heated to 30 °C, which is above the gelation temperature of the polymer in aqueous solution; it is probable that **P2** and **P3** gelled within the chamber causing aggregation of the polymer chains, during the analysis. Since AF4 uses a chamber the aggregated polymer will move through the chamber, however the molecular weights detected will be below the actual molecular weights of the polymers. Since, the [M]/[cat] ratios have been extensively studied with regard to the molecular weight of the polymer,[18] it is likely that the SEC results gave a more accurate indication of the molecular weight for **P2** and **P3**, in this case.

Circular dichroism (CD) spectroscopy experiments were carried out to study the secondary structure of the polyisocyanides, as seen in Figure 4.3. The results correspond to those seen in literature,[8] whereby a small negative Cotton effect is first observed followed by a larger positive Cotton effect. This indicates that the polymer adopts a left-handed (M) helical conformation.[15]

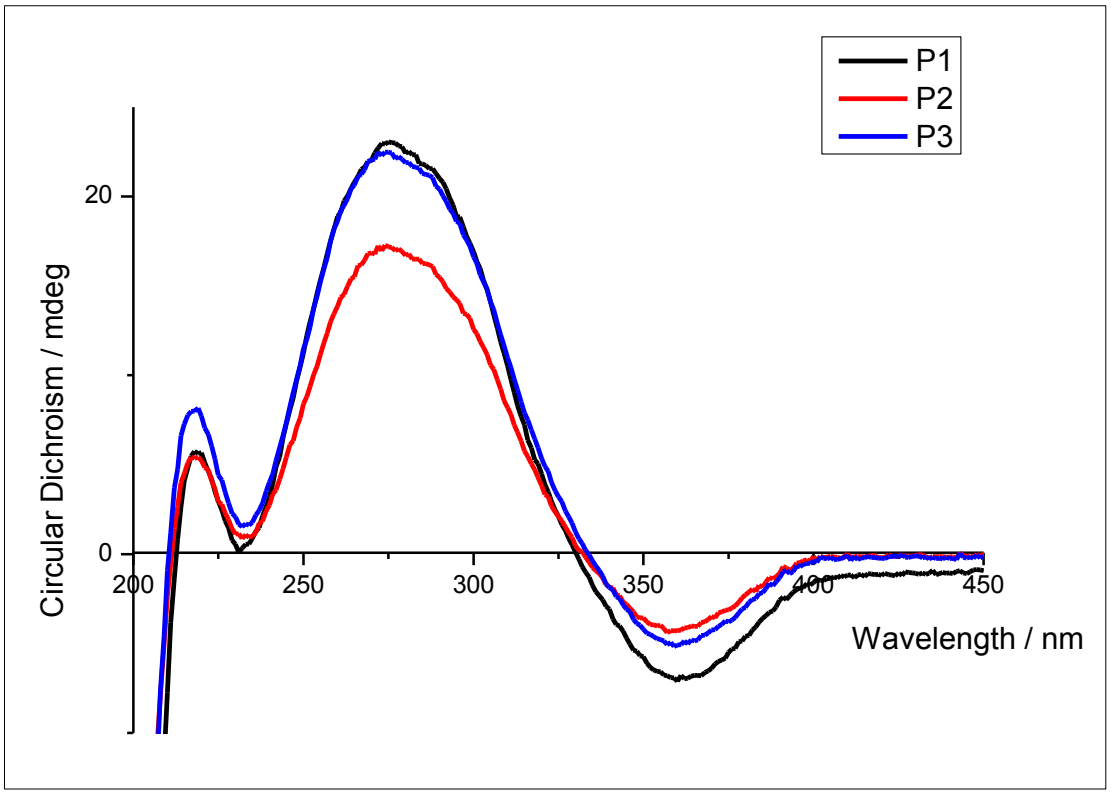

Figure 4.3 CD spectra of P1-P3 dissolved in PBS buffer at a concentration 0.5 mg/mL

4.2.2 Dye-Functionalising polyisocyanopeptide hydrogels

The incorporation of the azide monomer in the copolymer allowed for the possibility of functionalising the polymer, either with epitopes or dyes. Due to the low feed ratio of the azide monomer, ^{1}H NMR and FT-IR are not sensitive enough to be able to quantify the amount of azide monomer incorporated into the polymer. Thus, in order to determine the number of reactive sites, or free azides, available for functionalisation, 'dye tests' were conducted. In this test, the polymer is functionalised with 5-(*N*-(1-[(1*R*,8*S*,9s)-bicyclo[6.1.0]non-4-yn-9-yl]-3-oxo-2,7,10-trioxa-4-azadodecan-12-yl]sulfamoyl)-2-[6- (diethylamino)-3-(diethyliminio)-3*H*-xanthen-9-yl]benzenesulfonate rhodamine B conjugate (BCN-rhodamine), as seen in Scheme 4.3, through a Cu-free click reaction.

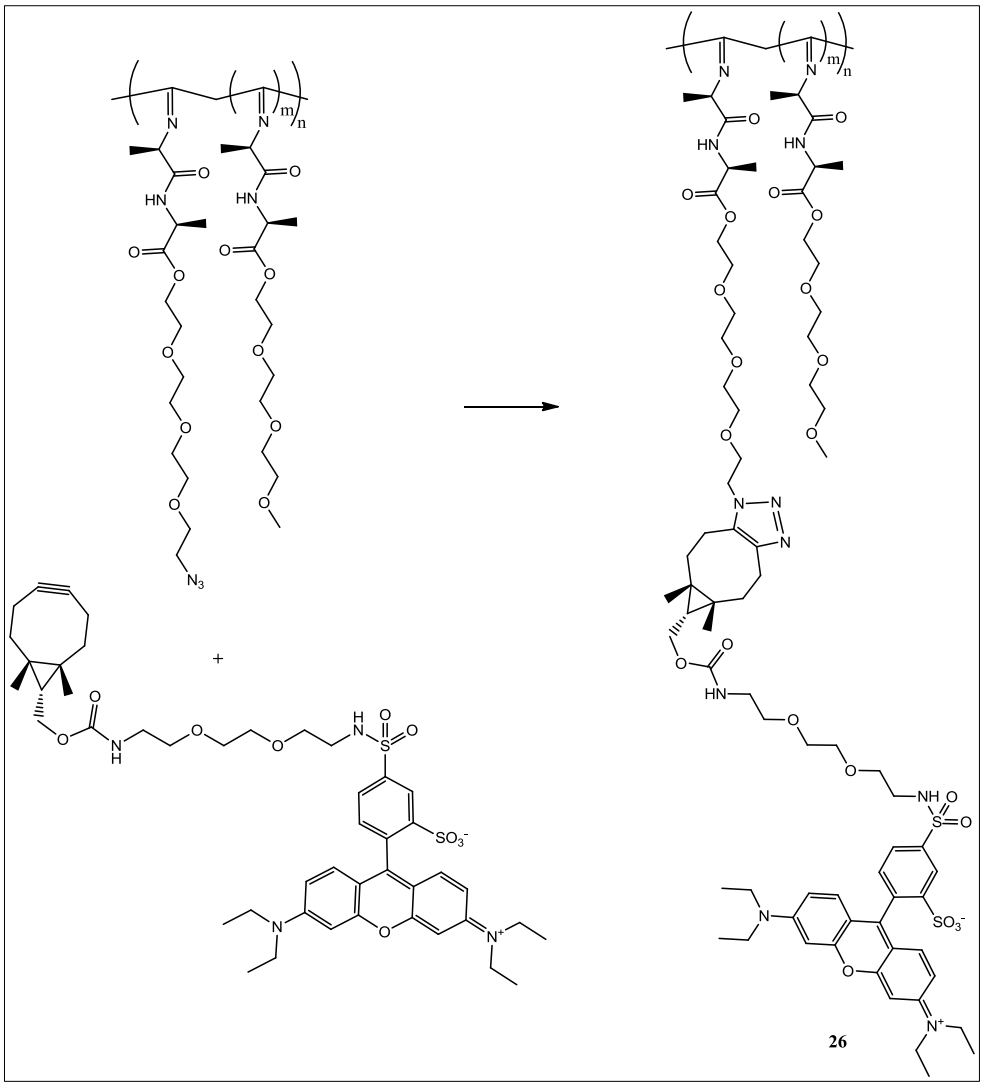

Scheme 4.3 Functionalisation of the polyisocyanide with BCN-rhodamine using 'click' chemistry.

The test exploits the fact that BCN-rhodamin has a UV-vis absorbance at 559 cm^{-1}, seen in Figure 4.4, whereas the polymer does not absorb at this wavenumber under UV-vis. Thus, if the polymer is dye-functionalised, it will absorb at 559 cm^{-1}, and this absorbance depends on the amount of BCN-rhodamine that is attached to the polymer. Therefore, it is possible to indirectly calculate the amount of azide monomer present in the polymer by measuring the UV-vis absorbance at 559 cm^{-1} of the dye-functionalised polymer.

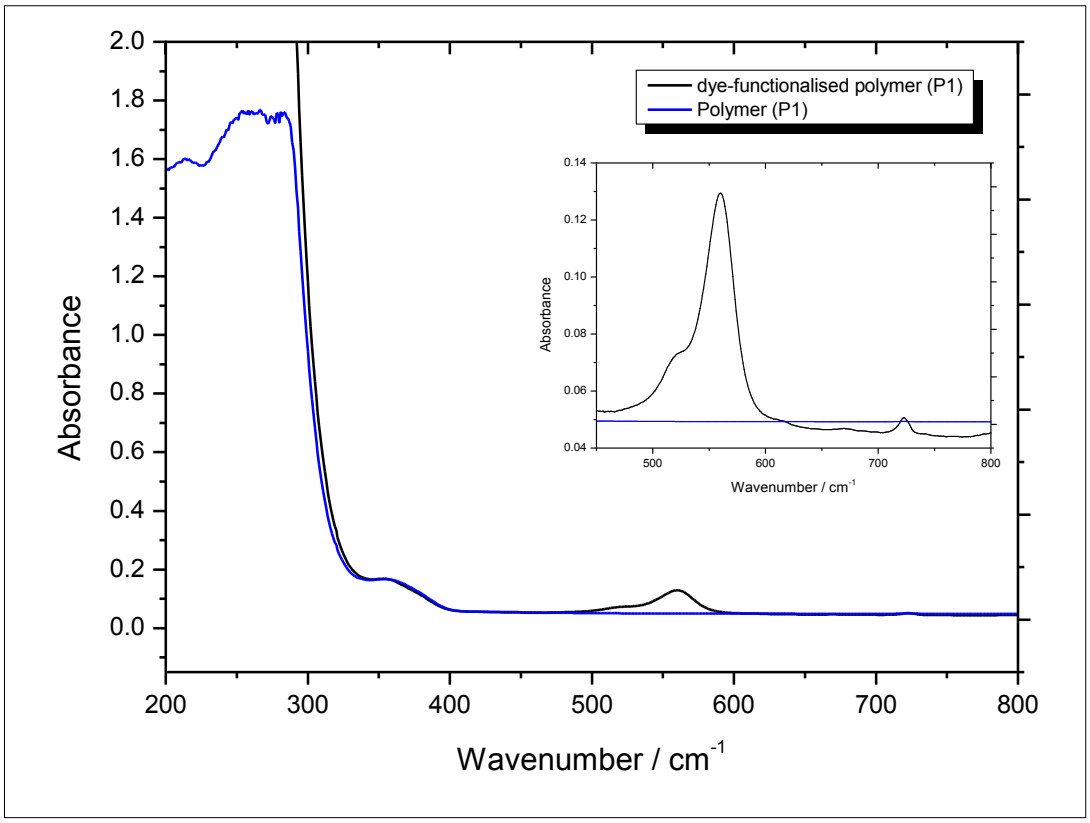

Figure 4.4 The UV-vis spectrum of BCN-rhodamin functionalised polymer in CH_2Cl_2 (black) shows that the compound absorbs at 559 cm^{-1}, whereas this absorbance is clearly missing in the UV-vis spectrum of the unfunctionalised polymer in CH_2Cl_2 (blue).

To carry out the 'dye' test, it was necessary to know the extinction coefficient of the BCN-rhodamin in CH_2Cl_2, which was calculated using the Beer-Lambert law:

$$A = \varepsilon C l \qquad 1$$

Where, A is the absorbance, C is the concentration, l is the path length and Ɛ is the extinction coefficient. The UV-vis absorbance of BCN-rhodamin in CH_2Cl_2 was plotted as a function of concentration, seen in Figure 4.5. From this it was possible to deduce that the extinction coefficient of BCN-rhodamin in CH_2Cl_2 is 10531 $M^{-1}cm^{-1}$ with an R^2 value of 0.997, was extracted.

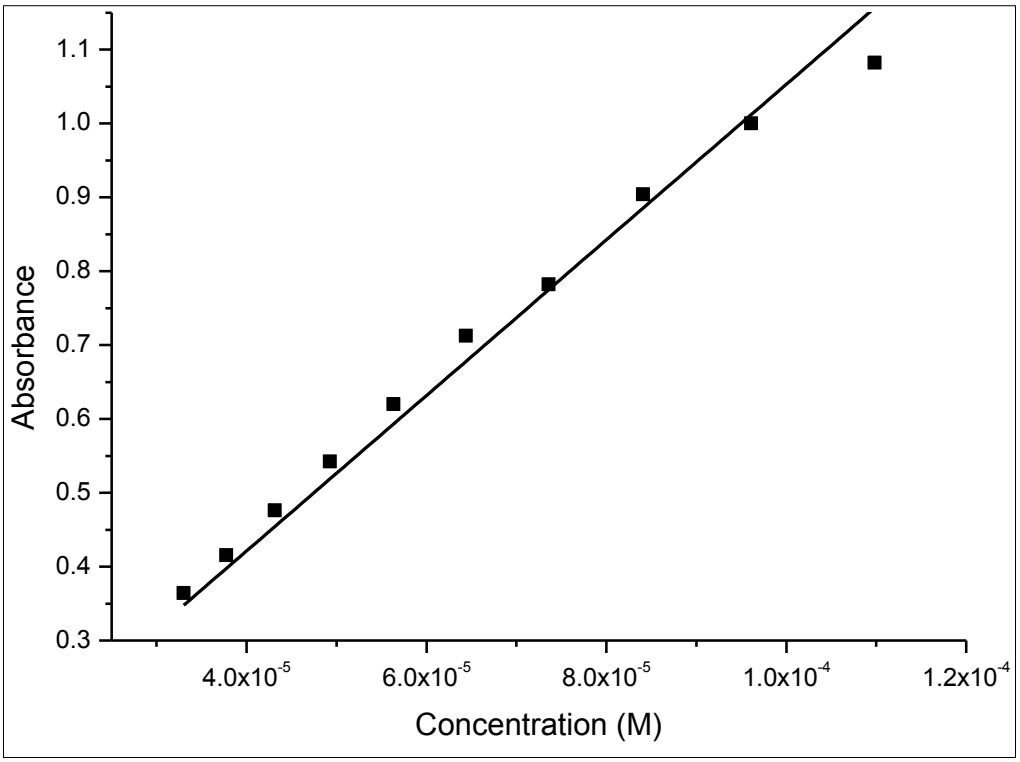

Figure 4.5 A plot of the absorbance versus the concentration of BCN-rhodamine at a wavenumber of 559 cm^{-1}, whereby the extinction coefficient can be obtained from the slope of the graph due to the Beer-Lambert law.

Using the calculated extinction coefficient, in theory, it would be possible to use the absorbance values at 559 cm^{-1} of the polymers clicked to the dye to calculate the actual ratios of the monomers in the synthesised polymers. Previously, there have been issues using BCN-rhodamin for the dye test, as there have been difficulties with removing free rhodamin from the system.[19] Therefore, in this study, the dye-functionalised polymers were dialysed to remove the free rhodamin from the system before conducting the 'dye' test. It was found that the actual ratios, seen in Table 4.1, depicted monomer ratios that were higher than those expected based on the ratios in the monomer mixture. Since, the major component of the polymer is the spacer monomer, pre-determined by the feed ratio of the monomers, it is believed that there is still free rhodamin in the system, accounting for the higher than expected results.

4.2.3 Gelation characteristics of polyisocyanopeptide hydrogels

The polyisocyanopeptides in aqueous medium were seen to be in liquid state below 18 °C, upon heating the solution gelled, as seen in Figure 4.6.

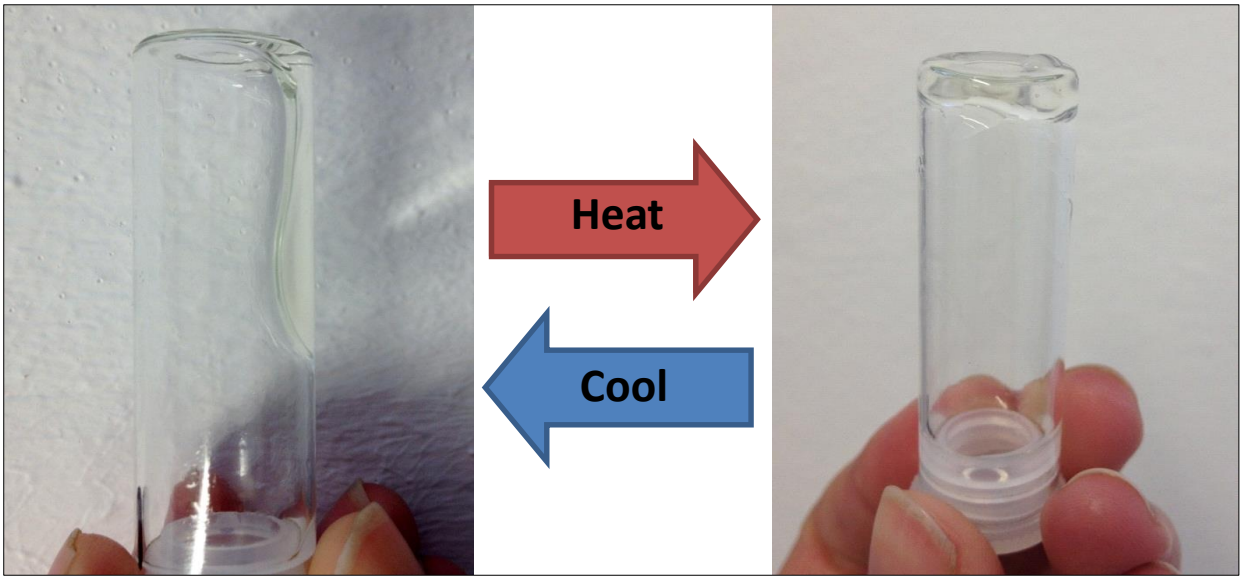

Figure 4.6 When heated, polyisocyanides in aqueous solution transition from liquid state (left, 12 °C) to gel state (right, 25 °C).

The theory of the bundle size being independent of concentration was investigated through fluorescence microscopy, as seen in Figure 4.7. A concentration series of **P3** in aqueous medium was visualised using super-resolution fluorescence microscopy, while the polymer was in gel state. The images seen in Figure 4.7 are three-dimensional structured illuminations of a conglomeration of z-stack images of the gels. Using POV-ray and a Python-based program, it was possible to create a reconstruction of the gels from the z-stacks.[20] These images are shown in Figure 4.8. These 3D-reconsititutions were carried out by Willie Pretorius (Department of Engineering, Stellenbosch University) under the guidance of Thomas Nielser.

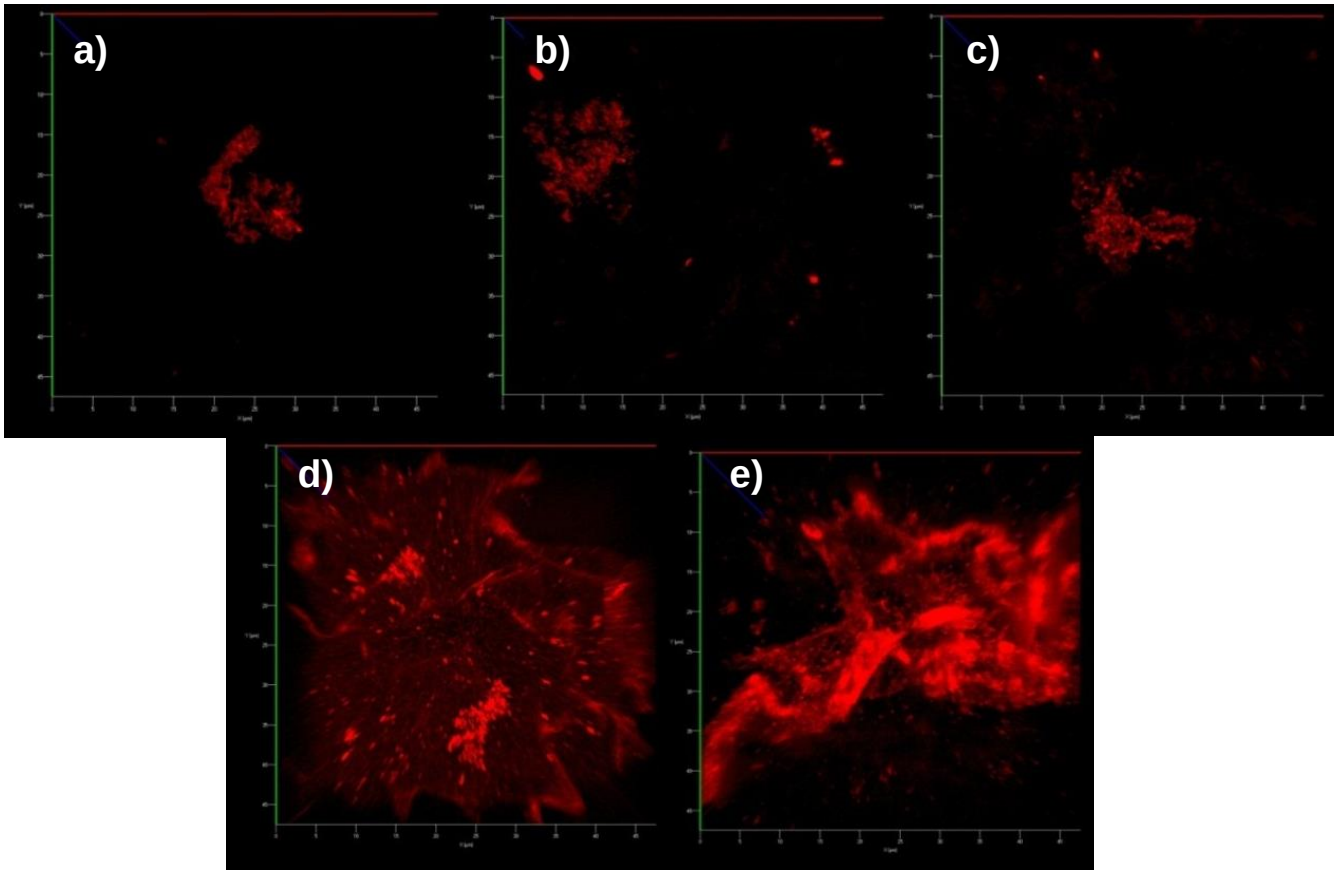

Figure 4.7 Visualisation of a concentration series of P3, with concentrations ranging from 0.125 to 2.00 mg/mL in water, using fluorescence microscopy, where a) 0.125 mg/mL, b) 0.25 mg/mL, c) 0.50 mg/mL, d) 1.0 mg/mL, and e) 2.0 mg/mL. 1 unit on Scale bar: 5 µm.

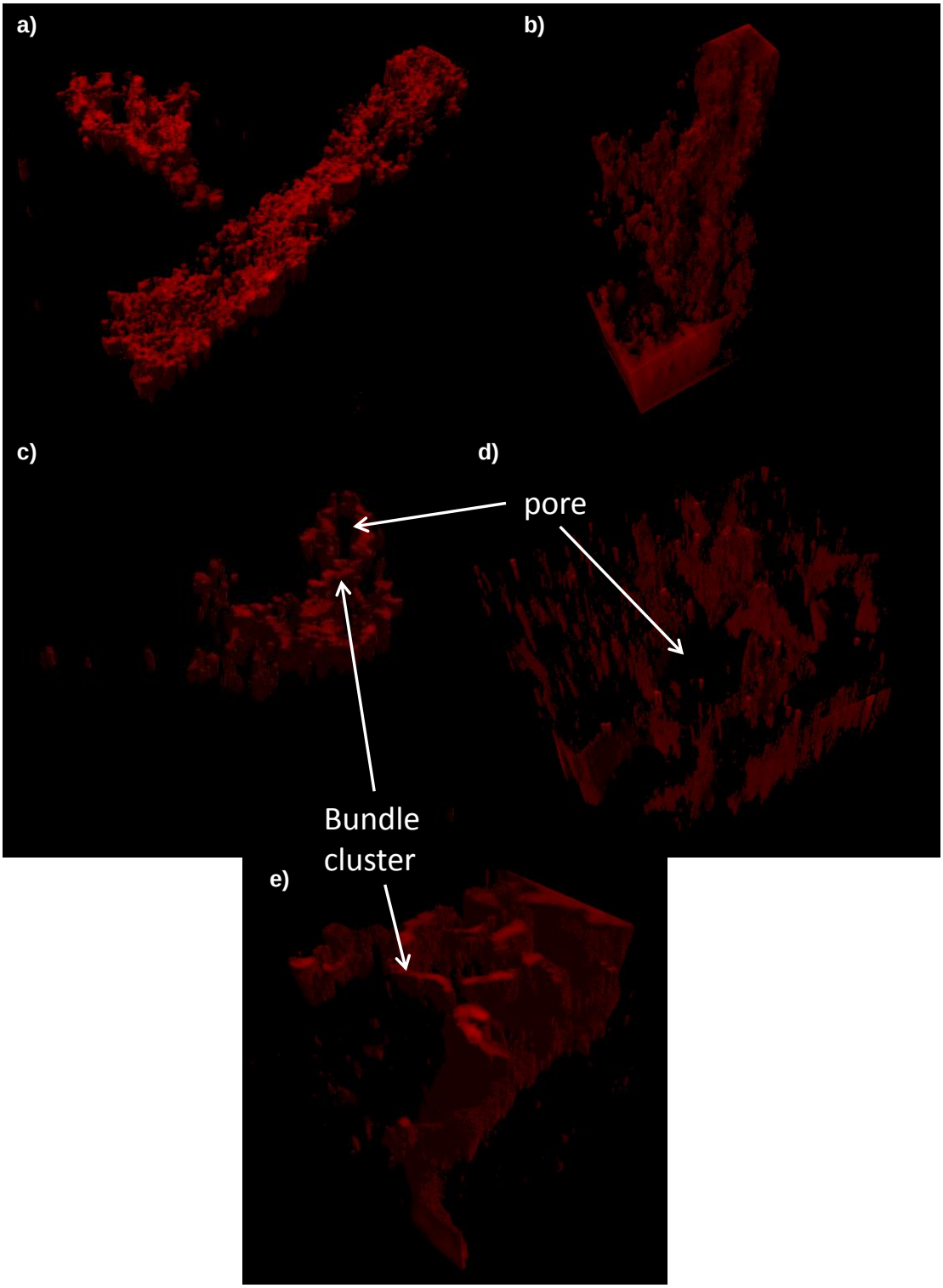

Figure 4.8 3D reconstruction of z-stacked fluorescence microscopy images of different concentrations of polymer in aqueous medium in gel state, where a) 0.125 mg/mL b) 0.25 mg/mL c) 0.5 mg/mL d) 1 mg/mL e) 2 mg/mL.

According to the results from AFM, as mentioned above, the bundles are approximately 1.4 nm in size, and bundle number is 6.9.[8] Since the super resolution fluorescence microscope has a resolution of 100 nm, it was not possible to visualise the individual cluster of bundles. Furthermore, the pores seem to be smaller or similar in size compared to the pixels of the images produced through the 3D reconstructions, due to this limiting resolution of the fluorescence microscope, thus, it was not possible to individually measure the size of the pores. The AFM images show pore sizes that are approximately 50 nm in diameter,[8] which would indeed be below the resolution of the microscope. As a consequence, comparative studies with the gelation theory, put forward by Rowan *et al*., were not possible. However, calculations were carried out whereby the amount of filled space in a set volume, *i.e*. the amount of gel in a pre-determine volume for each concentration sample, was determined. The calculations were carried out at three different thresholds, 15 %, 20 % and 30 %. The threshold is a measure of the intensity of the pixel colour where the pixel is seen as 'empty'. Thus a threshold of 0 % means that the pixel needs to be completely black to be regarded as 'empty', while a threshold of 200 % means that even a quite bright pixel is seen as empty. The results were plotted as a function of concentration in Figure 4.9.

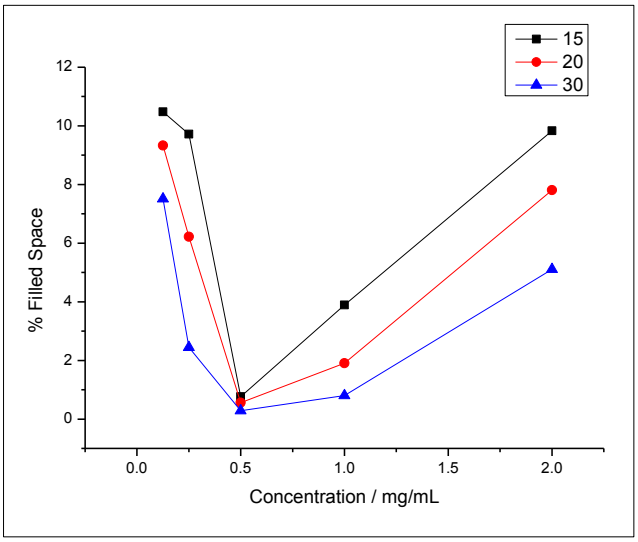

Figure 4.9 A plot of the calculated amount of the volume of space filled with polymer as a function as the concentration of polymer in the solution at three different thresholds, where black represents a threshold of 15%, red is 20 % and blue is 30 %.

A direct and linear relationship was predicted between the concentration and the percentage of filled space, or the amount of polymer in the system. This was verified between a concentration of 0.5 mg/mL and 2.0 mg/mL, where it is possible to see a linear plot, in Figure 4.9. However, samples below a concentration of 0.5 mg/mL do not fit within this linear relationship. It is believed that the limited resolution of the fluorescence microscope had an impact on the results that were obtained, especially at very low concentrations. Therefore, more investigations, at a higher resolution, would be necessary to further understand this gelation behaviour.

4.3 Conclusion

Three polyisocyanopeptide hydrogels were successfully synthesised using Ni(II)-catalysed polymerisation. The polymers were characterised using SEC, AF4, CD, FT-IR and 'dye' tests. The results correlated well to those seen in previous studies.[8] It was found that the 'dye' test cannot be used as an absolutely quantitative method to obtain the actual comonomer ratios in the polymer, due to the interference of free rhodamine in the system.

The bundling effect was studied using super resolution fluorescence microscopy, whereby z-stack images were taken of the gel and subsequently the images were re-constructed into 3D representations of the gel. Although, it was possible to see pores and bundles, no conclusions could be drawn regarding the influence of concentration on the pore size, as the resolution of the z-stack images was below the size of the pixels of the 3D simulations. The fluorescence microscope has a resolution of 100 nm, which should have been sufficient for the visualisation of the gel structures; however, due to the gel being a dynamic system, it is possible that the movement of the gel caused the images to blur slightly, which reduced the resolution of the images. The percentage of filled space of each 3D simulation was calculated, and thereafter plotted as a function of concentration. A linear relationship was found above a concentration of 0.5 mg/mL. It was concluded that more investigations, using higher resolution imaging, would be necessary to come to solid conclusions regarding the relationship between polymer concentrations and bundle and pore sizes of the gel.

4.4 Experimental

4.4.1 General

Chemicals

All chemicals were purchased from Merck or Sigma Aldrich and used without further purification, unless stated otherwise. The 'spacer monomer' was purchased from Chiralex. It was purified via column chromatography (eluent: 30 % Acetonitrile/CH_2Cl_2).

CD analysis

CD spectra were measured using a Chirascan-Plus CD spectrometer with a 150 W air cooled Xe lamp light source. A high-performance UV-vis photomultiplier tube was used as a detector. Pro-Data control and viewer, CDNN secondary structure analysis software and APL data converter were used for data acquisition. Samples were scanned between 200 and 800 nm at a temperature of 25 °C.

FT-IR analysis

All FT-IR measurements were performed using Thermo Nicolet iS10 FT-IR spectrometer. Omnic software (version 6.0a) was used for instrument control and data analysis. 32 scans were performed for each sample, and they were scanned between 650 and 4100 cm^{-1}.

SEC analysis

SEC was measured using a Shimadzu LC-10AT isocratic pump and a Waters 717+ autosampler. The column system was fitted with a PSS guard column (50×8 mm) in series with three PSS GRAM columns (300×8 mm, 10 µm, 2 × 3000 Å and 1 × 100 Å) and a temperature of 40 °C was maintained. The polymer was detected using a Waters 2487 dual wavelength UV detector and a Waters 2414 differential refractive index (DRI) detector. The eluent was dimethylacetamide (DMAc) which was stabilised with 0.05 % BHT (w/v) and 0.03 % LiCl (w/v). The flow rate was 1 $mL.min^{-1}$. Before injection, the polymer samples were filtered through 0.45 µm GHP filters. This was done to remove any possible impurities. PMMA standard sets (690 $g.mol^{-1}$ to 1.2 x 10^6 $g.mol^{-1}$) (Polymer Laboratories) were used as calibration standards. Millennium32 software (version 4) was used for data acquisition.

AF4 analysis

The experiments were performed on an ambient temperature AF4-Instrument (AF2000, Postnova Analytics, Landsberg/Germany) which was coupled to a MALLS- (PN3609, Postnova Analyticsm Landsberg/Germany) and a RI-detector (PN 3140, Postnova Analytics, Landsberg/Germany). The channel was connected to three different pumps (tip, focus and cross-flow) while the injection port was coupled to an autosampler (PN 5300, Postnova Analytics, Landsberg/Germany). The membrane was a regenerated cellulose membrane with an average cut-off of 10 000 Da. The Mylar spacer used for definition of the channel height had a thickness of 350 µm.

UV-vis analysis

An AnalytikaJena Specord 210 plus was used to measure UV-vis spectroscopy. The software used for data acquisition was WinASPECTPlus (Version 4.1.0.0). The absorbance of the samples was measured at 559 nm. (For the extinction coefficient study samples were measured between 200 and 800 nm.)

Fluorescence microscopy

A Carl Zeiss Confocal LSM 780 Elyra S1 with SR-SIM super resolution platform was used for confocal and super resolution imaging of the gels. An alpha Plan-Apochromat 100 x/1.46 Oil DIC M27 Elyra objective was used.

Time-lapse imaging was used for the liquid to gel transition visualisation. It was done using MBS: MBS 458/561, MBS_InVis: Plate and FW1: NoneLSM beam splitters and a 561 nm laser. The images were taken on a single plane, on time-lapse mode.

Super-resolution imaging was done with FW1: BP 570-620 + LP 750 Beam splitters and a 561 nm laser. The exposure time was 80.0 s and 3 SIM rotations were done. Z-stacking images were obtained with z scaling of 0.05-0.1 µm.

3D Simulations

POV-ray 3.7.0 (Persistence of Vision(tm) Ray Tracer Version 3.7.0) was used to create the 3D reconstructions from .TIF files obtained from the super resolution fluorescence microscope. The 3D images were then generated and the volumes were calculated using a Python (version 2.7.6)-based program. The simulations and calculations were carried out by Willie Pretorius, under the guidance of Thomas Niesler.

4.4.2 Polymerisation protocol

Stock solution for $Ni(II)(Cl_2O_4)_2 \cdot 6\ H_2O$ Catalyst

A 100 mL volumetric flask was charged with Ni(II) perchlorate hexahydrate (39 mg, 0.11 mmol) was dissolved in 10 mL absolute ethanol and stirred for ca. 1 h, or until fully dissolved. Thereafter, the solution was diluted with 90 mL freshly distilled toluene, and allowed to keep, up to a maximum of four weeks.

General polymerisation protocol

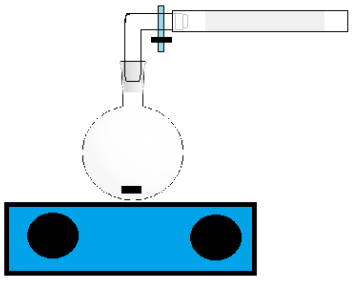

The glassware was dried for 2 h in an oven at 170 °C. A drying tube containing calcium chloride was placed onto the RBF as soon as it was removed from the oven.

The total mass of 'azide monomer' for all polymerisations was dissolved in 1 mL freshly distilled toluene.

The total mass of spacer monomer used in all polymerisations was dissolved in 1 mL freshly distilled toluene.

The two monomers were both added to the RBF in the correct ratios, as indicated in Table 4.1, and cooled to 0 °C. This mixture was stirred. Thereafter, the correct volume of Ni (II) catalyst (1:10 000, Ni(II) catalyst : spacer monomer) was added to the mixture. Freshly distilled toluene was added to make up a final monomer concentration of 25 mg/mL. The reaction was stirred at 0 °C and allowed to reach RT on its own, and the polymerisation reaction was ran for 72 h. Afterwards the reaction was stopped by opening the flask and diluting with minimal CH_2Cl_2, and the polymer was isolated by precipitation from diisopropyl ether and dried. The polymer was then re-dissolved in minimal CH_2Cl_2 and re-precipitated, this was repeated three times. Finally, the dried, brown polymer was weighed and stored in the freezer. Varying yields of 59 % – 86 % were obtained.

The 'dye test'

Polymer (3.0 mg) was dissolved in 3 mL CH_2Cl_2, and the solution was stirred for 1 h at r.t. A stock solution of BCN-rhodamine (1.64 mg/mL) was prepared in CH_2Cl_2. BCN-rhodamin was added in a mole ratio of 2:1 BCN-rhodamin to moles of azide functionality present in the polymer. The solution was stirred for 1 h at r.t. Afterwards the polymer was isolated by precipitation from diisopropyl ether, several times, until

colour of the dye was no longer visible in the filtrate. The polymer was then dried and weighed. The UV-vis absorbance at 559 cm^{-1} was measured and plotted as a function of concentration and the concentration of azide functionality present in the polymer was deduced. The results are shown in Table 4.1.

4.5 References

(1) Millich, F. *Chem Rev* **1972**, *72*, 101.
(2) Nolte, R. J. M. a. D., W. *Acc Chem Res* **1979**, *12*, 30.
(3) Nolte, R. J. M. *Chem Soc Rev* **1994**, *23*, 11.
(4) Cornelissen, J. J. L. M.; Rowan, A. E.; Nolte, R. J. M.; Sommerdijk, N. A. J. M. *Chem Rev* **2001**, *101*, 4039.
(5) Schwartz, E., Koepf, M., Kitto, H. J., Nolte R. J. M. & Rowan, A. E. *Polym Chem* **2011**, *2*, 33.
(6) Deming, T. J.; Novak, B. M. *Macromolecules* **1991**, *24*, 326.
(7) Koepf, M.; Kitto, H. J.; Schwartz, E.; Kouwer, P. H. J.; Nolte, R. J. M.; Rowan, A. E. *Eur Polym J* **2013**, *49*, 1510.
(8) Kouwer, P. H. J.; Koepf, M.; Le Sage, V. A. A.; Jaspers, M.; van Buul, A. M.; Eksteen-Akeroyd, Z. H.; Woltinge, T.; Schwartz, E.; Kitto, H. J.; Hoogenboom, R.; Picken, S. J.; Nolte, R. J. M.; Mendes, E.; Rowan, A. E. *Nature* **2013**, *493*, 651.
(9) Lutz, J. S., H. *Polymer* **2008**, *49*, 817.
(10) Kitto, H. J.; Schwartz, E.; Nijemeisland, M.; Koepf, M.; Cornelissen, J. J. L. M.; Rowan, A. E.; Nolte, R. J. M. *J Mater Chem* **2008**, *18*, 5615.
(11) Dommerholt, J.; Schmidt, S.; Temming, R.; Hendriks, L. J. A.; Rutjes, F. P. J. T.; van Hest, J. C. M.; Lefeber, D. J.; Friedl, P.; van Delft, F. L. *Angew Chem Int Ed* **2010**, *49*, 9422
(12) Agard, N. J.; Prescher, J. A.; Bertozzi, C. R. *J Am Chem Soc* **2004**, *126*, 15046.
(13) Turner, R. B., Jarrett, A. D., Goebel, P. & Mallon, B. J. *J Am Chem Soc* **1973**, *95*, 790.
(14) Cornelissen, J. J. L. M.; Sommerdijk, N. A. J. M.; Nolte, R. J. M., PhD Dissertation, Radboud University, 2001.
(15) Schwartz, E.; Palermo, V.; Finlayson, C. E.; Huang, Y.-S.; Otten, M. B. J.; Liscio, A.; Trapani, S.; González-Valls, I.; Brocorens, P.; Cornelissen, J. J. L. M.; Peneva, K.; Müllen, K.; Spano, F. C.; Yartsev, A.; Westenhoff, S.; Friend, R. H.; Beljonne, D.; Nolte, R. J. M.; Samorì, P.; Rowan, A. E. *Chem Eur J* **2009**, *15*, 2536.
(16) Giddings, J. C.; Yang, F. J. F.; Myers, M. N. *Science* **1976**, *193*, 1244.
(17) Giddings, J. C. *Science* **1993**, *260*, 1456+.
(18) Mabesoone, M.; Rowan, A. E.; Kouwer, P. H. J.; Jaspers, M., BSc Dissertation, Radboud University, 2013.
(19) Voerman, D.; Eksteen-Akeroyd, Z. H.; Rowan, A. E., MSc Dissertation, Radboud University, 2014.
(20) Pretorius, W. & Niesler, T. B.Eng(HONS) Dissertation, Stellenbosch University, 2014.

Chapter 5: Polymer Conjugation and Physiological Testing

Abstract

Polyisocyanopeptide hydrogels functionalised with oligo(ethylene glycol) side chains were decorated with C**IKVAV** and cyclo(**RGD**fC) epitopes attached to dibenzocyclooctyne-maleimide, through copper-free click chemistry. The Kaiser test was used to verify the attachment of the epitopes onto the polymer. Cell viability tests showed that the decorated polymers were non-cytotoxic. The decorated polymers were, subsequently, tested for their ability to facilitate the cell attachment and process formation of GT1-7 cells. After incubation, Hoechst viability assessment and also MitoTracker Green tests were used to assess this differentiation of cells. The extent of the formation of mitochondrial networks in the cells was assessed by calculating the surface area of the networks using Python. It was found that the **IKVAV** epitope promoted neurite outgrowth in the cells more than the **RGD** epitope. However, it was also seen that the cells show better differentiation with more prominent mitochondrial network formation in the growth medium control than in the growth medium containing the gel.

5.1 Introduction

Laminins are a family of glycoproteins that form a major component of basement membranes.[1,2] At least 14 isoforms of the five α, three β and three γ chains are known. Laminin-1 is made up of three chains, α1, β1, and γ1, held together by disulphide bonds, and it has been shown to be involved in many biological functions, such as cell adhesion, migration, neurite outgrowth, tumour metastasis and angiogenesis.[3] Studies have found that this glycoprotein is over-expressed in the brains of patients suffering from Alzheimers and Down syndrome.[4] There have been many investigations surrounding laminins, whereby all the chains have been cloned and sequenced. A peptide sequence, Ile-Lys-Val-Ala-Val **(IKVAV**), seen in Figure 5.1 (right), was found at the C-terminus of the α-1 chain. This motif has been identified as an active region within Laminin-1,[5] and it is required for the biological activity of the protein.

Arg-Gly-Asp (**RGD**), seen in Figure 5.1 (left) is another well-known peptide motif, which is found in the cell-binding domain of fibronectin.[6] This epitope has been extensively studied and identified as the cell adhesion site for many proteins within

the extracellular matrix (ECM), blood and on the cell's surface.[7,8] By incorporating the **RGD** sequence into synthetic peptides it is possible to mimic the binding activity of the adhesion proteins. It is therefore possible to use **RGD** peptides, and mimics thereof, to promote cell migration, growth, differentiation and apoptosis within biological systems. Moreover, **RGD**s are being studied with the intent to find applications within pharmaceuticals.

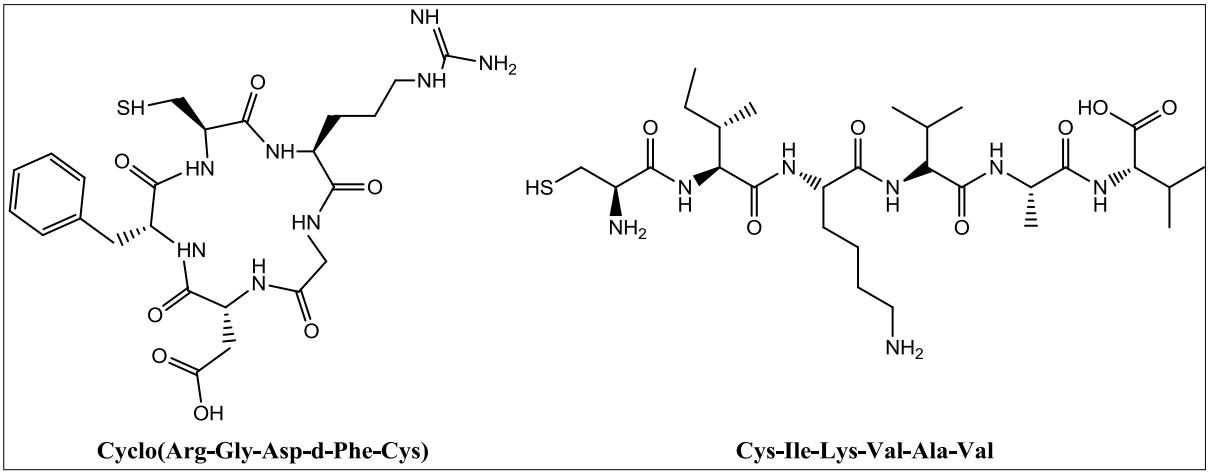

Figure 5.1 The structures of Cyclo(RGDfC) (left) and CIKVAV (right) are shown

The primary aim of the current study is to establish the ability of a hydrogel decorated with the C**IKVAV** epitope to promote neurite outgrowth in hypothalamic neuronal mouse (GT1-7) cells. As mentioned in **Chapter** 2, there have been various scaffolds that have been tested in this regard. However, none have shown as promising ECM-mimicking capabilities as seen in these polyisocyanopeptide hydrogels. Therefore, these polymers have been targeted as a possible tissue-engineering scaffold.

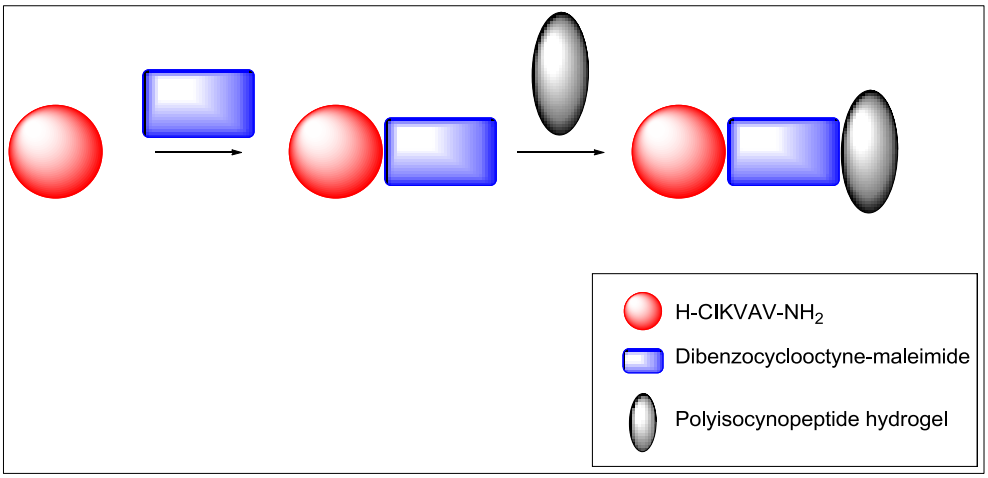

Scheme 5.1 General protocol for the preparation of the decorated polyisocyanopeptide hydrogels

In order to test the establish the ability of the polymers to promote process formation, the development and adhesion of cells, in GT1-7 cells, it will be necessary to be link the **IKVAV** epitope to the hydrogel through a dibenzocyclooctyne-linker, by copper-free click chemistry.[9] The general approach for this is seen in Scheme 5.1. The dibenzocyclooctyne-maleimide moiety will be introduced onto the C**IKVAV** epitope by means of a Michael addition. Thereafter, the hypothalamic neuronal mouse (GT1-7) cells will be seeded into the polymer solution in growth medium. The seeding will be carried out at a low enough temperature so that the polymer solution is in the liquid state, while ensuring that the cells do not die due to the cold. Thereafter, the seeded polymer solution will be incubated to 37 °C. The viability and efficacy of polyisocyanopeptide hydrogels decorated with **IKVAV** as scaffolds for the promotion of neurite outgrowth will be tested using fluorescence microscopy, with the aid of fluorescent markers, *i.e*. propidium iodide (PI), Hoechst 33342 (Hoechst) and MitoTracker Green (MTG). The hydrogels will also be decorated with cyclo(Arg-Gly-Asp-D-Phe-Cys) (Cyclo(RGDfC)) which will be used as a control in the cell testing. This decorated hydrogel will be prepared in the same manner as mentioned above.

5.2 Results and Discussion

5.2.1 Epitope preparation

The **IKVAV** peptide contains a cysteine amino acid attached to the isoleucine, H-C**IKVAV**-NH_2, so that the thiol functional group can be used to attach the peptide sequence to dibenzocyclooctyne-maleimide, seen in Scheme 5.2, to yield compound **27a**. Since cyclo(**RGD**fC) also contains a thiol group, the same general procedure can be followed in the synthesis of compound **27b**. The addition of the thiol to a cyclooctyne was done as illustrated in Scheme 5.2, whereby dibenzocyclooctyne-maleimide was reacted with the C**IKVAV** peptide through a Michael addition.[10] Since, dibenzocyclooctynes are stable and unreactive with thiols and amines, the Michael addition will only occur at the maleimide position, and thus it will not disrupt the cyclooctyne ring when coupling the peptide sequence to the cyclooctyne compound.[11]

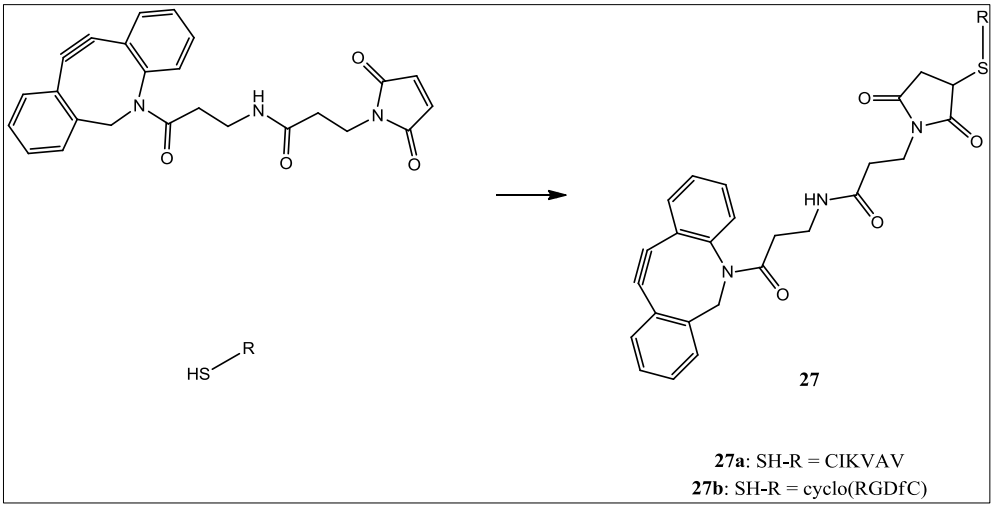

Scheme 5.2 Michael addition reaction between the thiol functional group on the CIKVAV and cyclo(RGDfC) peptide sequences with the dibenzocyclooctyne-maleimide to obtain the peptide with a functional group that can be 'clicked' copper free onto the polymer.

Both of the reaction mixtures formed precipitates, therefore, at the end of the reaction, the mixtures were centrifuged. The pellets were separated from the supernatant, and both the pellet and supernatant were analysed by LC-MS. The chromatograms for the pellets are seen in Figure 5.2 and Figure 5.3, for compounds **27a** and **27b**, respectively. It was found that the pellet contained a higher

concentration of the products and a lower concentration of the reagents, where **27b** was seen to elute at 4.66 minutes. The LC-MS spectrum for the pellet of **27a**, did not show a sharp peak as a representation of the product eluting. Instead, a broad band with a number of compounds eluting was seen. It is believed that this is possibly due to the formation of a mixture of diastereomers due to the chiral centre formed between the thiol and the maleimide. Furthermore, it is possible that intramolecular hydrogen bonds form, causing the compound to interact slightly differently with the LC column, thus the product shows a broad elution time.

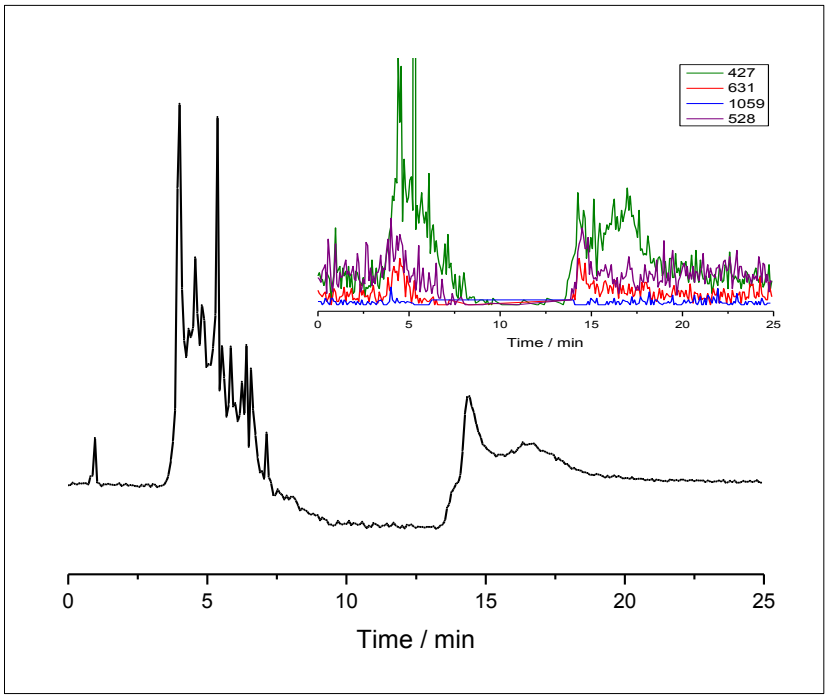

Figure 5.2 LC-MS Chromatogram of the pellet obtained in the synthesis of 27a. Main chromatogram: Total ion chromatogram (TIC); Insert: Extracted Ion Chromatogram with red representing the CIKVAV reagent (m/z 630-631), green represents the dibenzocyclooctyne-maleimide reagent (m/z 427-428) and the purple and blue chromatograms represent the product (m/z 529-531, which is the doubly charged species and m/z 1059-1060, respectively).

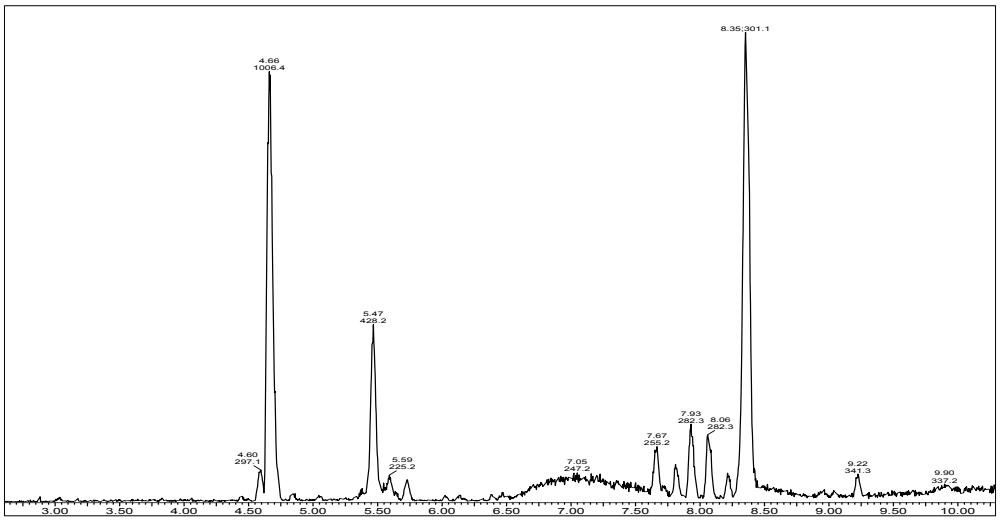

Figure 5.3 LC-MS spectra of the pellet of 27b. The peak that eluted at 4.66 minutes is compound 27b, and the compound that eluted at 5.47 minutes is the reagent dibenzocyclooctyne.

5.2.2 Polymer functionalization

Table 5.1 Sample names and components of each of the decorated polyisocyanopeptides

Sample name	Components
28a	P2 + dibenzocyclooctyne + CIKVAV + BCN-maleimide
28b	P2 + dibenzocyclooctyne + cyclo(RGDfC) + BCN-maleimide
28c	P2 + dibenzocyclooctyne + BCN-maleimide
28d	P2 + BCN-maleimide

It is then possible, using Cu-free click chemistry, to use the dibenzocyclooctyne as a linker between the polymer and the epitopes. It has been observed that electron-withdrawing groups, attached to the cyclooctyne, may increase the rate of the Cu-free click reaction.[11] Dibenzocyclooctyne has been shown to react quickly with azides to produce triazoles with quantitative yields. Due to difficulty in purifying **27a** and **27b**, the pellets for both were used without further purification to functionalise **P2** (Table 4.1 page 62) with the **IKVAV** and the **RGD** epitopes forming **28a** and **28b**, respectively, following the method described in Scheme 5.3. The polymer is only able to react with a cyclooctyne-containing compound in the Cu-free click reaction

conditions. Therefore, any remaining free-C**IKVAV** or cyclo(**RGD**fC) reagents in **27a** and **27b**, respectively, would be removed from dialysing the polymer system after conjugation. In order to eliminate any interference in possible results, a control, **28c**, was prepared whereby the polymer was clicked to unreacted dibenzocyclooctyne-maleimide, as this reagent was still present in both **27a** and **27b**. A final polymer control, **28d**, was prepared from **P2**-coupled only to BCN-rhodamine. **28d** was prepared due to the presence of BCN-rhodamine in each of the other decorated polymers. Each of the decorated polymers and their components are described in Table 5.1, above.

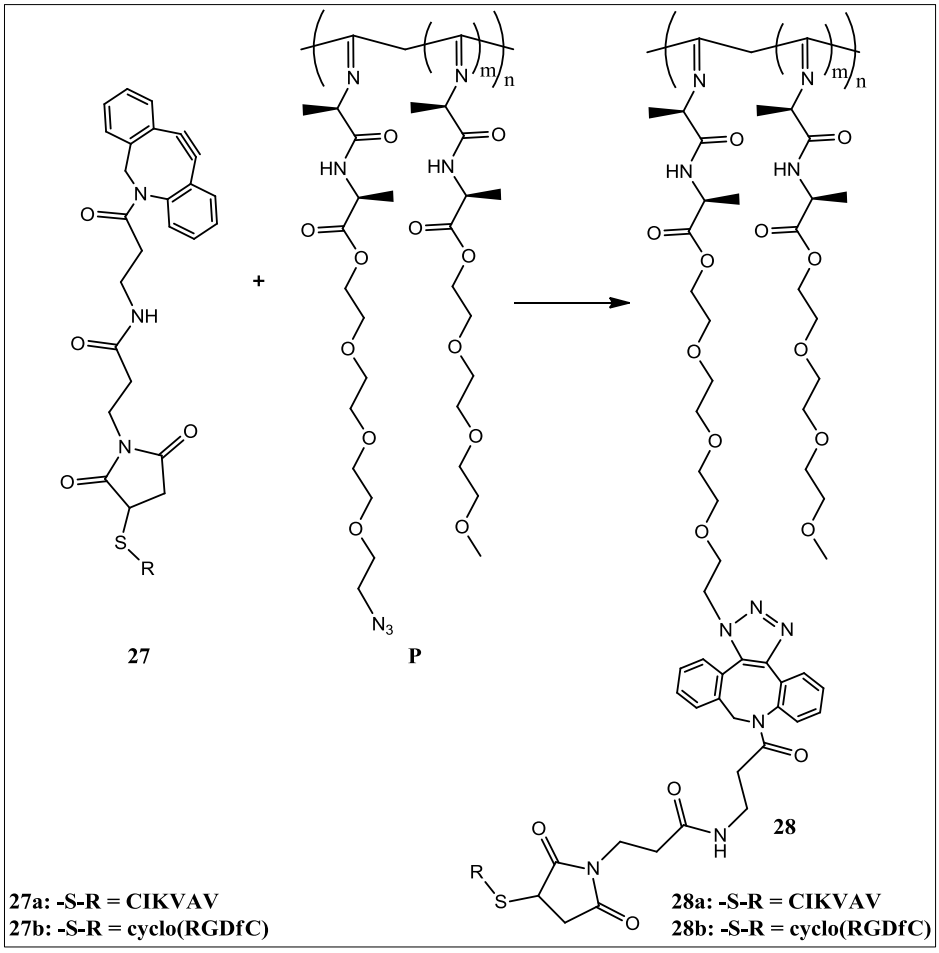

Scheme 5.3 This represents the Cu-free 'click' chemistry whereby CIKVAV or cyclo(RGDfC) epitopes attached to the dibenzocyclooctyne linker are reacted with the azide pendant group on the polymer.

Due to the low spacer monomer to 'azide monomer' feed ratio, NMR spectroscopy is not sensitive enough to show whether the epitopes were successfully conjugated to the polymer. Therefore, the Kaiser test was performed to verify this.[12] This test, also known as the ninhydrin test, is able to detect the presence of primary amines through a colour change from yellow (negative) to blue-green (positive). The strength of the colour is directly related to the concentration of primary amines. Dialysis was used in order to purify the decorated polymer, before the Kaiser test was performed. The results of the test are seen in Figure 5.4.

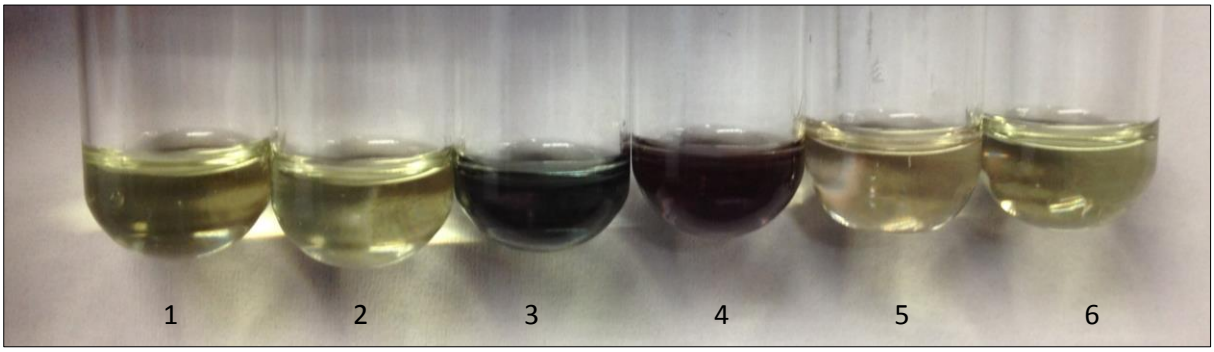

Figure 5.4 The visual results of the Kaiser test, where 1) Control, 2) P2, 3) 28a, 4) 28b, 5) 28c and 6) 28d.

Negative results for the Kaiser test are seen in the **Control** (Test tube 1), containing only DMF and the reagents for the Kaiser test, **P2** (Test tube 2), **28c** (Test tube 5), and **28d** (Test tube 6), as seen in Figure 5.4, which correspond to the lack of primary amines in all of the samples. However, the samples containing **28a** (Test tube 3) and **28b** (Test tube 4), also seen in Figure 5.4, show a positive result for the Kaiser test, which indicates that the **CIKVAV** and cyclo(**RGD**fC) epitopes were successfully clicked to **P2** in **28a** and **28b**.

5.2.3 Polymer testing with cells

Initially, a test reaction, S1, was done using GT1-7 cells and a solution of **28d** in growth medium (made from Dulbecco's modification of Eagle's medium (DMEM), antibiotics and anti-fungal agent) to acquire the cytotoxicity of the polymer. It has been found that a more desirable outcome is achieved when cell cultures are introduced to the hydrogel before the sol-gel transition has taken place. This is due

to the pores of the hydrogel being smaller than a cell's diameter.[13] Therefore, the GT1-7 cells were seeded into a solution of polymer in growth medium, below the gelation temperature. Thereafter the cell-polymer solution was incubated at 37 °C, which is the correct physiological temperature for the cells as well as being above the gelation temperature of the hydrogel, thus the cell-polymer solution was in gel state. In cell studies, it is important to have a way of identifying the viability of the cell as well as a manner in which to determine the effect that a specific study has on the cells being investigated. Staining cells with fluorescent compounds allows for visualisation of the cell and further provides a large amount of information about the cell function. It is possible to target specific cell activities as well as cell structures, including cell membranes, organelles, proteins and nucleotides. It has become convention to stain cells with various fluorescent markers for which the cell membrane is permeable or impermeable. The viability of the cells was visualised after 24 h of incubation by adding propidium iodide (PI) and Hoechst dye to the cell samples. PI intercalates with the DNA double helix,[14] whereas Hoechst attach themselves to the minor groves of the DNA double helix.[15,16] At physiological conditions, Hoechst molecules are positively charged and are, therefore, able to move through the viable cell membrane. Thus, they are used to evaluate the nuclear morphology of cells within the cytoplasm.[17] Hoechst can also be used to assess pathogen nuclear morphology, such as nuclear condensation, which is an indication for apoptotic cell death. If PI is able to permeate the cell membrane, *i.e*. the cell is stained red, it indicates necrotic cell death. Viable cell membranes are impermeable to PI.[18] No quantifiable difference was seen between the viability of the cells seeded in only growth medium (**Control**) and in the presence of **28d**. The images are seen in Figure 5.5 (**Control**) and Figure 5.6 (**28d**). Thus, the polymer was judged to be non-cytotoxic. Some debris was seen around the cells. However, the cells did not seem to show signs of distress as adhesion took place and there was little cell death. The debris did not contain DNA as they did not illuminate as blue from Hoechst dye. Therefore, it was concluded that the debris was not a bacterial contamination, and was not considered important to the cell study.

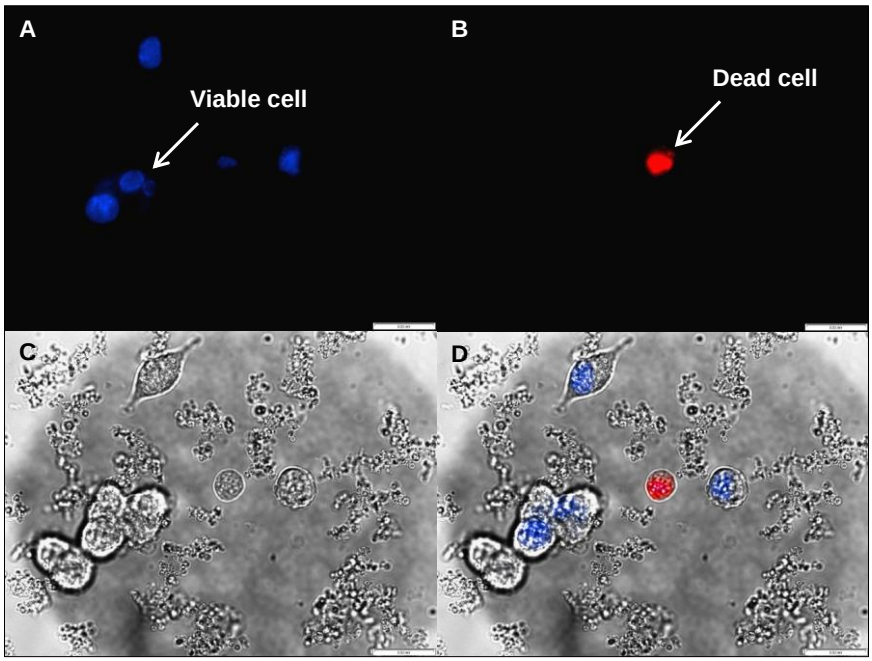

Figure 5.5 Fluorescence micrographs and transmission micrographs of the Control of the cytotoxicity test, S1, after incubation for 24 h and after PI and Hoechst dye were added to the samples. The channels used were A) blue, B) red, C) transmission and D) all channels. Scale bar: 20 µm .

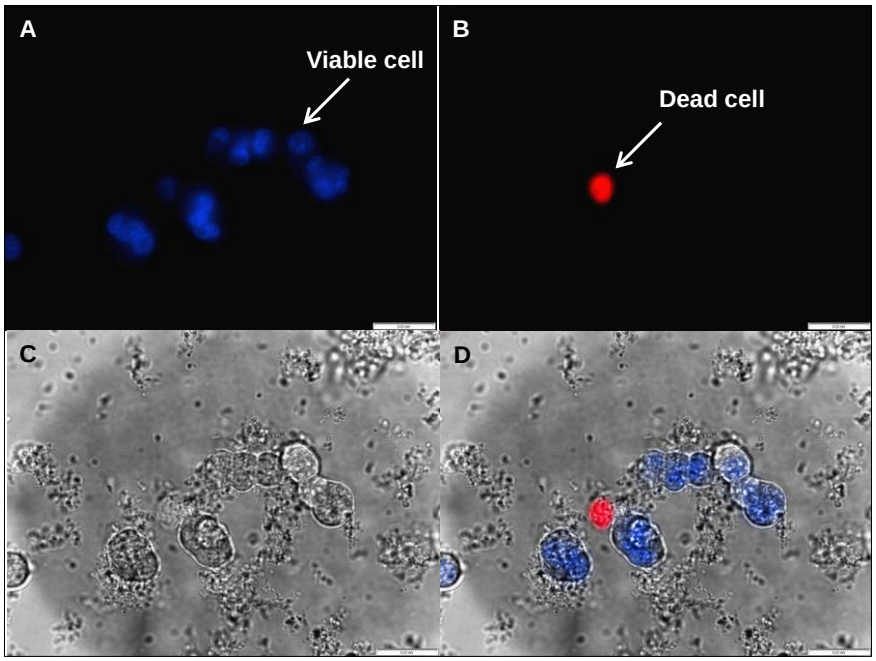

Figure 5.6 Fluorescence micrographs and transmission micrographs of the sample containing 28d (1.0 mg/mL) of the cytotoxicity test, S1, after incubation for 24 h and after PI and Hoechst dye were added to the samples. The channels used were A) blue, B) red, C) transmission and D) all channels. Scale bar: 20 µm.

Thereafter, GT1-7 cells were seeded into solutions of **28a, 28b**, **28c**, **28d** in growth medium as well as a **Control** at a cell density of 20 000 cells per sample, **S2**. After 72 h of incubation, the cell samples were stained with Hoechst and MTG. MTG is a fluorochrome that is used to stain mitochondria.[19] Mitochondria are important organelles when testing cell viability and cell function. This is due to their presence in almost all eukaryotic cells as they are the 'power house' of the cell, due to their assistance in producing adenosine triphosphate (ATP), the cell's major energy source.[20] The cell type, cell cycle and cell viability can be assessed through evaluating the shape, abundance and location of the mitochondria in the cell. MTG molecules are able to permeate the cell membrane, and their intensity signal is directly related to the concentration of ATP in the mitochondria.[19] After adding the fluorochromes to the cell samples, they were then viewed under the fluorescence microscope using blue, red, green and transmission (Trans) channels for illumination, see Figure 5.8. The images of **28c** and **28d** are in the Experimental Section below, see Figure 5.13. Due to the polymer being functionalised with BCN-rhodamine, the red illumination from the Red lamp is due to the presence of **P2**. After visualising that the decorated polymer material was not cytotoxic, use of PI was not necessary in the case of the further cell studies, as the viability of the cell can also be indicated by the morphology of the mitochondria, as they are very sensitive to the cellular health and play an important role in cell death.[21] Furthermore, a healthy and happy cell will adhere and then begin to spread, whereas a cell that is under stress or is in an undesirable environment will remain a small circle, as seen in Figure 5.7.

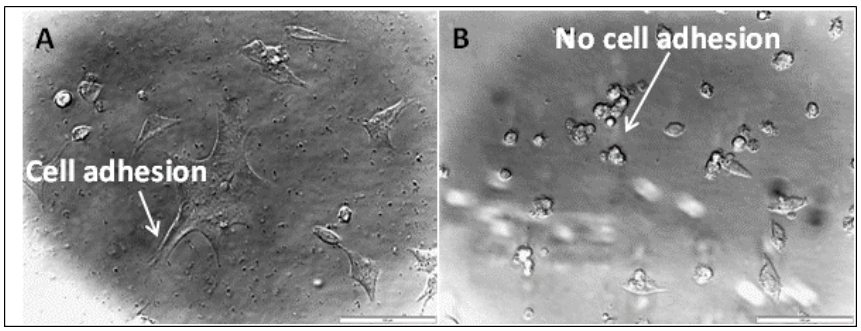

Figure 5.7 Examples of transmission micrographs indicating adhering (happy) cells (A) and cells that are not adhering (less happy) (B). Scale bar: 100 µm.

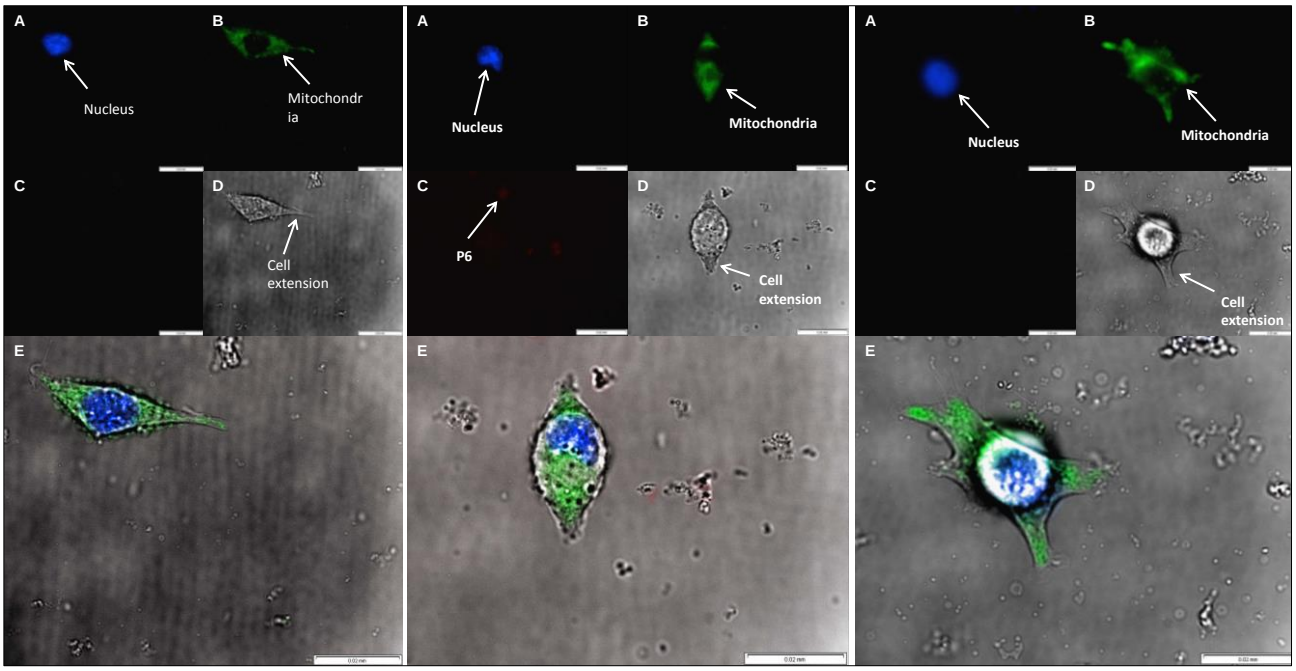

Figure 5.8 Fluorescence micrographs and transmission micrographs of the samples containing Control (left) 28a (middle) and 28b (right) in S2, after incubation for 72 h and after MTG and Hoechst dye were added to the samples. The channels used were A) blue, B) green, C) red, D) trans and E) all channels. Scale bar: 20 µm.

It was seen that the GT1-7 cells in all of the samples, including the **Control**, did not adhere as effectively as anticipated 72 hours post seeding. The seeding density was increased so that more cells per field of view could be assessed, to provide a better understanding of their adhesion. Therefore, the experiments were repeated with 30 000 GT1-7 cells per sample, **S3** and 60 000 GT1-7 cells per sample, **S4.** The cell-polymer samples were incubated for 48 h. The images for the **Control**, **28a** and **28b** in **S3** can be seen in Figure 5.9, and **28c** and **28d** can be seen in Figure 5.14, in the Experimental section. The images for **28a** and **28b** in **S4** can be seen in Figure 5.10, and **28c** can be seen in Figure 5.15. Since **S3** and **S4** were cultured on the same plate, only one **Control** was necessary for both tests, this control was cultured with 30 000 GT1-7 cell density.

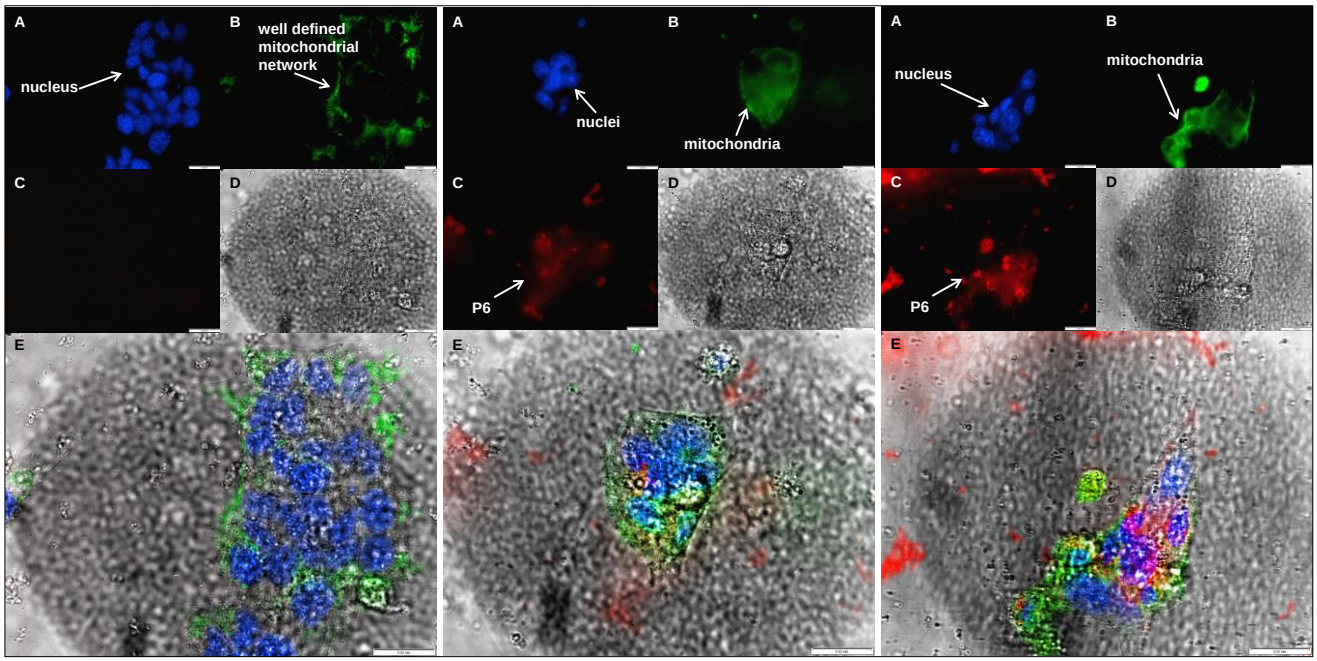

Figure 5.9 Fluorescence micrographs and transmission micrographs of the Control (left), 28a (middle) and 28b (right) for S3, after incubation for 48 h and after MTG and Hoechst dye were added to the samples. The channels used were A) blue, B) green, C) red, D) trans and E) all channels. Scale bar: 20 µm.

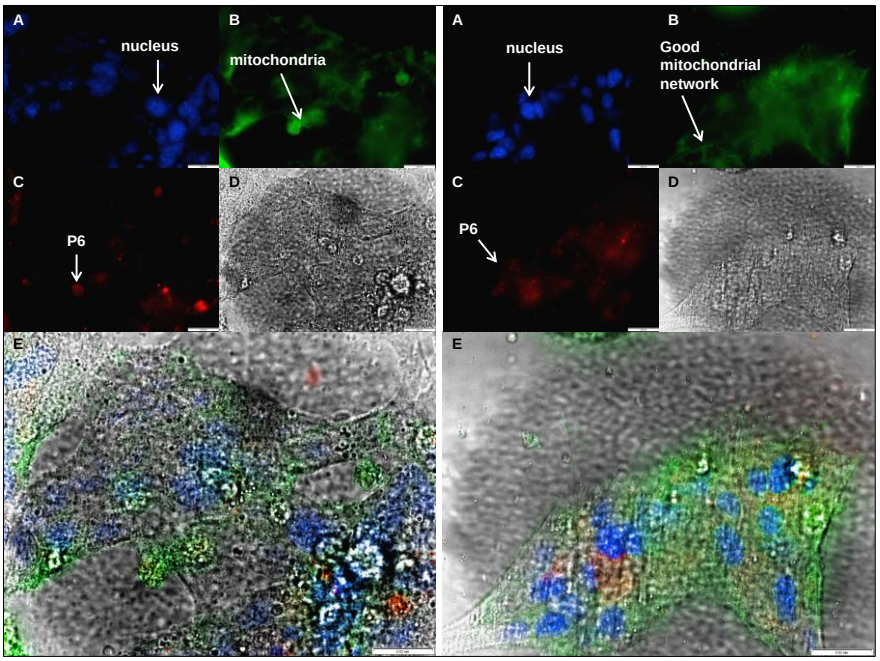

Figure 5.10 Fluorescence micrographs and transmission micrographs of the samples containing 28a (left) and 28b (right) in S4, after incubation for 48 h and after MTG and Hoechst dye were added to the samples. The channels used were A) blue, B) green, C) red, D) trans and E) all channels. Scale bar: 20 µm.

More process formation was seen with the increase in cell density. **S4**, which contained 60 000 cells per sample showed more process formation than **S3**, containing 30 000 cells per sample, seen in Figure 5.9 and Figure 5.10, for **S3** and **S4** respectively. In order to quantify this process formation one of the major techniques in life sciences was employed, whereby the mitochondrial networks, an interconnected and complex system of mitochondria,[22] are detected and quantified as a method of monitoring cell function and cell growth. Pixel-wise co-localisation analysis can be used in the determination and quantification of the extent of mitochondrial networking, although it is not always the preferred method for this analysis, as it is vulnerable to noise and background fluorescence.[23] A python-based program, was used to calculate, from images rendered by Pov-ray, the surface area of the mitochondrial network for each cell culture of **S3** and **S4.** The results are seen for **S3** in Figure 5.11 (green) and for **S4** in Figure 5.12 (green). Furthermore, it is possible to measure the surface area occupied by the cells relative to the total area within a fluorescence microscopy image. As shown in Figure 5.7, a more suitable cell environment would allow for more axon and dendrite formation, leading to larger cell surface areas. Small, round cells is an indication that the cells have undergone less process formation. Therefore, this measurement lends itself to being a quantitative measure of process formation. The surface area occupied by the cells was relative to the total area was measured using ImageJ, the results can be seen in Figure 5.11 (red) and Figure 5.12 (red), for **S3** and **S4**, respectively.

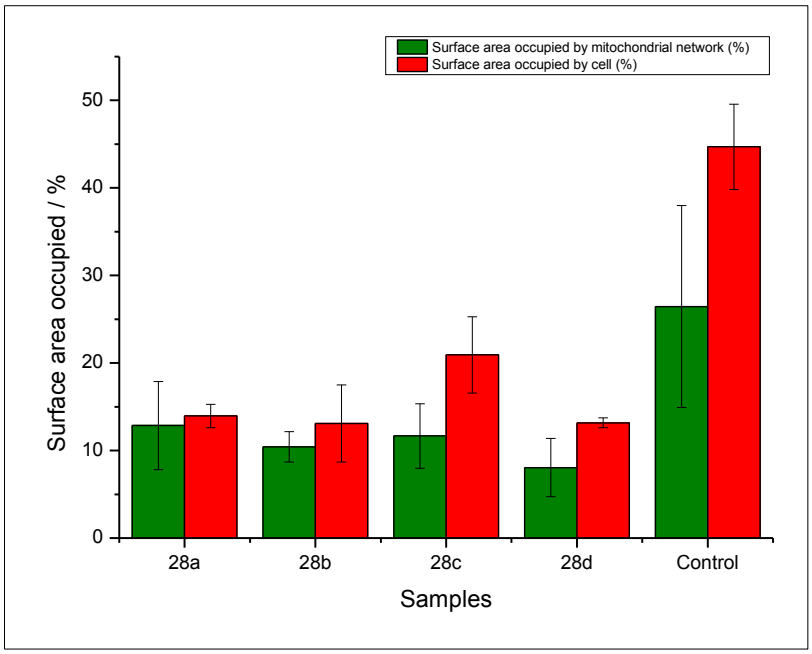

Figure 5.11 The surface area relative to the total area that is occupied by the cell (red) and by the mitochondrial network (green) in S3.

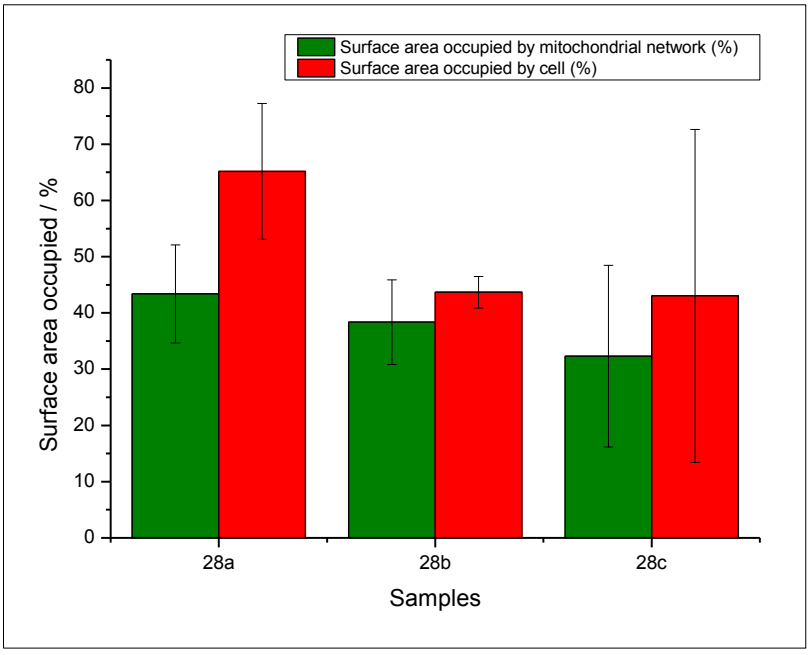

Figure 5.12 The surface area relative to the total area that is occupied by the cell (red) and the mitochondrial network (green) in S4.

The **Control** shows the largest surface area occupied by mitochondrial networking as well as the largest amount of surface area occupied by the cells. A more tubular network is seen in the **Control**, which shows that more mitochondrial fusion is taking place in the **Control** than in the rest of the samples, indicating a likely more viable environment for the cells. The cells within the **Control** have undergone more dendrite and axon formation than cells in any other sample of the same cell density. . No conclusions can be drawn regarding the influence of the epitopes conjugated to the polymers, on cell development. This is due to the fact that all of the cell samples, cultured in polymer, developed to a similar degree. However, it was observed that the cells were not inhibited from developing in the presence of the gel, since cell processing was observed in all of the cell studies. Therefore, this study can be viewed as a preliminary base for the physiological testing, however better refinement and optimisation is necessary to study the polymer's scaffolding abilities. This should include the optimisation of the concentration of the gel, as well as the concentration of the IKVAV epitopes conjugated to the polymer, in order to obtain the most suitable environment for cell differentiation. Further, the refinement of the composition of the growth medium is necessary, in order to obtain an environment that is fully dependent on the polymer for differentiation, in other words, no cell processing would be observed in the Control sample. Furthermore, the type of cells used in the cell studies should be revisited, since GT1-7 progenitor cells are perhaps not the best option for the study at hand.

5.3 Conclusion

It was possible to use a dibenzocyclooctyne-maleimide linker to decorate the azide pendent end group of polyisocyanopeptide hydrogels, functionalised with oligo(ethylene glycol) side chains, with C**IKVAV** and cyclo(**RGD**fC) epitopes, through Cu-free click chemistry. This decoration was verified using the Kaiser test, whereby the polymers decorated with both of the motifs tested positive for primary amines, whereas the polymers without the two epitopes tested negative.

Furthermore, the polyisocyanopeptides proved to be non-toxic to cells. This was shown through fluorescent microscopy by adding PI and Hoechst dye to samples containing GT1-7 neuronal cells after incubation for 24 h in a solution of growth medium containing the polymer. Moreover, it was shown that a cell density of 30 000 cells was necessary for cell attachment to take place, although a higher cell density

of 60 000 cells led to more process formation. In addition, it was noted that the cells surrounded by only growth medium, the **Control**, showed higher levels of cell attachment and mitochondrial networking than those seeded into growth medium containing polyisocyanopeptide hydrogels. The difference in neurite extension between the polymer-containing samples is not very conclusive, more testing would be necessary in the future, and a larger sample size would be required to achieve higher statistical relevance. Furthermore, a more viable polymer environment would be necessary for the cells. With this aim in mind, perhaps a lower concentration of gel, or a different approach for cell seeding could be attempted.

5.4 Experimental

5.4.1 General

Chemicals

All chemicals were purchased from Merck or Sigma Aldrich and used without further purification, unless stated otherwise. C**IKVAV** was purchased from jpt and cyclo(**RGD**fC) was purchased from GLS (GL Biochem (Shanghai) LTD).

Fluorescence Microscopy

An Olympus IX-81 inverted fluorescence microscope system was used for cell imaging with objectives of x40 and x60 and an F-view cooled CCD camera. The instrument uses a Xenon-Arc burner as a light source and it is equipped with 360 nm, 492 nm and 572 nm excitation filters as well as a U/B/G triple-band pass emission filters for the detection of blue, green and red fluorescent markers. The software used for data acquisition and processing was Cell R Live Imaging Software.

Mitochondrial network measurements

POV-ray (Persistence of Vision(tm) Ray Tracer Version 3.7.0) was used to create the reconstructions from .TIF files obtained from the Olympus fluorescence microscope. Two-dimensional images were then generated and the surface areas of the mitochondrial networks were calculated using a Python (version 2.7.6)-based program. Three images were assessed per sample group. The calculations were carried out by Willie Pretorius, under the guidance of Thomas Niesler.[25]

Measurements of surface area occupied by cell

ImageJ (version 1.48) was used to measure the cell surface area. Three images were assessed per sample group. In this method, random fields of view were selected.

5.4.2 Synthetic Protocol

Dibenzocyclooctyne-maleimide-C**IKVAV** (**27a**)

Dibenzocyclooctyne-maleimide (2.22 mg, 5.19 µmol) was dissolved in 50 µL dry DMSO. C**IKVAV** (1.635 mL, 2 mg/mL in PBS buffer) was added to the dibenzocyclooctyne-maleimide solution. A white precipitate formed immediately with the addition of the dibenzocyclooctyne-maleimide. The mixture was shaken/stirred for 12 h. Catalytic amounts (1 %) of ethylene diamine were added to the solution[24] and the reaction mixture was stirred for a further 12h. The solution contained a white precipitate. A pellet was obtained by centrifuging the mixture and removing the supernatant. Both the pellet and supernatant were analysed using LC-MS. **27a**, as well as the two reagents, were seen in the pellet. The pellet was used without further purification.

Dibenzocyclooctyne-maleimide-cyclo(**RGD**fC) (**27b**)

The same procedure was used as with **27a**, however, the reaction was allowed to stir for 72 h without adding any catalyst. LC-MS was used to analyse the pellet and supernatant. It was seen that the pellet containing mainly **27b** and dibenzocyclooctyne-maleimide reagent, while the supernatant contained more of the reagents. The pellet was used without further purification.

Dibenzocyclooctyne-C**IKVAV**-**P2** (**28a**)

P2 (20 mg) was dissolved in 15 mL acetonitrile, ensuring that the polymer was completely dissolved. The mass of **27a** corresponding to 75 % of the **P2** molar azide:spacer monomer ratio was added to the solution, as well as the mass of BCN-rhodamine corresponding to 25 % of the **P2** molar azide:spacer monomer ratio were added to solution of **P2**, and the reaction was stirred at 4 °C for 4 days. The solution was dialysed in 50 % MeOH/Water for 48 h and then 100 % MeOH for a further 12 h. The polymer was precipitated into diisopropyl ether, as described above, and then dried.

Dibenzocyclooctyne-cyclo(**RGD**fC)-**P2** (**28b**)

The same procedure was followed as for **28a**, but using **27b** instead of **27a**.

Dibenzocyclooctyne-**P2** (**28c**)

The same procedure was followed as for **28a**, but using dibenzocyclooctyne-maleimide instead of **27a**.

BCN-rhodamine-**P2** (**28d**)

The same procedure was followed as for **28a**, except only the BCN-rhodamine was added.

Cell-polymer seeding cytotoxicity test (**S1**)

28d was dissolved, at 4 °C, at a concentration of 1.0 mg/mL and 2.0 mg/mL in aqueous growth medium made up of Dulbecco's Modified Eagle's medium *(*DMEM) and antibiotic/antimycotic solution from Sigma Aldrich, containing penicillin and amphotericin B. After the polymer was fully dissolved, 200 µL of each of the solutions was separately added to 200 µL of GT1-7 cells in the same growth medium (20 000 cells per sample), at 12 °C, making a final concentration of 0.5 mg/mL and 1.0 mg/mL of polymer, respectively. The cell-polymer solution was incubated at 37 °C for 24 h.

Process formation test 1 (**S2**)

28a, 28b, 28c and 28d were dissolved in aqueous growth medium at 2.0 mg/mL, at 4 °C. 100 µL of the 2.0 mg/mL solutions were separately added to 150 µL of the GT1-7 cells in growth medium (20 000 cells per sample), at 12 °C. The cell-polymer solutions were incubated at 37 °C for 16 h and then imaged on the fluorescence microscope. Thereafter, the cells were incubated at 37 °C for a further 56 h.

Process formation test 2 (**S3**)

28a, 28b, 28c and 28d were dissolved in aqueous growth medium, at 4 °C, at a concentration of 2.0 mg/mL. 200 µL of the polymer solutions were separately added to 200 µL of the GT1-7 cells in growth medium (30 000 cells per sample), at 12 °C. The cell-polymer solutions were incubated at 37 °C for 48 h.

Process formation test 3 (**S4**)

28a, 28b, 28c were dissolved in aqueous growth medium at a concentration of 2.0 mg/mL, at 4 °C. 200 µL of the polymer solutions were separately added to 200 µL of the GT1-7 cells in growth medium (30 000 cells per sample), at 12 °C. The cell-polymer solutions were incubated at 37 °C for 48 h.

5.4.3 Supplementary images

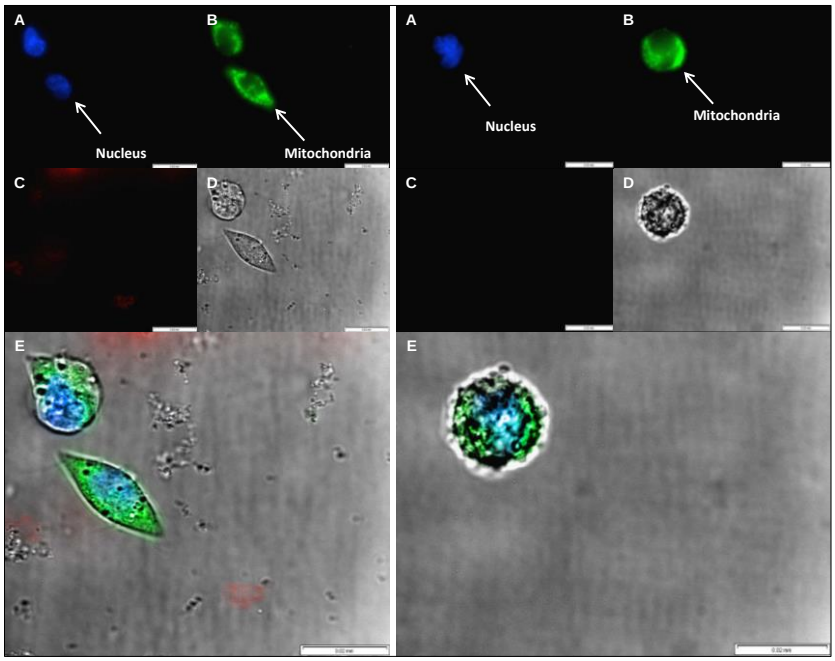

Figure 5.13 Fluorescence micrographs and transmission micrographs of the samples containing 28c (left) and 28d (right) in S2, after incubation for 72 h and after MTG and Hoechst dye were added to the samples. The channels used are A) blue, B) green, C) red, D) trans and E) all channels. Scale bar: 20 µm.

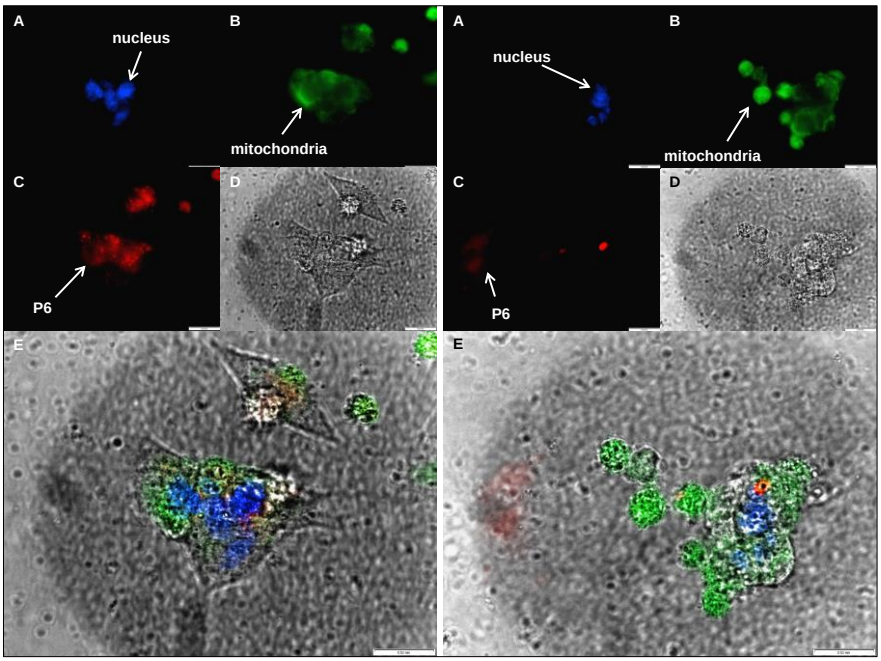

Figure 5.14 Fluorescence micrographs and transmission micrographs of the samples containing 28c (left) and 28d (right) in S3, after incubation for 48 h and after MTG and Hoechst dye were added to the samples. The channels used are A) blue, B) green, C) red, D) trans and E) all channels. Scale bar: 20 µm.

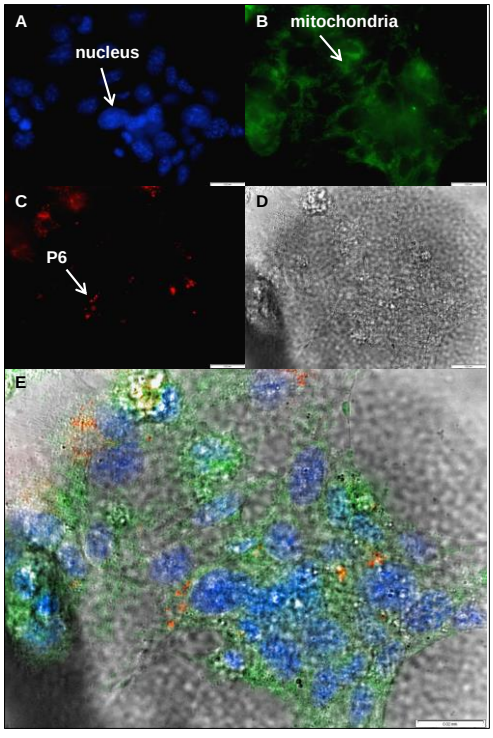

Figure 5.15 Fluorescence micrographs and transmission micrographs of the samples containing 28c in S4, after incubation for 48 h and after MTG and Hoechst dye were added to the samples. The channels used are A) blue, B) green, C) red, D) trans and E) all channels. Scale bar: 20 µm.

5.5 References

(1) Timpl, R.; Rohde, H.; Robey, P. G.; Rennard, S. I.; Foidart, J. M.; Martin, G. R. *J Biol Chem* **1979**, *254*, 9933.

(2) Chung, A. E.; Jaffe, R.; Freeman, I. L.; Vergnes, J.-P.; Braginski, J. E.; Carlin, B. *Cell*, *16*, 277.

(3) Engel, J.; Furthmayr, H. In *Methods in Enzymology*; Leon, W. C., Ed.; Academic Press: 1987; Vol. Volume 145, p 3.

(4) Yamada, M., Kadoya, Y., Kasai, S., Kato, K., Mochizuki, M., Nishi, N., Watanabe, N., Kleinman, H.K., Yamada, Y. & Nomizu, M. *FEBS Letters* **2002**, *530*, 48.

(5) Kanemoto, T.; Reich, R.; Royce, L.; Greatorex, D.; Alder, S. H.; Shiraishi, N.; Martin, G. R.; Yamada, Y.; Kleinman, H. K. *Proc Natl Acad Sci USA* **1990**, *87*, 2279.

(6) Pierschbacher, M. D.; Ruoslahti, E. *Nature* **1984**, *309*, 30.

(7) Pierschbacher, M. D.; Ruoslahti, E. *Proc Natl Acad Sci* **1984**, *81*, 5985.

(8) Yamada, K. M.; Kennedy, D. W. *J Cell Biol* **1984**, *99*, 29.

(9) Agard, N. J.; Prescher, J. A.; Bertozzi, C. R. *J Am Chem Soc* **2004**, *126*, 15046.

(10) Collman, J. P.; Zhang, X.; Herrmann, P. C.; S., U. E.; Boitrel, B.; Straumanis, A.; Brauman, J. I. *J Am Chem Soc* **1994**, *116*, 2681.

(11) Ning, X., Guo, J., Wolfert, M. A. & Boons, G. *Angew Chem Int Ed* **2008**, *47*, 2253.

(12) Kaiser, E.; Colescott, R. L.; Bossinger, C. D.; Cook, P. I. *Anal Biochem* **1970**, *34*, 595.

(13) Brandl, F.; Sommer, F.; Goepferich, A. *Biomaterials* **2007**, *28*, 134.

(14) Schmid, I.; Uittenbogaart, C. H.; Giorgi, J. V. *Cytometry* **1994**, *15*, 12.

(15) Foglieni, C.; Meoni, C.; Davalli, A. M. *Histochem Cell Biol* **2001**, *115*, 223.

(16) Hoorens, A.; Van de Casteele, M.; Kl; xF; ppel, G.; Pipeleers, D. *J Clin Invest* **1996**, *98*, 1568.

(17) Hubbard, K.; Gut, I.; Scheeler, S.; Lyman, M.; McNutt, P. *BMC Res Not* **2012**, *5*, 437.

(18) Harrison, R. A.; Vickers, S. E. *J Reprod Fertil* **1990**, *88*, 343.

(19) Poot, M.; Pierce, R. H. *Cytometry* **1999**, *35*, 311.

(20) Poot, M.; Zhang, Y. Z.; Krämer, J. A.; Wells, K. S.; Jones, L. J.; Hanzel, D. K.; Lugade, A. G.; Singer, V. L.; Haugland, R. P. *J Histochem Cytochem* **1996**, *44*, 1363.

(21) Mitra, K.; Lippincott-Schwartz, J. In *Current Protocols in Cell Biology*; John Wiley & Sons, Inc.: 2001.

(22) Hales, K. G. *Nature Edu* **2010**, *3*, 12.

(23) Rizk, A.; Paul, G.; Incardona, P.; Bugarski, M.; Mansouri, M.; Niemann, A.; Ziegler, U.; Berger, P.; Sbalzarini, I. F. *Nat. Protocols* **2014**, *9*, 586.

(24) Scales, C. W.; Convertine, A. J.; McCormick, C. L. Biomacromolecules 2006, 7, 1389.
(25) Pretorius, W. & Niesler, T. B.Eng(HONS) Dissertation, Stellenbosch University, 2014.

Chapter 6: Conclusion and Future Perspectives

6.1 Conclusion

The current study investigated the possibility of using polyisocyanopeptide hydrogels functionalised with oligo(ethylene glycol) side chains, as scaffolds for tissue engineering. The particular focus on these polymers was due to the claims that they are able to mimic, in almost in every manner, the extracellular matrix of cells.[1] Polyisocyanopeptide hydrogels were decorated with the laminin-derived epitope, **IKVAV**, in the hope of promoting neurite extension and differentiation of neuronal GT1-7 progenitor cells.

Furthermore, the study explored the mechanism with which the polyisocyanides in question are able to gel. Previous studies, using atomic force microscopy, have shown that the polymers form clusters of bundles and pores in the gel state.[1] These bundles have been shown to be independent of concentration, but the number of bundles in a cluster increases with increased concentration of polymer; and in so doing, it causes an inverse relationship between pore size and concentration. This theory was investigated using fluorescence microscopy, and further through three-dimensional reconstruction of the gel.

Chapter 1 gave a brief introduction to polyisocyanopeptide hydrogels functionalised with oligo(ethylene glycol) side chains. The chapter also described the primary objectives of the study, whereby the polymer would be decorated with **IKVAV** epitope and tested for its ability to act as a scaffold for the promotion of GT1-7 neuronal progenitor cells into neurons. **Chapter 2** presented a more in-depth discussion on the importance of an ECM-mimicking scaffold. In addition, it also described other important characteristics of scaffolds, such as biocompatibility, non-toxic biodegradability, mechanical strength, *etc*. The chapter also introduced scaffolds that have been studied previously in neuronal tissue engineering. It especially discussed the importance of the work from Stupp *et al.* in this field, focusing especially on their peptide amphiphile systems. Moreover, **Chapter 2**, motivated the study of polyisocyanides functionalised with oligo(ethylene glycol) side chains as potential tissue engineering scaffolds. This was achieved by first

describing previous work that has been carried out on a range of polyisocyanopeptides, and subsequently focusing on the hydrogel system at hand.

Chapter 3 described the various methods that were attempted in producing the 'azide monomer'. It was found that the method described in literature did not yield the desired results. Instead, the monomer was synthesised by first attaching the azide functionality to the tetraethylene glycol. Thereafter, DCC- and EDC-mediated *Boc*-alanine coupling reactions were performed, with a Boc-deprotection step between the two coupling steps. After a second deprotection, the primary amine was formylated, and finally dehydrated, forming the 'azide monomer'. This monomer was used in **Chapter 4**, where it was copolymerised with a bought, non-functional spacer monomer, in different monomer feed ratios and Ni(II) catalyst to monomer ratios. The resulting polymers were characterised using ^{1}H NMR, SEC, AF4, CD, FT-IR and 'dye' tests.

The mechanism of gelation was also a focal point in **Chapter 4**. The theory brought forward by Rowan *et al.* regarding the gel being a porous structure due to the formation of clusters of bundles of the polymer, was investigated using SR-SIM fluorescence microscopy. The z-stack images that were obtained were thereafter reconstructed into a three-dimensional representation of the gels. However, due to the limited resolution of the obtained microscopy images relative to the feature sizes in the gel, no conclusive evidence was obtained to prove or disprove the theory. However, it was possible to calculate and plot the percentage of filled space within the simulated image as a function of concentration. A linear relation was found between 0.5 to 2.0 mg/mL. However, below 0.5 mg/mL inconclusive results were obtained. It was believed that this could be due to the low concentration of polymer in combination with the limited resolution of the microscope.

Chapter 5 described the preparation of the C**IKVAV** and cyclo(**RGD**fC) epitopes. This included the Michael addition of the thiol moiety of these peptides to a dibenzocyclooctyne-maleimide linker. Thereafter, Cu-free click chemistry was utilised in order to conjugate the epitopes to the polymer. These click reactions were verified by use of the Kaiser test, which indicates the presence of free amines. The polymer was then tested to ascertain the absence of cytotoxicity. It was found that after 24 h of incubation, the cells, seeded in a polymer-growth medium solution, showed equal

viability to that seen in the **Control** (containing just growth medium). Moreover, these decorated polymers, as well as two control polymers, were seeded with GT1-7 cells. Thereafter, their ability to differentiate the cells into neurons was tested. It was found that the cells formed better and obtained more mitochondrial networks in the **Control** containing no polymer, than in the samples containing the gel. However, within the polymer samples, it was seen that the **IKVAV**-decorated polymer showed the highest levels of neurite outgrowth. This was measured by calculating the surface area of the mitochondrial network, as well as the occupied surface area of cells related to the total area.

6.2 Future Perspectives

To further establish whether polyisocyanopeptide hydrogels grafted with oligo(ethylene glycol) side chains can act as an ECM-mimicking scaffold, it is necessary to investigate a number of other factors. One such factor is the biodegradability of the polymer. The strength of the polyisocyanide carbon backbone could pose problems with regard to the degradation of the polymer. Since very low concentrations of the polymer are necessary for it to act as a 3D scaffold, it is possible that this degradation is unnecessary. This must be established. Another route would to perhaps look at using a helical polypeptide backbone that is able to attain similar properties as the polyisocyanide carbon backbone. This polymer would then possibly be able to break-down after it has performed its function as a scaffold, in order to allow for the ECM of the cells/tissue to take over.

A study has been proposed whereby the density of **IKVAV** along the backbone**,** necessary to promote neurite outgrowth, is tested. A polymer would be decorated with varied concentrations of the **IKVAV** epitope. These polymers would then be seeded with GT1-7 cells. After incubation, the cells would be stained with fluorescent markers in order to track their process (axon and dendrite) formation. In a manner similar to the one reported in this study, this process formation can then be quantified by measuring the surface area occupied by the cells, as well as by the mitochondrial network as a function of the total surface area. A similar study is suggested, which allows for the establishment of the optimum concentration of gel. A concentration gradient of each of the above-mentioned **IKVAV**-decorated polymers

would be seeded with GT1-7 cells and thereafter the process formation would be tracked, as above. Furthermore, in order to gain higher statistical power, larger sample size should be used for the cell seeding experiments. In order to obtain better quality results, a number of refinements should be made, such as ensuring that the cells do not clump together, or form a homogenous layer. This could possibly be achieved by using a different approach for the cell seeding.

The possible information to be drawn from the three-dimensional reconstructions of the gels was restricted, due to the limited resolution of the SR-SIM fluorescent microscope. It would be interesting to use a higher resolution microscope, capable of taking z-stacks of the gel, to further investigate the mechanism of gelation of the polymer in solution state. It would then be possible to generate reconstructions of these images, in the same manner as in the current study, whereby it would be possible to infer more information regarding bundle and pore size. In so doing, there may be some possibility to increase the understanding of the mechanism of gelation.

6.3 Reference

(1) Kouwer, P. H. J.; Koepf, M.; Le Sage, V. A. A.; Jaspers, M.; van Buul, A. M.; Eksteen-Akeroyd, Z. H.; Woltinge, T.; Schwartz, E.; Kitto, H. J.; Hoogenboom, R.; Picken, S. J.; Nolte, R. J. M.; Mendes, E.; Rowan, A. E. *Nature* **2013**, *493*, 651.